



**THE DEVELOPMENT OF THERMOGELLING AZITHROMYCIN
FOR PERIODONTITIS TREATMENT**



**A DISSERTATION SUBMITTED IN PARTIAL FULFILLMENT
OF THE REQUIREMENTS FOR
THE DEGREE OF DOCTOR OF PHILOSOPHY IN PHARMACY
COLLEGE OF PHARMACY**

**GRADUATE SCHOOL, RANGSIT UNIVERSITY
ACADEMIC YEAR 2022**

Dissertation entitled

**THE DEVELOPMENT OF THERMOGELLING AZITHROMYCIN
FOR PERIODONTITIS TREATMENT**

by

KUNCHORN KERDMANEE

was submitted in partial fulfillment of the requirements
for the degree of Doctor of Philosophy in Pharmacy

Rangsit University
Academic Year 2022

Assoc.Prof. Watcharee Khunkitti, Ph.D.
Examination Committee Chairperson

Assoc.Prof. Pienkit Dangprasert, Ph.D.
Member

Asst.Prof. Orawan Theanphong, Ph.D.
Member

Apirada Sucontphunt, Ph.D.
Member

Asst.Prof. Sucharat Limsitthichaikoon, Ph.D.
Member and Advisor

Approved by Graduate School

(Asst.Prof.Plт.Off. Vannee Sooksatra, D.Eng.)

Dean of Graduate School

December 21, 2022

Acknowledgments

I would like to express my deepest appreciation to my advisor Asst. Prof. Sucharat Limsiththichaikoon for her invaluable patience and guidance. I also could not have undertaken this journey in the world of pharmacy without my defense committee, who generously provided knowledge and expertise. Additionally, this endeavor would not have been possible without the generous support from Prof. Thawatchai Phaechamud and Asst. Prof. Chuencheewit Thongsiri who shared their expertise and practical support in the critical parts of this research.

I am also grateful to my classmate, Nuttawut Supachawaroj for his advice and suggestions along with the inspiration in these difficult tasks.

Lastly, I would be remiss in not mentioning my family. Their belief in me has kept my spirits and motivation high during this process.

Kunchorn Kerdmanee
Researcher

มหาวิทยาลัยรังสิต Rangsit University

6105286 : Kunchorn Kerdmanee
 Dissertation Title : The Development of Thermogelling Azithromycin
 for Periodontitis Treatment
 Program : Doctor of Philosophy in Pharmacy
 Dissertation Advisor : Asst.Prof. Sucharat Limsitthichaikoon, Ph.D.

Abstract

The objective of this study was to develop an efficient dosage form of azithromycin (AZM) for intra-periodontal pocket administration in periodontitis treatment. A niosome system of span 60 (S60) and cholesterol (CHL) was utilized to improve the bioavailability of AZM. AZM-loaded niosome (NAZ) was fabricated by the modified reverse phase evaporation method. The influence of S60 and CHL on physicochemical properties was investigated. The 3² full factorial experimental design was employed. The results indicated that niosome with S60:CHL at the molar ratio of 3:3 exerted nano-sized with adequate charged stability. Controlled release of AZM was achieved for 8 hrs following the zero-order kinetic. NAZ exhibited biocompatibility with low toxicity. NAZ was further developed into the injectable formulation, thermoresponsive AZM-loaded niosome gel (AZG), utilizing poloxamer 407 (P407) and hyaluronic acid (HA) interactions. At the concentration of 19% P407 and 2% HA, AZG exhibited phase transition within the periodontal pocket temperature, acceptable drug content, stability, and injectability with the pseudoplastic flow. Textural properties indicated proper gel strength without interfering with the tissue-repairing process. AZG exhibited bioadhesive to mucosa and tooth structure which aids in the retention time in the pocket. The release was sustained for 3 days with enhanced drug retention in the biological tissue. The gel-state of AZG gradually degraded within 5 days. AZG accelerated cell proliferation contributed to scratch wound closure. AZG showed biocompatibility and antibacterial activity against periodontal pathogens. The anti-inflammatory effects investigation revealed significant decreases in the inflammatory cytokines (IL-1 β , TNF- α) expression with the tendency to reduce inflammatory cytokines secretion. The developed AZG provided optimal physicochemical with potential therapeutic properties for intra-periodontal pocket administration for adjunctive periodontitis treatment.

(Total 95 pages)

Keywords: Azithromycin, Hyaluronic acid, Hydrogel, Niosome, Periodontitis, Poloxamer 407

Student's Signature Dissertation Advisor's Signature

Table of Contents

	Page
Acknowledgments	i
Abstracts	ii
Table of Contents	iii
List of Tables	vii
List of Figures	viii
Abbreviations	xi
Chapter 1 Introduction	1
1.1 Background and significance of the problem	1
1.2 Research Objectives	3
1.3 Research Framework	4
Chapter 2 Literature Review	5
2.1 Periodontitis	5
2.2 Treatment of periodontitis	6
2.3 Antibiotics in periodontitis treatment	7
2.4 Local antibiotics for periodontitis treatment	8
2.5 Azithromycin in periodontal therapy	9
2.6 Desirable formulation for periodontal formulation	12
2.6.1 Poloxamer 407 (P407)	13
2.6.2 Hyaluronic Acid (HA)	14
Chapter 3 Research Methodology	16
3.1 Fabrication of AZM-loaded niosomes	16
3.1.1 Solubility of azithromycin dihydrate (AZM)	16
3.1.2 Preparation of AZM-loaded niosomes (NAZ)	16

Table of Contents (Cont.)

	Page
3.1.3 Determination of particle size and zeta potential	17
3.1.4 Utilization of experimental design for the determination of particle size and zeta potential	17
3.1.5 Differential scanning calorimetry (DSC), thermogravimetric analysis (TGA)	17
3.1.6 Powder X-ray diffraction analysis (PXRD)	18
3.1.7 Fourier transform infrared spectroscopy (FTIR)	18
3.1.8 Confocal microscopy, scanning electron microscopy (SEM), transmission electron microscopy (TEM)	18
3.1.9 Entrapment efficiency of niosome	19
3.1.10 <i>In vitro</i> drug release study	19
3.1.11 Cell viability evaluation	20
3.2 Formulation of thermoresponsive AZM-loaded niosomes gel	20
3.2.1 Preparation of thermoresponsive niosomes gel (AZG)	20
3.2.2 Physicochemical Properties	21
3.2.3 Mechanical properties	22
3.2.4 Stability of the formulation	25
3.2.5 Model drug analysis	25
3.2.6 Biocompatibility	26
3.3 Efficacy evaluation of thermoresponsive AZM-loaded niosomes gel	27
3.3.1 Antibacterial activity	27
3.3.2 Wound healing effects	27
3.3.3 Anti-inflammatory effects	28
 Chapter 4 Research Results	 31
4.1 Fabrication of azithromycin-loaded niosomes (NAZ)	31

Table of Contents (Cont.)

	Page
4.1.1 Solubility of azithromycin dihydrate (AZM)	31
4.1.2 Preparation of AZM-loaded niosomes (NAZ)	31
4.1.3 Determination of particle size and zeta potential	32
4.1.4 Utilization of experimental design for the determination of particle size and zeta potential	35
4.1.5 Differential scanning calorimetry (DSC), thermogravimetric analysis (TGA)	38
4.1.6 Powder X-ray diffraction analysis (PXRD)	40
4.1.7 Fourier transform infrared spectroscopy (FTIR)	41
4.1.8 Confocal microscopy, scanning electron microscopy (SEM), transmission electron microscopy (TEM)	42
4.1.9 Entrapment efficiency of niosomes	44
4.1.10 <i>In vitro</i> drug release study	44
4.1.11 Cell viability evaluation	47
4.2 Formulation of thermoresponsive AZM-loaded niosomes gel (AZG)	48
4.2.1 Preparation of thermoresponsive niosomes gel	48
4.2.2 Physicochemical Properties	51
4.2.3 Mechanical properties	55
4.2.4 Stability of the formulation	63
4.2.5 Model drug analysis	65
4.2.6 Biocompatibility	69
4.3 Efficacy evaluation of thermoresponsive AZM-loaded niosomes gel	72
4.3.1 Antibacterial activity	72
4.3.2 Wound healing effects	73
4.3.3 Anti-inflammatory effects	75

Table of Contents (Cont.)

	Page
Chapter 5 Conclusion	80
5.1 Conclusion	80
5.2 Further study	82
References	83
Appendix	93
Biography	95



List of Tables

	Page
Tables	
3.1 Primers used for IL-1 β , TNF- α , and GAPDH	29
4.1 Composition of azithromycin-loaded niosomes (NAZ), particle size, polydispersity index (PDI), zeta potential and entrapment efficiency (EE) of NAZ formulations.	33
4.2 Experimental design layout for NAZ formulation optimization.	35
4.3 Kinetic models fitting of AZG formulations.	46
4.4 Composition of thermoresponsive azithromycin-loaded niosomes gel (AZG) and physicochemical properties of AZG includes pH, drug content, gelation temperature and gelation time.	50
4.5 Experimental design layout for AZG formulation optimization.	53
4.6 Mechanical properties of thermoresponsive azithromycin-loaded niosomes gel (AZG) such as viscosity, injectability and textural properties.	56
4.7 Percentage of AZM content and pH of each formulation in different storage conditions at 0, 7, 14, and 30 days.	64
4.8 Kinetic models fitting of AZG formulations.	67
A1 Validation data of azithromycin dihydrate	94

List of Figures

Figures	Page
1.1 Research framework of this study	4
2.1 Chemical structure of azithromycin dihydrate	11
2.2 Chemical structure of poloxamer 407	14
2.3 Chemical structure of hyaluronic acid	14
4.1 Niosomes particle size of AZM-loaded niosomes (a), blank niosomes (b) related to polydispersity index.	34
4.2 Niosomes particle size of AZM-loaded niosomes (a), blank niosomes (b) related to the zeta potential.	34
4.3 Response surface plot indicating the effect of variables A (S60) and B (CHL) on the responses: particle size (a) and zeta potential (b).	36
4.4 Contour plot of the responses: particle size (a), zeta potential (b), and the superimposed contour plots of both responses (c).	37
4.5 DSC thermograms of span 60 (S60), cholesterol (CHL), blank niosome (BLN), azithromycin (AZM), and azithromycin-loaded niosome (NAZ).	38
4.6 TGA investigation presenting the percentage of weight loss of span 60 (S60), cholesterol (CHL), blank niosome (BLN), azithromycin (AZM), and azithromycin-loaded niosome (NAZ).	39
4.7 PXRD analysis of span 60 (S60), cholesterol (CHL), blank niosome (BLN), azithromycin (AZM), and azithromycin-loaded niosome (NAZ).	40
4.8 FTIR spectra of span 60 (S60), cholesterol (CHL), blank niosome (BLN), azithromycin (AZM), and azithromycin-loaded niosome (NAZ).	41
4.9 Confocal laser scanning microscopy of AZM-loaded niosome.	42
4.10 SEM image of AZM-loaded niosome at 5000x (a) and 20000x magnification (b).	43
4.11 TEM image of AZM-loaded niosome.	43

List of Figures (Cont.)

Figures	Page
4.12 <i>In vitro</i> percent cumulative release of azithromycin-loaded niosomes (NAZ).	44
4.13 Cell viability of HGF cultured with AZM-loaded niosomes (NAZ) formulations (a), blank niosome (b), azithromycin solution (AZM) compared to the culture medium (Control), which served as a negative control.	47
4.14 Response surface plot indicating the effect of variables C (P407) and D (HA) on the responses: gelation temperature (a) and gelation time (b).	54
4.15 Shear stress and shear rate plots indicated rheological behavior of all AZG formulations at 4 °C.	58
4.16 Bioadhesive force of AZG formulations represented the adhesion to the mucosa and tooth-root surface.	61
4.17 Percent cumulative drug release of AZG formulations.	65
4.18 Cumulative permeated drug from <i>ex vivo</i> mucosal permeation model.	68
4.19 Percentage of cell viability of AZG formulations in various concentrations.	70
4.20 Biodegradability of the formulation represented by the percentage of weight loss.	71
4.21 Antibacterial activity of AZG against major periodontal pathogens, namely <i>Aggregatibacter actinomycetemcomitans</i> (Aa.) and <i>Porphyromonas gingivalis</i> (Pg.).	72
4.22 Scratch wound assay of gingival fibroblast at 0, 6, 12, 18, 24 hrs.	73
4.23 Percentage of wound closure.	73
4.24 Cell proliferation assay indicated the percentage of cell viability of cultured macrophage at 48 and 72 hrs incubation periods.	75
4.25 IL-1 β mRNA expression of RAW 264.7 in control (Ctrl), LPS-stimulated (LPS), pretreated with AZG followed by LPS stimulation group (LPS + AZG7, 8 and 9).	77

List of Figures (Cont.)

	Page
Figures	
4.26 TNF- α mRNA expression of RAW 264.7 in control (Ctrl), LPS-stimulated (LPS), pretreated with AZG followed by LPS stimulation group (LPS + AZG7, 8 and 9).	77
4.27 IL-1 β secretion of RAW 264.7 in control (Ctrl), LPS-stimulated (LPS), pretreated with AZG9 extract at different concentration followed by LPS stimulation.	79
4.28 TNF- α secretion of RAW 264.7 in control (Ctrl), LPS-stimulated (LPS), pretreated with AZG9 extract at different concentration followed by LPS stimulation.	79
A1 HPLC chromatogram of standard azithromycin dihydrate.	94



Abbreviations

Abbreviation	Meaning
%	percentage(s)
% EE	percent of entrapment efficiency
% w/v	percent weight by volume
°C	degree Celsius
μl	micro liter
μg	micro gram
<i>Aa.</i>	<i>Aggregatibacter actinomycetemcomitans</i>
AZG	thermoreponsive azithromycin-loaded niosome gel
AZM	azithromycin
cDNA	complementary deoxy-ribonucleic acid
CHL	cholesterol
CO ₂	carbon dioxide
cps	centipoise
DMEM	Dulbecco's modified eagle's medium composition
DOE	design of experiment
DSC	differential scanning calorimetry
EE	Entrapment efficiency
ELISA	enzyme linked immunosorbent assay
FBS	fetal bovine serum
FTIR	Fourier transform infrared spectroscopy
g	gram
g-Force	gravitational force
GAPDH	glyceraldehyde-3-phosphate dehydrogenase
GCF	gingival crevicular fluid
HA	hyaluronic acid
HGF	human gingival fibroblast

Abbreviations (Cont.)

Abbreviation	Meaning
HPLC	high performance liquid chromatography
hr (s)	hour (s)
H ₂ S	hydrogen sulfide
IL-1 β	interleukin one beta
IL-6	interleukin six
IL-8	interleukin eight
kDa	kilodalton (s)
KH ₂ PO ₄	potassium dihydrogen phosphate
LPS	lipopolysaccharide
M	molar
MeOH	methanol
mg	milligram
min (s)	minute (s)
ml	milliliter
mm	millimeter
mN	millinewton
MTT	3-(4,5-dimethylthiazol-2-yl)-2,5-diphenyl-2H-tetrazolium bromide
MWCO	molecular weight cut off
mV	millivolts
N	newton
NAZ	niosome of azithromycin
NH ₄	ammonium
nm	nanometer
OD	optical density
P407	poloxamer 407
PBS	phosphate buffer solution

Abbreviations (Cont.)

Abbreviation	Meaning
PCR	polymerase chain reaction
PDI	polydispersity index
<i>Pg.</i>	<i>Porphyromonas gingivalis</i>
pH	potential of hydrogen ion
pKa	acid dissociation constant
PLGA	poly (lactic-co-glycolic acid)
PXRD	powder X-ray diffraction
RNA	ribonucleic acid
rpm	revolutions per minute
rt-qPCR	real-time reverse transcriptase quantitative polymerase chain reaction
r^2	coefficient of determination
s	second
S60	span 60
SEM	scanning electron microscopy
TEM	transmission electron microscopy
TGA	thermogravimetric analysis
TNF- α	tumor necrosis factor alpha

Chapter 1

Introduction

1.1 Background and significance of the problem

Periodontitis is an inflammatory disease triggered by bacterial infection. The periodontium or the framework supporting the teeth was destroyed as a result of periodontitis. According to statistics from the most recent national oral health survey in 2017, the prevalence of periodontitis in the Thai adult population aged 35 to 44 was 25.9%, and in those aged 60 to 74 was increased to 36.3% (Bureau of dental health, 2018). The high prevalence of periodontitis among the population is a great concern for oral health problems in Thailand. Untreated periodontitis can lead to multiple tooth losses and may complete loss of dentition. When there are no teeth, eating becomes problematic. These diseases have a serious impact on a patient's quality of life.

The hygienic phase and surgical phase constitute up the gold standard of treating periodontal disease. During the hygienic phase, mechanical cleansing of tooth structure is performed to get rid of periodontal pathogens. However, it is generally accepted that the treatment outcome of non-surgical treatment is limited because of the following factors. It is impossible to get rid of all bacteria from the tooth structure with complicated root morphology. The cementum is still contaminated with infiltration of bacterial endotoxin. The periodontal pathogen may reside in the gingival tissue resulting in the recolonization of the bacteria. If the disease is persistent, the patient would be referred for complex surgical treatment. In the past decade, various adjunctive therapeutic methods have been proposed to improve periodontal treatment outcomes.

Since the nature of this disease is a bacterial infection, systemic antibiotic in oral dosage form was used concomitantly with scaling and root planing. Herrera and colleagues conducted a systematic review of using systemic antibiotics as an adjunct to mechanical debridement from 25

randomized controlled trials. They concluded that systemic antibiotics as the adjunct to scaling and root planing showed the benefit over scaling and root planing alone in aspects of pocket reduction and clinical attachment level gain. (Herrera, Sanz, Jepsen, Needleman, & Roldán, 2002) In agreement with the systematic review of Haffajee and colleagues which also presented greater clinical improvement over the treatment without systemic antibiotics. (Haffajee, Socransky, & Gunsolley, 2003) The antimicrobial agents included in both reviews such as amoxicillin, metronidazole, tetracycline, clindamycin, and doxycycline were extensively used in periodontal treatment.

However, the systemic drug needs to pass through whole body metabolism not only the site of infection. In periodontitis treatment, the periodontal pocket is considered the site of action. To reach a therapeutic dose of medication in this area, a high dose of the oral drug is required. The unwanted side effect of a systemic antibiotic such as nausea, vomiting, diarrhea, as well as bacterial resistance, could happen. (Jepsen, K. & Jepsen, S., 2016) For this reason, the concept of local drug delivery was invented to be used as a carrier to bring the medication directly to the periodontal pocket. Intra-periodontal pocket administration may be the ideal route for the treatment of chronic periodontitis (Nair & Anoop, 2012). The advantage of bringing the drug directly into the periodontal pocket may avoid the undesirable effects of the systemic antibiotic. The concentration of the drug can be lower with this administration route. Drug administration by the dentist may avoid patient compliance problems.

Intra-periodontal pocket administration has caught many researchers' attention. The treatment of periodontitis would benefit from the local delivery of active medications to the active site of infection. Chlorhexidine chip, tetracycline fiber, doxycycline gel, metronidazole gel, and minocycline microspheres were developed for adjunctive treatment (Quirynen, Teughels, De Soete, & van Steenberghe, 2002).

One macrolide antibiotic with intriguing features is azithromycin (AZM). In addition to its susceptibility to the principal periodontal pathogens, the anti-inflammatory effectiveness has

been well-documented (Hirsch, Deng, & Laohachai, 2012). AZM exhibits a long half-life with good tissue penetration. These properties are suitable for the nature of periodontitis. However, only a few studies of AZM as a local delivery were published. With today's modern cutting-edge pharmaceutical technology, creating a reliable vehicle could enable AZM's intra-periodontal pocket administration for treating periodontitis to work more effectively.

Therefore, the goals of this study are to develop the optimum thermogelling azithromycin formulation for local delivery. This formulation would achieve the maximum potency for periodontitis treatment in terms of antibacterial activities, anti-inflammatory effect, and promote the healing process.

1.2 Research objectives

Objectives of the development of thermogelling azithromycin formulation for periodontitis treatment were as follows,

1.2.1 To prepare an optimal thermogelling azithromycin formulation by observing the mixing method, the appearance of the prepared formulation, drug content, and thermogelling properties.

1.2.2 To conduct comprehensive characterizations of thermogelling azithromycin formulation including physicochemical properties, mechanical properties, drug analysis as well as stability of the formulation.

1.2.3 To assess the efficacy of the formulation as a therapeutic agent by investigating cytotoxicity, antimicrobial activities, effects on the wound healing process, and anti-inflammatory activities.

1.3 Research Framework

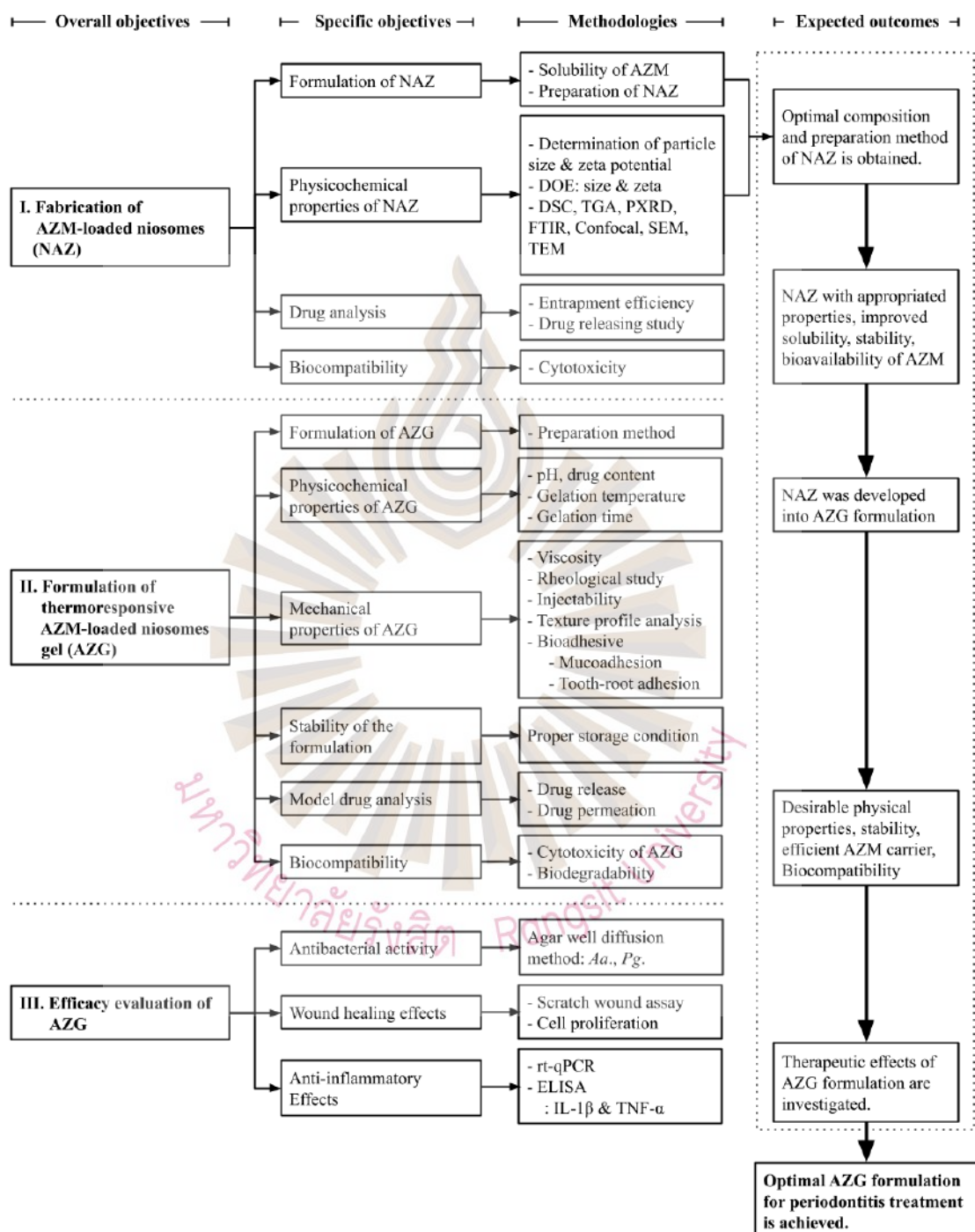


Figure 1.1 Research framework of this study

Chapter 2

Literature Review

2.1 Periodontitis

An inflammatory disease known as periodontitis affects the tooth-supporting structure or the periodontium, which is made up of cementum, periodontal ligament, alveolar bone, and gingiva. From the data of the latest national oral health survey in 2017, the prevalence of periodontitis in the Thai adult population aged 35 to 44 was 25.9%, and in those aged 60 to 74 was increased to 36.3% (Bureau of dental health, 2018). Which are considered high-prevalence diseases.

Pathogenesis of periodontitis is associated with the accumulation of dental plaque biofilm which leads to the imbalance of host and bacteria. The relation between host and bacteria shifts from symbiosis to dysbiosis stage. This condition stimulates the host's immune response in the form of inflammation in order to eliminate the invasion of bacteria. Unfortunately, inflammatory response causes collateral damage to the periodontium, which resulted in the destruction of adjacent periodontal tissues.

Signs and symptoms of periodontitis are gingival inflammation, bleeding, halitosis, gingival recession, periodontal pocket formation, tooth mobility, and alveolar bone loss. The unique characteristic of this disease is the formation of the periodontal pocket. After the crestal bone of the alveolar process is damaged by periodontitis, the periodontal pocket is formed. The periodontal pocket is pathologically deepened of the physiological gingival sulcus. In healthy gingiva, the gingival sulcus, or the gap between tooth and gingiva is 2-3 mm in depth. When the alveolar bone is destroyed by periodontitis, this gap becomes deeper to 4 mm or more. It is uncleanable by patient routine self-care. This causes more bacterial plaque buildup in the form of dental plaque biofilm, which promotes higher intensity of the inflammation and progression of the disease.

According to the current periodontal pathogenesis model, dental plaque biofilms are considered the main etiologic factor of periodontal disease (Meyle & Chapple, 2015). Although biofilms are the polymicrobial complex of various kinds of bacteria, a limited number of bacteria are associated with periodontitis. The pathogenicity criteria are based on the disease association, elimination of specific bacteria results in remission of the disease, pathogenicity in animal experiments, host immune response induction, and virulent factors production (Haffajee & Socransky, 1994). Two bacterial species that matched all criteria are *Aggregatibacter actinomycetemcomitans* (*Aa.*) and *Porphyromonas gingivalis* (*Pg.*). The virulent factors of *Aa.* are leukotoxin, collagenase, protease, endotoxin, fibroblast inhibition factor, and bone resorption factor. While the virulent factors of *Pg.* include proteases, collagenase, hemolysin, endotoxin, fatty acid, H₂S, and NH₄. Both pathogens are greatly associated with the destruction of the periodontal lesion, as a result, they could be indicated as key periodontal pathogens (Popova, Dosseva-Panova, & Panov, 2013).

The advanced stage of periodontitis extensively destroys tooth-supporting structures until no supporting bone is left. Eventually, patients with untreated periodontitis can lead to multiple tooth losses and may complete tooth loss. When there are no teeth, eating becomes problematic. These conditions significantly affect a patient's quality of life.

2.2 Treatment of periodontitis

The treatment of periodontitis begins with the initial phase or non-surgical periodontal treatment. The objective of this phase is to control inflammation of the periodontium by eliminating dental plaque biofilms and any factors involved in its deposition. In this phase, dental plaque biofilms and supragingival and subgingival calculus are removed by mechanical debridement performed by the dentist. Mechanical debridement aimed to get rid of bacterial deposits by scraping on the tooth-root surface with a specifically designed curette. The dentist must also provide oral hygiene instructions to prevent the new formation of dental plaque biofilms. Mechanical debridement employing scaling and root planing is considered the gold standard for non-surgical

treatment. Scaling and root planing can be accomplished with an ultrasonic scaler and manual-hand scalers. After non-surgical treatment, in case of the periodontal pocket or the defect caused by periodontitis are persist. It should be managed by the surgical treatment performed by a periodontist. The patients would be referred for more complex surgical procedures.

However, it is generally accepted that the treatment outcome of non-surgical treatment is limited because of many factors. Mechanical debridement by scaling and root planing is impossible to get rid of all subgingival calculus from the tooth structure with complicated root surface morphology. The remaining bacteria in subgingival calculus can lead to reinfection by the recolonization of bacteria. Although cementum, tooth-root surface, is cleaned by scaling and root planing, it was found in the scanning electron microscopy that the ultrastructure of cementum is still infiltrated with bacterial endotoxin. Moreover, periodontal pathogens may be left inside gingival tissue and recolonize over time. These factors result in prolonged dysbiosis and are difficult to reverse back to the symbiosis relationship between host and bacteria (Meyle & Chapple, 2015).

Therefore, periodontitis patients may need complicated surgical treatment afterward. However, some patients may have difficulty receiving complex periodontal treatment such as patients who live in remote areas of the faraway province, patients who cannot afford the expenditure of periodontal surgery, and medically compromised patients who cannot undergo surgical procedures. The improvement of non-surgical treatment methods can be beneficial to these patients. This aspect can be a research challenge to developing an adjunctive therapeutic method for improving the outcome of non-surgical periodontal treatment.

2.3 Antibiotics in periodontitis treatment

In order to improve the treatment outcome of nonsurgical treatment, many adjunctive treatment modalities were proposed. Applications of laser and photodynamic, medication are used in periodontal therapy. Since the nature of periodontitis is an inflammatory disease caused by bacterial infection, antibiotic drugs are thought to be useful in the treatment protocol. Systemic

antibiotics in oral dosage form were used concomitantly with scaling and root planing. The antimicrobial agents included in both reviews such as amoxicillin, metronidazole, tetracycline, clindamycin, azithromycin, and doxycycline were extensively used in periodontal treatment. Herrera and colleagues conducted a systematic review of using systemic antibiotics as an adjunct to mechanical debridement from 25 randomized controlled trials. They came to the conclusion that adding systemic antibiotics to scaling and root planing has advantages over doing so alone in terms of pocket reduction and clinical attachment level gain. (Herrera et al., 2002). In agreement with the systematic review of Haffajee et al. (2003), which also presented greater clinical improvement over the treatment without systemic antibiotics.

However, the systemic drug needs to pass through whole-body metabolism before entering the site of action. In periodontitis treatment, the periodontal pocket is considered the site of action. In order to reach a therapeutic dose in this area, a high dose of the peroral drug is required. The unwanted side effect of a systemic antibiotic such as nausea, vomiting, and diarrhea may occur (Jepsen, K. & Jepsen, S., 2016). Antibiotic resistance of bacteria is also a major concern. For this reason, the concept of local drug delivery was proposed to be used as a carrier to bring the active ingredient to the site of action. Intra-periodontal pocket administration could be the ideal route for the treatment of periodontitis. The major advantage of local drug delivery is to directly bring the drug to the periodontal pocket. This may avoid the undesirable effects of systemic antibiotics. The concentration of the drug can be lower with this local administration route. The use of local antibiotics may reduce the developing bacterial resistance. Drug administration by the dentist may also avoid patient compliance problems.

2.4 Local antibiotics for periodontitis treatment

Various kinds of antibiotics and antiseptics were intended to deliver to the periodontal pocket with different carriers. The purpose of local antimicrobial agents is to eliminate or reduce bacterial remnants in the periodontal pocket which could reduce the chance of recolonization and reinfection of the disease. Examples of the intra-periodontal delivery system are chlorhexidine in

the form of a chip, varnish, and gel, doxycycline gel, metronidazole gel, minocycline in the form of gel and microsphere, tetracycline in the form of film, fiber, and gel. The efficacy of these products was proven to add benefit to the treatment of deep and recurrent pockets (Matesanz-Pérez et al., 2013). When compared to the efficacy of systemic antibiotics which added the clinical benefit of pocket reduction and clinical attachment gain of 0.3 and 0.2 mm, respectively, the local antibiotics provide more clinical benefit of 0.4 mm and 0.3 mm, respectively (Jepsen, K. & Jepsen, S., 2016). Moreover, in a recent systematic review of local antibiotics, the authors emphasized the importance of drug vehicles which should be sustained release formulation long enough to eliminate pathogens depending on each type of antibiotic. Other factors such as ease of handling, application time, and cost must be considered with these products (Matesanz-Pérez et al., 2013). The development of a novel dosage form with prolonged and controlled release of antibiotics may improve the treatment outcome of chronic periodontitis treatment.

Apart from the antibiotic effect, it was found that some antibiotics exhibit immunomodulatory activities, which regulate destructive host inflammatory response. For example, tetracycline was found to have an anti-collagenase effect. That can be useful in the treatment of collagen degradation diseases like periodontitis. Sub-antimicrobial dose of doxycycline, the tetracycline descendant, was found to reduce matrix metalloproteinase enzyme activities when used adjunct to periodontal treatment (Gu, Walker, Ryan, Payne, & Golub, 2012). These drugs can be good examples of host modulation therapy which is the future trend of periodontal treatment. Host modulation therapy aims to manage inflammatory response besides the elimination of bacteria.

2.5 Azithromycin in periodontal therapy

A second-generation macrolide antibiotic is called AZM. By inhibiting bacterial protein synthesis, AZM has a bacteriostatic effect. The bacteriostatic mechanism involves the binding of AZM at the bacterial ribosome. The translocation of aminoacyl transferase is blocked, resulting in premature termination of the peptide chain. With regard to both gram-positive and gram-negative bacteria, AZM is a broad-spectrum antibiotic. In periodontitis, significant periodontal pathogens

such as *Aggregatibacter actinomycetemcomitans*, *Porphyromonas gingivalis*, and *Prevotella intermedia* are susceptible to AZM (Hirsch et al., 2012). It is a long half-life antibiotic (68 hours) with good penetration to the periodontal tissue. These properties are suitable for the nature of periodontitis. The oral form of AZM was used as an adjunctive in periodontitis treatment in many clinical studies. Hirsch summarized the results of previous AZM clinical trials in a review article. They concluded that the adjunctive use of AZM in periodontal treatment improved therapeutic outcomes compared with periodontal treatment without AZM administration. In general, the dosage regimen of AZM is 500 mg once daily, for three days. AZM has a lengthy half-life, hence, the regimen is shorter than other antibiotics. This can be beneficial in terms of better patient compliance. After three days of oral administration, AZM levels in the gingival crevicular fluid were found to be above the minimal inhibitory concentration of the periodontal pathogens continuously for 7 days. This is because AZM was accumulated in the periodontal tissues (Hirsch et al., 2012).

Moreover, the distinctive feature of AZM is its immunomodulatory properties. It was shown that AZM decreased the expression of pro-inflammatory cytokines including interleukin (IL)-1 β , IL-6, IL-8, and tumor necrosis factor (TNF)- α . The reduction of pro-inflammatory cytokines results in anti-inflammatory effects (Singh et al., 2018).

AZM was used as local drug delivery in 2008, from the clinical study by Pradeep et al. poly (lactic-co-glycolic acid) (PLGA) with 0.5% AZM was used for periodontitis treatment. The results indicated that the treated group with adjunctive AZM had improvement in clinical and microbiologic parameters compared to the treated group without adjunctive AZM (Pradeep, Sagar, & Daisy, 2008). However, tissue penetration, and mucoadhesion, may not achieve with PLGA-based formulation.

In the pharmaceutical aspect, AZM is available in the form of anhydrous, monohydrate, and dihydrate with molecular weights of 748.984, 767.02, and 785.0, respectively. The structural formula of AZM is shown in figure 2.1. AZM appears as a powder that is either white or off-white. In water, AZM is essentially insoluble. The water solubility of AZM is only 1.1 mg/ml with pKa =

7.34. AZM is stable with heated up to 80 °C and changed from dihydrate to anhydrous form but the crystalline lattice is remained unchanged (Bakheit, Al-Hadiya, & Abd-Elgalil, 2014).

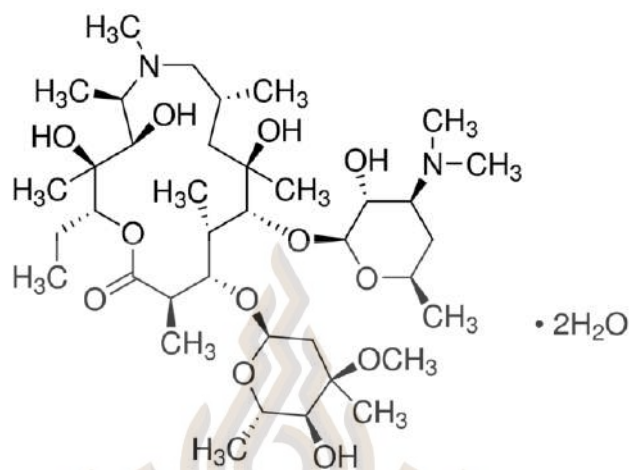


Figure 2.1 Chemical structure of azithromycin dihydrate

Source: Al-Rimawi & Kharoaf, 2010

As mentioned above, AZM is a high-potential drug. The antibacterial effect against periodontal pathogens along with anti-inflammation are useful for periodontitis treatment since the pathogenesis of periodontitis is involved with bacterial infection accompanied by the inflammatory effects of the host immune response. The development of an efficient vehicle may synergistically enhance the efficacy of AZM for local drug delivery systems. According to the long half-life of AZM, three days of oral administration could provide the therapeutic drug level for 7 days. It could be postulated that the local delivery form of AZM, which is directly brought to the target site without entering the first-pass metabolism, should be more efficient and avoid undesirable side effects of the systemic drug.

However, AZM is classified as a BCS class II medication (Idkaidek, Najib, Salem, & Jilani, 2014). The poor solubility of AZM could be problematic to the bioavailability of the drug in biological tissue. Therefore, this disadvantage of AZM must be corrected. Several methods have been proposed to improve drug dissolution such as chemical modification, solid dispersion, and carrier systems. The vesicle system can be used as a carrier for hydrophobic drugs.

Niosome is a vesicular system that is capable of delivering both hydrophilic and hydrophobic drugs owing to the bilayer structure. Non-ionic surfactants and cholesterol or their derivatives are the major ingredients of niosomes. Non-ionic surfactants such as Span 60 (sorbitan monostearate) consist of two distinct regions in one molecular structure, which are a hydrophilic head and a hydrophobic tail. After forming a niosome structure, the molecular structure arranges into the lipid bilayer with an aqueous core inside. The hydrophilic material can be carried with the aqueous core while the hydrophobic substance can entrap into the lipophilic domain in the lipid bilayer shell. The addition of cholesterol enhanced vesicle stability, entrapment efficiency, storage, and release (Moghassemi & Hadjizadeh, 2014).

2.6 Desirable formulation for periodontal formulation

The first thing to be considered in the development of intra-periodontal pocket administration is the biology of the periodontal pocket. The periodontal pocket is the unique pathologic feature of periodontitis. Within the pocket, one side is the hard tissue of the tooth-root surface, whereas another side is the soft tissue of the pocket epithelium and the connective tissue of the gingiva. At the bottom of the pocket, junctional epithelium, gingival crevicular fluid (GCF) is secreted from epithelial cells of the periodontal pocket. GCF is an extracellular fluid responsible for the defense mechanism of the periodontium. The normal flow rate of GCF is 2-3 μl per hr per tooth which increases up to ten-fold during the inflammation stage. The pH range varies from 6.9 to 7.4. The temperature of the pocket is 2 $^{\circ}\text{C}$ less than the sublingual temperature and increases by 0.65 $^{\circ}\text{C}$ during inflammation.

The intra-periodontal pocket formulation must be designed to overcome the restricted environment of the periodontal pocket in the following aspects. The periodontal formulation needs to reside inside the pocket and sustained release therapeutic agent long enough for the therapeutic period of each active ingredient. The formulation that can form a semi-solid stage may have advantages in this aspect. In addition, the required property to ensure prolonged residence time inside the pocket is mucoadhesion. However, the pocket epithelium has a high turnover rate. The

formulation can be flushed out of the pocket prematurely. The key property of the periodontal formulation may be the adhesion to the tooth-root surface (Agossa et al., 2017). The formulation could achieve prolonged retention time inside the pocket with good bioadhesive, which includes both mucoadhesion and tooth-root surface adhesion.

To invent the desirable formulation specialized for periodontal pockets, the following polymers are chosen.

2.6.1 Poloxamer 407 (P407)

The in situ forming formulation can be achieved with various mechanisms such as solvent exchange, pH-dependent, stimulation by specific wavelength light source, and temperature. The human body possesses a specific temperature range and it can be used as a stimulation for in situ forming systems without the need for an external stimulator. P407 is a thermosensitive polymer that has the extraordinary ability to transition into a semi-solid state when the temperature is increased. The P407 structure (figure 2.2) is a triblock copolymer with two hydrophilic domains made of ethylene oxide and one hydrophobic domain made of propylene oxide. Below the transition temperature, the P407 solution remains in the liquid stage. Above transition temperature, P407 molecules form micelles by dehydration of the hydrophobic parts at the core with the outer shell of hydrophilic parts. The packing of multiple micelles initiates the gelation process of the polymer and finally forms a semi-solid or gel stage (Dumortier, Grossiord, Agnely, & Chaumeil, 2006). Gel formation by the body temperature is possible with this characteristic. P407 has been constantly used in many dosage forms, especially in ocular drugs as well as periodontal administration (Bansal et al., 2018; Garala, Joshi, Patel, Ramkishan, & Shah, 2013; Talasaz et al., 2008). The gel stage of P407 could extend the formulation's duration in the periodontal pocket. P407 is considered an inactive ingredient with biocompatibility and biodegradability. However, the gel matrix of this polymer is poor durability, and low mechanical strength and causing rapid drug release (Gong et al., 2013). The addition of the second type of polymer may help improve these drawbacks.

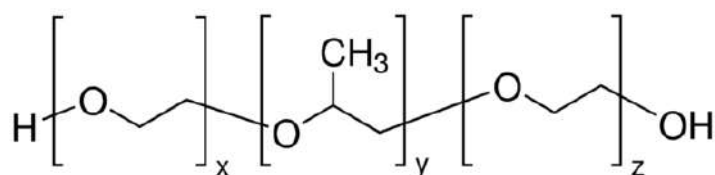


Figure 2.2 Chemical structure of poloxamer 407

Source: Braun, 2011

2.6.2 Hyaluronic Acid (HA)

HA is a naturally occurring polymer that is found in the connective tissue of the organ's extracellular matrix. HA is the main component of periodontal tissues which maintains the physiological and structural function of these organs. In the pharmaceutical aspect, HA is highly biocompatible non immunogenicity, and biodegradable. Due to its hygroscopic property, it retains water and forms a gel-like matrix. In the study of poloxamer incorporated with HA, the addition of hyaluronic acid to the formulation increased viscoelasticity but not much affected the transition temperature of the formulation. The model drug's release increased the ability for sustained release (Mayol, Quaglia, Borzacchiello, Ambrosio, & Rotonda, 2008). HA also possessed mucoadhesive properties. The structure of hyaluronic acid is composed of random coils which entangle into the mucous layer and adhere. A large number of studies used HA as a mucoadhesive polymer, especially in the ophthalmic formulation. HA was reported to prolong resident at cornea increasing the bioavailability of therapeutic drugs (Liao, Jones, Forbes, Martin, & Brown, 2005).

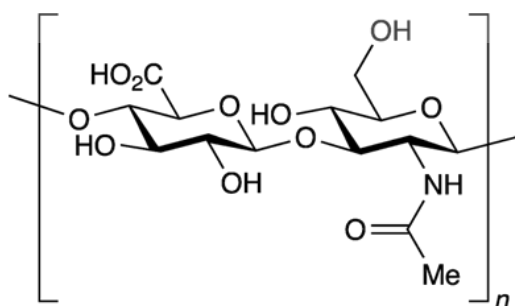


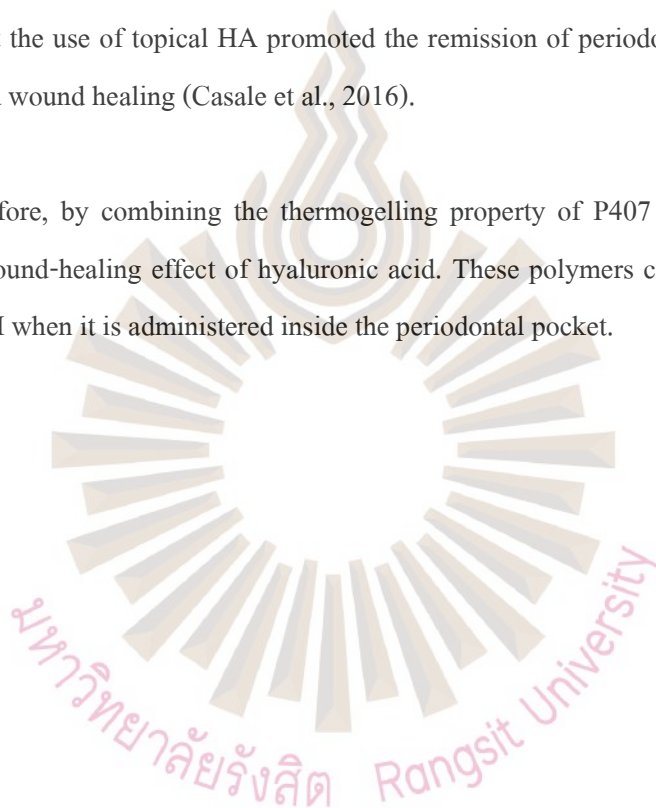
Figure 2.3 Chemical structure of hyaluronic acid

Source: Dahiya & Kamal, 2013

Apart from the versatile physicochemical property of HA, it was found that HA aids in the wound healing process. Various cell functions are related to the presence of HA such as cell adhesion, proliferation, and migration (Dahiya & Kamal, 2013).

In periodontal treatment, HA was prepared in the form of topical gel at a concentration of 0.2 and 0.8%. It was used as the adjunctive treatment with conventional periodontal treatment. Casale et al. summarized the previous clinical studies of topical HA formulation in dental treatment. They stated that the use of topical HA promoted the remission of periodontal disease in terms of tissue repair and wound healing (Casale et al., 2016).

Therefore, by combining the thermogelling property of P407 with the mucoadhesive property and wound-healing effect of hyaluronic acid. These polymers could serve as a delivery system for AZM when it is administered inside the periodontal pocket.



Chapter 3

Research Methodology

The development of the formulation for periodontal disease treatment consisted of three major sections including (1) fabrication of AZM-loaded niosomes, (2) formulation development of thermogelling AZM-loaded niosomes gel, and (3) efficacy evaluation of the thermogelling AZM-loaded niosomes gel.

3.1 Fabrication of AZM-loaded niosomes (NAZ)

3.1.1 Solubility of azithromycin dihydrate (AZM)

The exact weight of AZM dihydrate powder was dissolved in various kinds of solvents including deionized water, ethanol, and phosphate buffer pH 6.8 - 7.4 with magnetic stirring. The solubility behavior of the drug was investigated. The appearance of the obtained mixtures was visually observed for turbidity and clarity. The optimal solvent for AZM dihydrate dissolution was determined and selected for further formulation development.

3.1.2 Preparation of AZM-loaded niosomes (NAZ)

According to the findings of studies on solubility (details available in chapter 4), the formulation of AZM was decided to develop with the niosome system. The minimum inhibitory concentration of the principal periodontal pathogens was used to determine the concentration of AZM (Hirsch et al., 2012). NAZ formulations were created using a slightly modified reverse-phase evaporation process (Szoka & Papahadjopoulos, 1978). Absolute ethanol was used to dissolve the amounts of S60 and CHL in a 3:3 molar ratio (0.42 and 0.38 g, respectively, in the preparation of the 30 ml niosomal suspension), along with 1 % of AZM. The mixture was then placed in an

ultrasonic bath (POWERSONIC CP230T, Crest Ultrasonics, Ewing Township, NJ, USA) for 30 minutes. The secondary solvent, deionized water, was added and the mixture was subjected to continuous ultrasonication for a period of half an hour. After the mixture was homogenized, ethanol was removed using a rotary evaporator (N-1001, Eyela, Tokyo, Japan). To allow vesicle development until the start of the studies, the niosomal solution was maintained at 4 °C for 24 hours.

3.1.3 Determination of particle size and zeta potential

Three samples of each of the NAZ formulations were produced. The nanoparticle size and zeta potential analyzer (NanoPlus-3®, Particulate Systems, Georgia, USA) was used to measure the particle size, polydispersity index (PDI), and zeta potential of each formulation.

3.1.4 Utilization of experimental design for the determination of particle size and zeta potential

Using the design of experiment (DOE) principle, the optimal S60 and CHL concentrations in the NAZ formulations were identified. Two factors and three levels of full factorial design were utilized in this study. The S60 to CHL ratio was designated as an independent variable. The dependent variables or responses were particle size and zeta potential. Response data were analyzed by DOE software (Design-Expert® v.11.0.3, Stat-Ease, Minnesota, USA) to obtain polynomial equations and response surface plots fitted with results. The desirability optimization of the formulation was also analyzed.

3.1.5 Differential scanning calorimetry (DSC), thermogravimetric analysis (TGA)

Each sample was put into a punctured aluminum pan and heated using a nitrogen flush at a rate of 20 ml/min from 25 °C to 300 °C at a scanning rate of 10 °C per min. As a reference, a bare metal pan was used. The melting points and transition temperatures were then calculated using thermographs and a differential scanning calorimeter (DSC 8000, PerkinElmer Inc., Waltham,

Massachusetts, USA). By observing weight loss during heating, a simultaneous thermal analyzer (STA 6000, PerkinElmer Inc., Waltham, Massachusetts, USA) was utilized to identify physical changes in the materials.

The five mg of each sample in an aluminum pan that had already been weighed were analyzed using a thermal gravimetric analyzer (TGA, STA 6000, PerkinElmer Inc., Waltham, Massachusetts, USA) and a cooling device in a nitrogen bath (20 ml/min). The pan was covered with a lid, and it was heated from 25 °C to 400 °C at a steady rate of 20 °C/min.

3.1.6 Powder X-ray diffraction analysis (PXRD)

The MiniFlex II diffractometer (Rikaku, Tokyo, Japan) was used to examine the PXRD pattern, which was obtained at 30 kV and 15 mA in the 2 range. Using Cu K α radiation ($\lambda = 0.154$ nm), the temperature was raised from 5 to 45 °C at a rate of 5 °C per minute.

3.1.7 Fourier transform infrared spectroscopy (FTIR)

In order to ascertain the changes in functional groups, the dried niosome compositions were examined using Fourier transform infrared spectroscopy (FTIR). After being lyophilized and mixed with potassium bromide, niosome samples were placed under 10 tons of hydraulic pressure. The molecular fingerprint of each composition was confirmed using an FTIR spectrometer (PerkinElmer Inc., Spectrum One software, Waltham, Massachusetts, USA).

3.1.8 Confocal microscopy, scanning electron microscopy (SEM), transmission electron microscopy (TEM)

Confocal microscopy was used to analyze the prepared niosomal vesicles' morphology. Nile red was used to dye the niosomes, and a confocal laser scanning microscope was used to detect the vesicle staining (DMi8, Leica, Wetzlar, Germany). Scanning electron microscopy was utilized

in order to investigate the surface topography of the niosome (SEM, FEI Quanta FEG 450, ThermoFisher Scientific, Hillsboro, Oregon, USA). Transmission electron microscopy was used to analyze the morphology of niosomes (FE-TEM, TALOS F200, ThermoFisher Scientific, Waltham, Massachusetts, USA).

3.1.9 Entrapment efficiency of niosome

NAZ formulation was loaded in centrifugal filter units (Amicon[®] Ultra-4, Merck Millipore, Ireland) with a molecular weight cut-off (MWCO) of 3000 kDa in order to exclude unentrapped drugs. After that, the filter units underwent a 30-minute 4000 G centrifugation. Unentrapped drugs passed the filtrate through the membrane filter and were quantified using high-performance liquid chromatography (HPLC, LC-10, Shimadzu, Kyoto, Japan). The percentage of entrapped drugs was then indirectly analyzed.

3.1.10 *In vitro* drug release study

Using Franz cell apparatus and a 12 kDa MWCO dialysis membrane (Sigma-Aldrich, USA), the releasing behavior of the produced NAZ formulations was examined. The upper compartment of the Franz cell, which was positioned above the dialysis membrane, was injected with the niosomes formulation (1.5 ml). The total volume of the lower compartment was loaded with 11 ml of phosphate buffer solution, pH 6.8, which served as a release medium and established the sink condition throughout the experiment. The circulating system was maintained at 37 °C. During periodic intervals, medium samples containing releasing drugs were taken and replaced with an equivalent volume of the new medium. HPLC (LC-10, Shimadzu, Kyoto, Japan) was used to measure the amount of AZM released. The following release kinetic models were fitted to cumulative data on drug release.

$$\text{Zero-order} \quad Q_t = Q_0 - K_0 \cdot t \quad (3-1)$$

$$\text{First-order} \quad \ln Q_t = \ln Q_0 - K_1 \cdot t \quad (3-2)$$

$$\text{Higuchi} \quad Q_t = Q_0 - K_H \cdot t^{1/2} \quad (3-3)$$

$$\text{Korsmeyer–Peppas} \quad D_t/D_\infty = K_{KP} \cdot t^n \quad (3-4)$$

where Q_t is the amount of drug released at time t ; Q_0 is the initial amount of the drug in the formulation; and K_0 , K_1 , and K_H are the release rate constants of the zero-order, first-order, and Higuchi models, respectively. In Equation (3-4), D_t/D_∞ is the proportion of drug released at time t , K_{KP} is the kinetic constant, and n is the exponent of drug release.

3.1.11 Cell viability evaluation

Human gingival fibroblasts (HGF) were cultured in 96-well plates at a density of 10,000 cells/well using DMEM, 10% FBS, L-glutamine, and antibiotics. The cells were then incubated until confluence was reached. HGF were cultivated with 10 g/ml concentrations of AZM and NAZ to assess the cytotoxic activity of each formulation. The MTT assay was carried out four times. Consequently, using the absorbance values that the microplate reader measured, the percent of cell viability was determined.

3.2 Formulation of thermoresponsive AZM-loaded niosomes gel

3.2.1 Preparation of thermoresponsive AZM-loaded niosomes gel (AZG)

From niosomes filled with AZM, AZG formulations were further developed. After one percent of NAZ was prepared with S60:CHL at the ratio of 3:3, thermoresponsive niosomes gel formulations were created by adding sodium hyaluronate (HA) and mixing thoroughly with a propeller stirrer (RW 20 digital, IKA, Staufen, Germany). Following that, P407 was added to the formulations using the cold technique. The measured amount of P407 was slowly introduced to the AZM-loaded niosomes with HA pre-mix that had been maintained at 4 °C. Overnight, the AZG formulation mixes were kept at 4 °C. Until uniformed mixes were achieved, the formulations were

intermittently swirled. Prior to further testing, the produced formulations were kept in sealed containers at 4 °C.

3.2.2 Physicochemical Properties

3.2.2.1 pH determination

A digital pH meter was used to assess each formulation's pH. (Eutech pH 700, Eutech Instruments Pte Ltd, Singapore).

3.2.2.2 Drug content

In order to determine the quantity of AZM present, one gram of each formulation was weighed into a volumetric flask that had a capacity of 10 ml. Methanol was used as the extraction solvent and made up the entire volume. The mixture was left for 4 hrs. The gel formulation then turned into a clear solution after being entirely dissolved. The drug content of each formulation's extracted sample (n = 3) was quantitatively examined using HPLC techniques (Al-Rimawi & Kharoaf, 2010). The analysis was done using a C18 column (Zorbax Eclipse XDB-C18, Agilent Technologies, USA) equipped with an HPLC system (LC-10, Shimadzu, Kyoto, Japan). With regard to the parameters of 1 ml/min flow rate, 50 °C, detected with diode array at 210 nm, the mobile phase was made up of 80% MeOH and 20% 0.3 M KH_2PO_4 pH 7.56 with samples' volume of 20 μl .

3.2.2.3 Gelation temperature and gelation time

The phase transition temperature of the developed thermoresponsive formulations was used to define gelation temperature, which was assessed by a viscometer (DV-II+ viscometer, Brookfield Engineering Laboratories, Middleborough, MA, USA). The sample container was filled with the formulations, and it was enclosed with a temperature-controlled jacket. To monitor the change in viscosity, a fixed rotating speed was set. While monitoring the formulation's viscosity, the system's temperature was adjusted to elevate from 3 to 40 °C. Each

formulation's gelation temperature was determined by observing the substantial increase in viscosity at a given temperature ($n = 3$).

Gelation time was described as the amount of time required for the formulation to transition from a solution state to a gel state. The test tube inversion technique was used to measure gelation time. The formulations were placed in the thin-walled scintillation glass vials and immersed in a water bath that was kept at a regulated temperature of 37 °C. The phase change was observed visually. Each formulation's gelation time was measured by the total amount of time required for the meniscus to stop shifting when tilted ($n = 3$). The relationship of the concentration of P407 and HA to the gelation temperature and gelation time was also investigated with experimental design.

3.2.3 Mechanical properties

3.2.3.1 Viscosity

Using a viscometer (DV-II+ viscometer, Brookfield Engineering Laboratories, Middleborough, MA, USA), the viscosity of the produced formulations was assessed. A temperature-controlled jacket was attached to the sample container. The formulation was measured in its solution state at 4 °C and in its gel state at 37 °C ($n = 3$).

3.2.3.2 Rheological study

The Kinexus pro rheometer (Malvern Instruments Ltd., Worcestershire, UK) and a PL20 stainless steel parallel plate (20 mm diameter) were used to measure the rheological behavior of the AZG solution state in order to assess the liquid flow during the injection. During the measurement, the temperature was kept at 4 °C. Shear rate was varied from 0.1 to 100 s^{-1} and shear stress was considered relative to the shear rate. ($n = 3$). The acquired information was examined by rSpace Rheometry software for Kinexus version 1.75.2326, and were fitted with various rheological equations such as Newtonian (Equation 3-5), Power law (Equation 3-6), Bingham (Equation 3-7), Hershel-Bulkley (Equation 3-8), and Casson model (Equation 3-9).

$$\tau = \eta\gamma \quad (3-5)$$

$$\tau = K \cdot \gamma^n \quad (3-6)$$

$$\tau = \tau_0 + \eta_p \cdot \gamma \quad (3-7)$$

$$\tau = \tau_0 + K \cdot \gamma^n \quad (3-8)$$

$$\tau^{0.5} = \tau_0^{0.5} + K \cdot \gamma^{0.5} \quad (3-9)$$

where τ is shear stress, η is viscosity, γ is the shear rate, η_p is plastic viscosity, K is the consistency index, τ_0 is the yield value, and n is the flow index.

3.2.3.3 Injectability

The produced formulations were dispensed into 1-ml syringes using a stainless steel needle that was 22-gauge and 0.7 mm in diameter, as intended to be used in a clinical setting. The syringe was mounted using a vertical holder that was positioned at the texture analyzer's base platform (TA.XT PlusC, Stable Micro Systems, Surrey, UK). The plunger rod of the syringe was pushed downward at a speed of 10 mm/s using a cylindrical probe (Model P/0.5, 12.7 mm in diameter). An evaluation was done to determine the maximum force required to inject the solution from the barrel of the syringe through the needle tip. The measurements were obtained as soon as each formulation was withdrawn from the refrigerator, while each formulation was in the sol stage. (4 ± 5 °C).

3.2.3.4 Texture profile analysis

The texture analyzer (TA.XT PlusC, Stable Micro Systems, USA) was used to study the gel condition of the prepared formulations for texture profile properties. Each formulation was placed onto a 55 mm culture dish and allowed to form a gel state. The double compression approach was applied (Agossa et al., 2017). The texture analyzer probe was pushed downward at a speed of 2 mm/s until it made contact with the surface of the gel formulation. The probe was then operated to penetrate the gel matrix for half its height and withdrawn upward to the first contact position. The probe was maintained in this position for 15 seconds before the second compression was performed in the same way as the first. The hardness, springiness, and resilience values of each

formulation were computed using the force-time graphs provided by the texture analyzer software (n = 3).

3.2.3.5 Bioadhesive property

The attachment of the formulation to biological tissue was categorized into two in this investigation. The soft tissue adhesive strength was aimed to measure the adhesion force to the mucosal tissue, whereas the hard tissue adhesive strength is measured by the adhesion force of the formulation to the tooth-root specimen.

(1) Mucoadhesion

The mucoadhesion of each formulation was assessed using a modified mucin discs model (Agossa et al., 2017; Bassi da Silva, Ferreira, Reis, Cook, & Bruschi, 2018). The texture analyzer (TA.XT PlusC, Stable Micro Systems, Surrey, UK) was used to measure the mucoadhesive force. Mucin discs were made from 250 mg of crude mucin powder using a 13-mm diameter die and vacuum ring compression at 10 tons for 30 s. One mucin disc was affixed to the center of the 60 mm petri dish, which was held to the texture analyzer's base platform. Another mucin disc was mounted to the texture analyzer's cylindrical probe tip. For 0.1 ml, the formulation was applied between the two mucin discs. The probe was lowered until a 1 mm gap between the discs was reached. The formulation was induced into a gel state. The probe was then instructed to compress and hold for 30 s before moving upward at a rate of 10 mm/s. The mucoadhesion force of each formulation was assessed as the maximal force necessary to separate mucin discs from each other (n = 3).

(2) Tooth-root surface adhesion

With minor alterations from the previous investigation, tooth-root surface specimens were produced from extracted human teeth (Agossa et al., 2017). Flat-surface roots were equally sectioned into 6.6 x 6.6 mm specimens with a thickness of 1.5 mm using a micro motor (Saeshin Strong 90, Saeshin, Korea) and a diamond cutting disc. Three root specimens were glued on a 25 × 25 mm acrylic plate using cyanoacrylate adhesive (UHU Super Glue, UHU GmbH & Co. KG, Bühl, Germany). The acrylic plate was placed in the center of the 60 mm petri dish and

was held by the texture analyzer's base platform. Three additional root specimens were similarly prepared and mounted to a second acrylic plate that was identical to the first acrylic plate. The second acrylic plate was aligned with the texture analyzer's cylindrical probe. The formulation was applied between samples of the tooth-root surface. Similar to the mucoadhesive study, the tooth-root surface adhesive force of each formulation was assessed by the texture analyzer ($n = 3$).

3.2.4 Stability of the formulation

Temperatures of 4 °C, 25 °C, and 45 °C were used to preserve AZG formulations. Each sample's pH and drug content were measured at 7, 14, and 30 days in comparison to freshly prepared formulations in order to assess the formulation stability.

3.2.5 Model drug analysis

3.2.5.1 *In vitro* drug release and kinetic profiles

Franz diffusion cell apparatus was used to evaluate the drug release properties of the prepared formulations. The dialysis membrane with an MW cutoff of 12 kDa (Sigma-Aldrich, St. Louis, MO, USA) was used. One milliliter of each AZG formulation was pipetted precisely to the donor compartment. The dissolution medium, phosphate buffer pH 6.8, was supplied into the receptor compartment's volume (11 ml) and magnetically stirred at 300 rpm under the controlled temperature of 37 °C. At predefined time intervals, samples of the medium containing the released medication were collected and refilled with an equivalent volume of fresh media. Throughout the experiment, the sink condition was maintained. The amounts of released AZM in each sample were determined using the previously reported HPLC method. The kinetic models were used to mathematically fit the drug release characteristics as described in section 3.1.10.

3.2.5.2 *Ex vivo* drug permeation study

The Franz diffusion cell apparatus method was used to examine mucosal permeation behavior. As a permeation membrane, porcine esophageal mucosa was employed (Diaz

del Consuelo, Pizzolato, Falson, Guy, & Jacques, 2005). Fresh porcine esophagi of equivalent size and appearance were purchased from a local slaughterhouse. The esophagus was dissected to eliminate muscular portions and excised to get mucosal specimens measuring 30 x 30 mm with a thickness of 2 mm. The specimens were placed the epithelial side to the donor compartment and placed the connective tissue side to the receptor compartment. As a dissolution media, the receptor compartment was filled with phosphate buffer pH 6.8. At 37 °C, the system was constantly agitated at 300 rpm and retained in sink condition. At periodic intervals, medium samples were obtained and replenished with an exact amount of new medium. As previously stated in section 3.2.5.1, permeated drugs in the sample were measured using HPLC (n= 3).

3.2.6 Biocompatibility

3.2.6.1 Cytotoxicity of AZG

Cytotoxicity of the prepared formulations was examined. The gel stage of the formulations was extracted by immersing in the cell culture medium for 24 hrs period. Then, the medium is filtered to remove the remaining gel matrices. The extract of the formulation was prepared in various concentrations, which was used as the culture medium for human gingival fibroblast. The cell viability test with MTT assay is performed to evaluate the cytotoxicity of each concentration.

3.2.6.2 Biodegradability

To investigate the biodegradability of the formulations, the custom-made silicone specimens were prepared to simulate the periodontal pocket anatomy. Dental putty silicone material was adapted to a cylindrical mold to obtain the cylinder shape specimen. The narrow chamber size with the dimension of $2 \times 5 \times 10 \text{ mm}^3$ was created inside the silicone specimen to mimic the narrow gap of the periodontal pocket. The formulation was injected to fill up the chamber within the silicone specimens. Then, the specimens were submersed in a container filled with PBS pH 6.8, which was set on the shaking bath at 60 rpm at 37 °C temperature. The weight of the gel

matrix was measured at various time intervals. The percent weight loss of the gel was calculated, which represented the degradability of the formulation in the various predetermined period.

3.3 Efficacy evaluation of thermoresponsive AZM-loaded niosomes gel (AZG)

3.3.1 Antibacterial activity

Antibacterial assays were performed on AZG formulations with periodontal pathogens such as *Aggregatibacter actinomycetemcomitans* (*Aa.*, ATCC 43718) and *Porphyromonas gingivalis* (*Pg.*, ATCC 33277). The agar well diffusion technique was employed. In brief, the lyophilized bacterial strains were cultivated for 36 hours at 37 °C in an anaerobic jar with GasPak (Becton, Dickinson, and Company, Maryland, USA) in tryptic soy broth (TSB, Himedia Laboratories, Mumbai, India). The turbidity of organism broth suspensions was measured using the 0.5 McFarland standard. The standardized inoculum of *Aa.* and *Pg.* were swabbed on the surface of sheep blood agar (Medex Solutions Ltd., Saraburi, Thailand). Before adding 0.1 ml of formulations to the well, a sterile cork borer was used to punch an 8 mm diameter well on the inoculated agar. For the comparison, an identical concentration of AZM diluted in phosphate buffer pH 6.8 solution and soaked in a sterile-paper disc was utilized. The examined samples were incubated for 24 hours in an anaerobic incubator. The inhibitory zone on the agar surface was determined (n = 3).

3.3.2 Wound healing effects

3.3.2.1 *in vitro* scratch wound closure

In vitro scratch wound assay was used to evaluate the wound healing effect of the formulation. Human gingival fibroblasts were seeded and cultured on the culture plates until 80% confluence. A sterile pipette tip was used to create a scratch wound gap over the adherent fibroblasts. Non-adherent cells were washed with PBS. Cell migration into the scratch area was observed and recorded by an attached digital camera module of an inverted microscope. The Scratch

area was measured and analyzed by the scientific image analysis software (ImageJ, U. S. National Institutes of Health, Bethesda, Maryland, USA).

3.3.2.2 Cell proliferation

The cell proliferation effect of the formulation was evaluated with the principle of the cell viability test at two cultured periods of 48 and 72 hrs. The extract of the formulation is prepared in the same manner as the cytotoxic test and cultured with mouse macrophage cell line RAW 264.7 (TIB-71; ATCC, Manassas, VA, United States). Cell viability was conducted with WST-8 assay with Cell Counting Kit 8 (CCK8, ab228554, Abcam, Waltham, MA, USA). The living cell would reduce the water-soluble tetrazolium salt into orange formazan crystal. The optical density read by a microplate reader would quantify the number of viable cells.

3.3.3 Anti-inflammatory effects

The anti-inflammatory effects of the prepared AZG formulation were investigated by observing the inflammatory cytokine productions of the mouse macrophage cell line RAW 264.7 (TIB-71; ATCC, Manassas, VA, United States), which was stimulated into the inflammatory stage by the lipopolysaccharide (LPS) of *Aa*. The expressions of TNF- α and IL-1 β genes were investigated by real-time reverse transcriptase quantitative polymerase chain reaction (rt-qPCR) technique, while the protein secretion of TNF- α and IL-1 β was investigated by enzyme-linked immunosorbent assay (ELISA). The cells were grown in DMEM containing 10% FBS with an antibiotic-antimycotic mixture and incubated in a CO₂ incubator. The cultured macrophages were sub-cultured to a new culture dish when the cell density reached 80% confluent or every 3 days. To induce the inflammatory response of the cultured macrophage, a preliminary study was conducted to determine the suitable concentration of LPS and the stimulated duration. The results indicated that at the concentration of 10 μ g/ml of *Aa*. LPS solution, the expression of the inflammatory cytokines namely TNF- α and IL-1 β could be able to discriminate between LPS-stimulated and unstimulated groups. The stimulated duration was 3 hrs. The anti-inflammation efficacy of the AZG

formulations was evaluated by pre-incubating the macrophages with the AZG formulation extract for 1 hr before the LPS stimulation.

3.3.3.1 Real-time reverse transcriptase quantitative polymerase chain reaction (rt-qPCR)

The treated macrophages were extracted for the total RNA by RNeasy mini kit (Qiagen Inc., Valencia, CA, USA) and converted into the complementary DNA (cDNA) by Revertra ACE™ qPCR RT Mastermix kit (Toyobo Co. Ltd., Osaka, Japan) followed the instructions provided by the manufacturers. The prepared cDNA samples were kept at -20 °C. The primers of the investigated gene including TNF- α , IL-1 β , and Glyceraldehyde-3-phosphate Dehydrogenase (GAPDH) were present in Table 3.1 The prepared cDNA samples were used as the PCR template for mRNA gene expression of TNF- α , IL-1 β , and GAPDH which was used as the internal control gene. The rt-qPCR procedure was carried out on the LightCycler® 480 unit (Roche Diagnostics, Rotkreuz, Switzerland) utilizing the PCR reagents (LightCycler® 480 SYBR Green I Master, Roche Diagnostics, Rotkreuz, Switzerland). The procedure parameters were applied with pre-incubation at 95 °C for 5 mins. Then, the reactions consisted of denaturation at 95 °C for 10 s, annealing at 58 °C for 40 s, extension at 72 °C for 45 s, were operated for 40 cycles, and ending with cooling at 40 °C for 30 s. The obtained results were analyzed with the manufacturer's provided rt-PCR software (LightCycler® 480, Roche Diagnostics, Rotkreuz, Switzerland).

Table 3.1 Primers used for IL-1 β , TNF- α , and GAPDH

Gene	Sequence	Base pairs
IL-1 β	Forward primer 5' CATCTTCTCAA AATTCGAGTGACAA 3'	175
	Reverse primer 5' TGGGAGTAGACAAGGTACAACCC 3'	
TNF- α	Forward primer 5' AAGCTCTCCACCTCAATGGACAG 3'	260
	Reverse primer 5' CTCAA ACTCCACTTTGCTCTTGA 3'	
GAPDH	Forward primer 5' GAGAACTGCGCAAGTATGATGAC 3'	212
	Reverse primer 5' TAGCCGTATTCATTGTCATACCAG 3'	

3.3.3.2 Enzyme-linked immunosorbent assay (ELISA) assay

The cultured medium samples were collected to investigate the production of the inflammatory cytokines by mouse TNF- α and IL-1 β Immunoassay Quantikine™ ELISA kit (R&D Systems, Minneapolis, USA). The ELISA strip plates were prepared following the instruction of the manufacturer. To quantify the production of IL-1 β and TNF- α from the macrophages, the cultured medium was collected. The ELISA protocol was conducted following the manufacturer's instructions. The amount of secreted cytokine in each sample was calculated by the optical density (OD) and concentration plots of the cytokine standard provided in the ELISA kit.



Chapter 4

Research Results

4.1 Fabrication of azithromycin-loaded niosomes (NAZ)

4.1.1 Solubility of azithromycin dihydrate (AZM)

The solubility of AZM was evaluated by dissolving AZM in various kinds of solvent at a 1% w/v concentration as intended to use in the formulation. The results indicated that AZM was able to dissolve in phosphate buffer at pH 6.8, ethanol, and methanol. AZM was unable to dissolve in water. For thermogelling formulation development, poloxamer 407 (P407) was chosen as a gelling agent. However, the micellization of P407 was disturbed by the addition of salt in the formulation (Fakhari, Corcoran, & Schwarz, 2017). During the preliminary formulation preparation, it was discovered that the formulation was unable to form a gel state with the presence of salts. Therefore, in this study, the formulation of AZM was developed by utilizing the vesicular system of the niosome.

4.1.2 Preparation of azithromycin-loaded niosomes (NAZ)

In this study, niosome was prepared by reverse phase evaporation described by Szoka and Papahadjopoulos (Szoka & Papahadjopoulos, 1978). The organic phase was prepared by the addition of S60 and CHL to ethanol. The aqueous phase was prepared by first dispersing AZM in ethanol and mixed with deionized water. The two solutions were mixed in a round bottom flask and ultrasonicated for 30 mins, the milky-white emulsion was obtained. Then, ethanol in the mixture was removed by a rotary evaporator. This procedure was modified by prolonging evaporation time during the ethanol removal process. The preliminary works indicated that the evaporation time should be in the range of 30 to 45 mins, which could achieve by reducing the vacuum pressure of a

rotary evaporator. It was observed in preliminary formulation preparation that the niosome obtained with prolonged evaporation time appeared in smaller vesicle sizes without precipitation. The appearance of niosome suspension was in a homogeneous-white-milky suspension due to the incorporation of S60 and CHL in the composition. The reproducibility and simplicity of this preparation procedure were its benefits. The niosome suspension can be easily made using basic laboratory instruments such as an ultrasonic bath and a rotary evaporator. Niosome formulations were prepared for further testing by altering the composition ratio of S60 and CHL, as shown in Table 4.1.

4.1.3 Determination of particle size and zeta potential

Table 4.1 shows that the particle sizes of the prepared niosomes ranged from 241.1 to 803.6 nm, and exhibited PDI values less than 0.4. According to the inclusion of CHL, the zeta potential of all formulations was negative. It was discovered that the concentration of surfactant and CHL influenced the properties of niosomes. It was revealed that increasing the concentration of S60 in a composition decreased the particle size, whereas increasing the concentration of CHL tended to increase the particle size of niosomes. The group of formulations with a high ratio of S60 content (NAZ7, 8, 9) showed decreased particle sizes (241.1 to 319 nm). This tendency was also expressed in a group of blank niosomes (Figure 4.1a, b).

In this study, the correlation between particle size and PDI was observed (Figure 4.1a). The PDI of formulations with bigger particle sizes (NAZ3, 6) was greater. Relative to particle size, a rise in CHL concentration led to an increase in PDI value. When the S60 amount ascended until the ratio of S60 to CHL was equivalent, the PDI value decreased to approximately 0.2. (NAZ1, 5, 9). The influence of the ratio of S60 and CHL was also manifested in the group of blank niosomes (Figure 4.1b)

Table 4.1 Composition of azithromycin-loaded niosomes (NAZ), particle size, polydispersity index (PDI), zeta potential and entrapment efficiency (EE) of NAZ formulations. Data are reported in mean \pm S.D.

Formulation code	AZM (%)	S60:CHL (molar ratio)	Particle size (nm)	PDI	Zeta potential (mV)	EE (%)
NAZ1	1	1:1	310.2 \pm 5.4	0.198	-27.14 \pm 0.64	92.24 \pm 0.027
NAZ2	1	1:2	472.9 \pm 3.0	0.273	-33.67 \pm 0.97	93.79 \pm 0.016
NAZ3	1	1:3	803.6 \pm 51.6	0.398	-37.99 \pm 0.89	94.20 \pm 0.001
NAZ4	1	2:1	286.7 \pm 13.9	0.285	-38.51 \pm 0.26	94.72 \pm 0.002
NAZ5	1	2:2	335.9 \pm 3.3	0.282	-38.93 \pm 0.45	92.70 \pm 0.015
NAZ6	1	2:3	606.0 \pm 35.9	0.346	-44.34 \pm 1.60	94.47 \pm 0.002
NAZ7	1	3:1	314.1 \pm 1.3	0.271	-30.42 \pm 1.00	95.51 \pm 0.002
NAZ8	1	3:2	241.1 \pm 7.1	0.273	-34.69 \pm 0.88	94.54 \pm 0.001
NAZ9	1	3:3	319.0 \pm 3.3	0.293	-39.57 \pm 0.49	94.21 \pm 0.001

The zeta potential of synthesized niosomes ranged from -27.14 to -44.34 mV as displayed in Table 4.1. The higher the concentration of CHL, the greater the zeta potential with negative charge. Regardless of particle size, the produced niosomes had a higher zeta potential based on the higher concentration of CHL (Figure 4.2a). The zeta charge of NAZ2 to NAZ9 was sufficient to inhibit the aggregation of niosomal vesicles, confirming colloidal stability (Jiang, Oberdörster, & Biswas, 2009). This occurrence was also found in the blank niosome group (Figure 4.2a). However, blank niosomes apparently possessed higher stability since the absolute zeta value was higher.

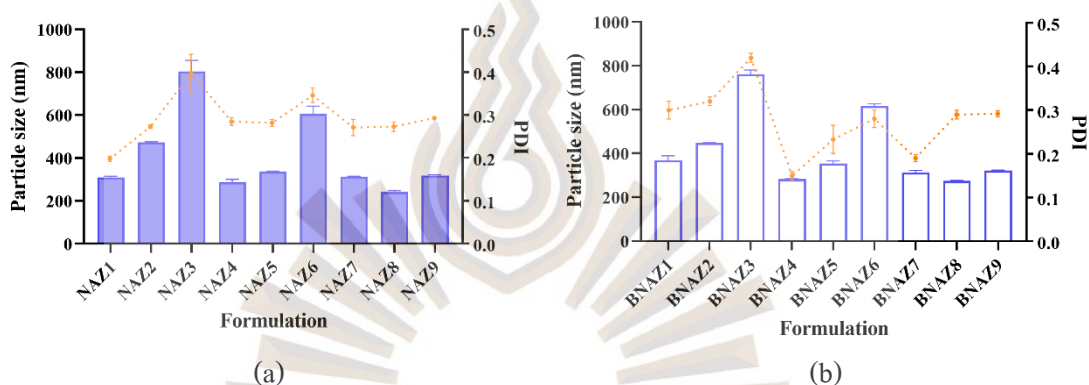


Figure 4.1 Niosomes particle size of AZM-loaded niosomes (a), blank niosomes (b) related to polydispersity index. PDI is displayed as an orange line graph with a scale on the right Y-axis. Data are presented in mean value, error bars signify S.D.

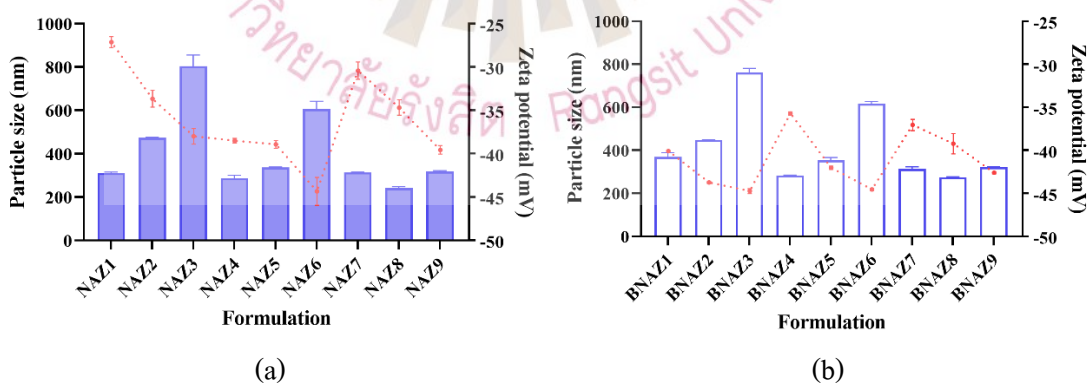


Figure 4.2 Niosomes particle size of AZM-loaded niosomes (a), blank niosomes (b) related to the zeta potential. Zeta potential is displayed as a red line graph with a scale on the right Y-axis.

Data are presented in mean value, error bars signify S.D.

Nonetheless, NAZ1 had a lesser particle charge stability (-27.14 mV). This may be due to the low concentration of surfactant and CHL, which was significantly lower than the concentration of AZM. The forming niosomes may not adequately entrap AZM in the composition; hence, the remaining drugs may disperse throughout the formulation, causing aggregation and instability of the formulation.

4.1.4 Utilization of experimental design for the determination of particle size and zeta potential

Two factors and three levels of the full factorial design were employed. The concentration of S60 and CHL were defined as the independent variables A and B, respectively. Particle size (Y_1) and zeta potential (Y_2) were the responses of this study. To evaluate the main, quadratic effects and interactions of the independent variables, the ratio of variables A and B was varied to three levels as listed in Table 4.2.

Table 4.2 Experimental design layout for NAZ formulation optimization.

Run	S60:CHL (molar ratio)	S60 (A)	CHL (B)
1	1:1	-1	-1
2	1:2	-1	0
3	1:3	-1	1
4	2:1	0	-1
5	2:2	0	0
6	2:3	0	1
7	3:1	1	-1
8	3:2	1	0
9	3:3	1	1
10	2:2	0	0

The analytical results indicated that response data of particle size (Y_1), and zeta potential (Y_2) significantly fit with quadratic models ($P < 0.01$, $P < 0.05$ respectively). The models were presented as the following equations.

$$Y_1 = 349.56 - 118.75A + 136.27B - 122.13AB + 0.6167A^2 + 89.97B^2 \quad (4-1)$$

$$Y_2 = -40.22 - 0.98A - 4.30B + 0.43AB + 6.68A^2 - 0.57B^2 \quad (4-2)$$

The model equation of particle size (Equation 4-1) expressed the correlation coefficient (r^2) at 0.9924. Each independent variable was analyzed by ANOVA for the quadratic model. From the equation, S60 (A) showed a significant reverse relationship to response Y_1 ($P < 0.05$) while CHL (B) exhibited a direct relationship to Y_1 ($P < 0.05$) as presented in the 3D response surface plot Figure 4.3(a). The interaction of S60 and CHL (AB) had a negative effect on response Y_1 significantly ($P < 0.05$). The quadratic model of zeta potential (Equation 4-2) was derived with r^2 equal to 0.9532. Each variable was analyzed for the effect on the zeta potential response (Y_2). It revealed that the increase of the S60 (A) value produced a quadratic effect on response Y_2 significantly ($P < 0.05$). Conversely, CHL (B_2) caused a significant inverse relationship to zeta potential ($P < 0.05$). The 3D surface plot of Equation 4.2 is shown in Figure 4.3(b).

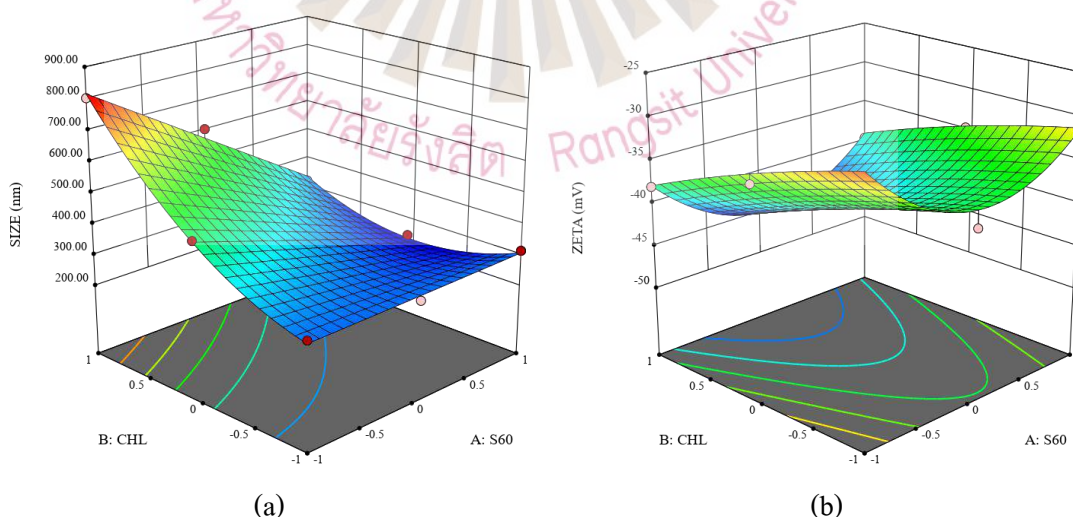


Figure 4.3 Response surface plot indicating the effect of variables A (S60) and B (CHL) on the responses: particle size (a) and zeta potential (b).

To acquire the optimal characteristics of the formulation, the contour plot of each response: particle size, and zeta potential as present in Figure 4.4(a) and Figure 4.4(b), respectively, were superimposed.

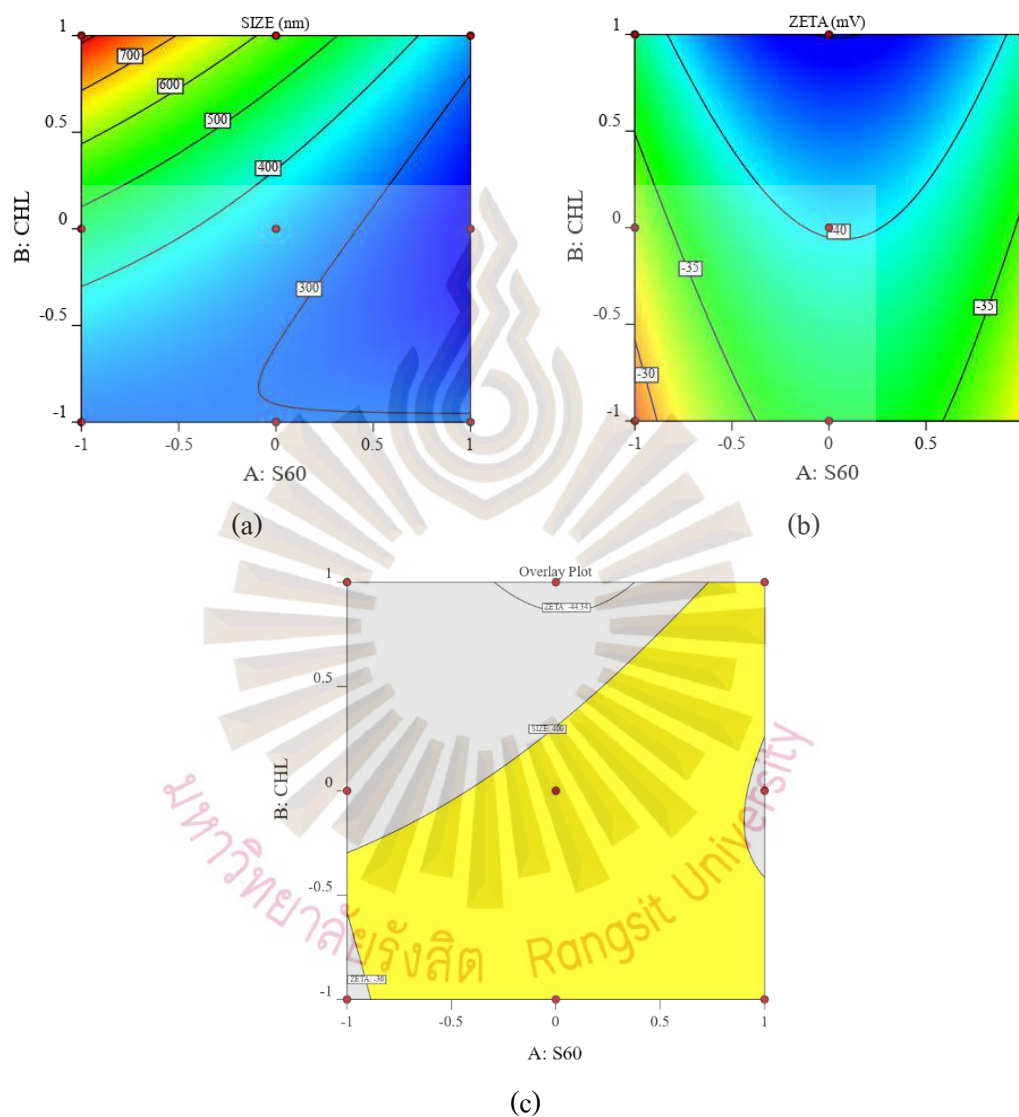


Figure 4.4 Contour plot of the responses: particle size (a), zeta potential (b), and the superimposed contour plots of both responses (c).

The optimal range of particle size was set to the range of 241.1 to 400 nm to achieve nanosized particles, while zeta potential was set at -44.34 to -30 mV for colloidal stability. The overlay plot was acquired as shown in Figure 4.4(c). The yellow plotting area indicated the optimal

values of both independent variables. Considering the prepared formulation, NAZ5 (0, 0), NAZ7 (1, -1), and NAZ9 (1, 1) matched the desired criteria, which were in nanosized particles (241.1 – 400 nm) and stable in charge since zeta potential was less than -30 mV (Jiang et al., 2009). The utilization of the experimental design indicated that the equal S60, CHL concentration ratio produced the nanosized, charged-stable niosome (NAZ5, 9). However, NAZ7 also occupied optimal particle size but its zeta potential was too close to the acceptable baseline (-30.42 ± 1.00 mV).

4.1.5 Differential scanning calorimetry (DSC), thermogravimetric analysis (TGA)

The interactions of CHL, surfactants, and AZM were investigated utilizing DSC presented in Figure 4.5.

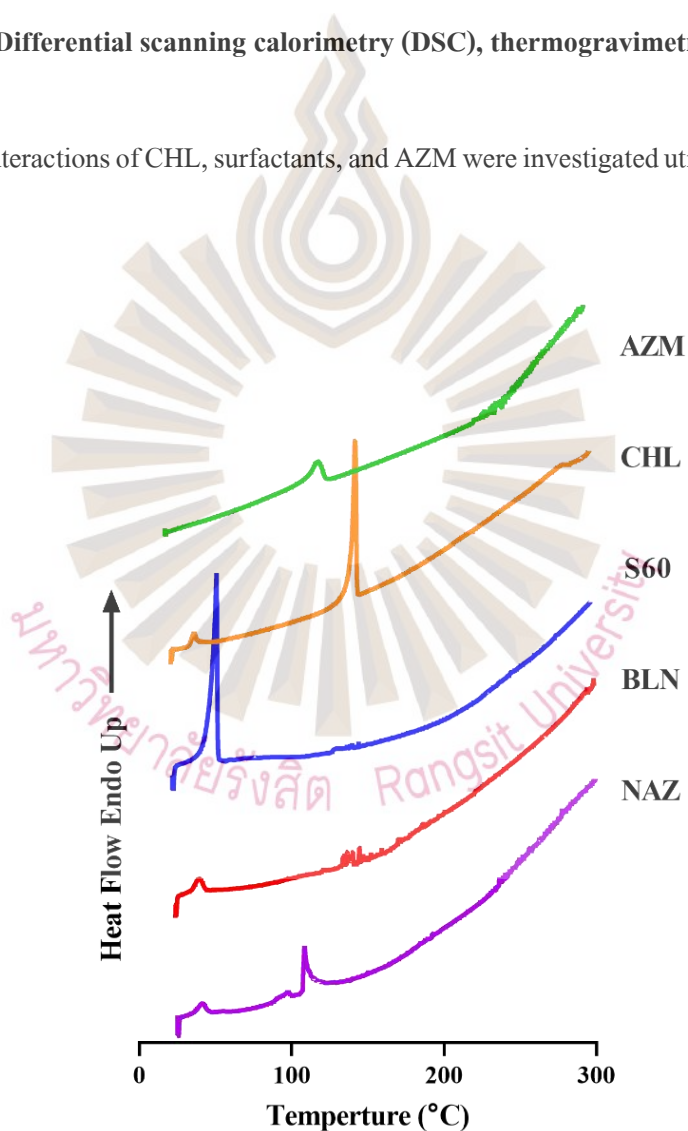


Figure 4.5 DSC thermograms of span 60 (S60), cholesterol (CHL), blank niosome (BLN), azithromycin (AZM), and azithromycin-loaded niosome (NAZ).

DSC thermograms revealed the endothermic peak of niosome component S60 and CHL at 54.1 and 146.2 °C, respectively. After blank niosome (BLN) forming, at the equal concentration ratio of surfactant and CHL, the endothermic peak markedly reduced to the group of flat peaks between 136.2 to 146.0 °C. This may cause by the influence of adding CHL, which was found to decrease the melting temperature of self-assembly niosomal structure (Abdelkader, Ismail, Kamal, & Alany, 2010). AZM exhibited an endothermic peak at 126.1°C. After being entrapped into the niosome, AZM-loaded niosome (NAZ) showed a slight reduction in melting temperature to 108.7 °C. However, the endothermic peak of NAZ was apparently higher than pure AZM. This may be because higher energy was needed to break the hydrophobic interaction of S60 and CHL after AZM entrapment.

A TGA graph of niosome composition is shown in Figure 4.6. TGA thermogram of S60 indicated an initial weight loss at 160.8 °C, while CHL started losing its weight at 245.9 °C. After assembling into the blank niosome, the initial weight loss became 236.1°C. Pure AZM exhibited initial weight loss at 131.2 °C but after being entrapped in the niosome vesicle, initial weight loss was increased to 232.5 °C.

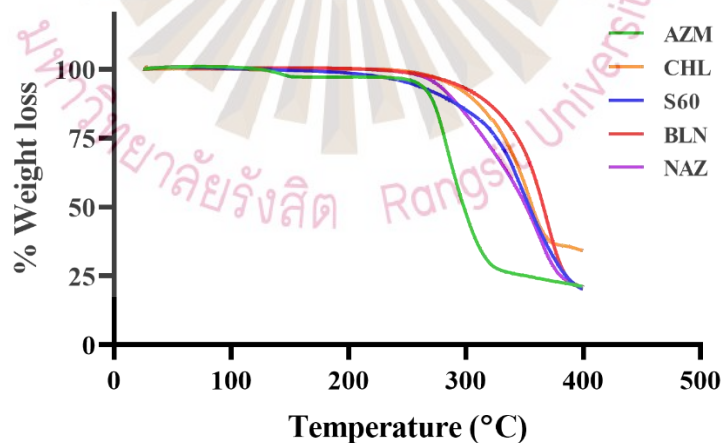


Figure 4.6 TGA investigation presenting the percentage of weight loss of span 60 (S60), cholesterol (CHL), blank niosome (BLN), azithromycin (AZM), and azithromycin-loaded niosome (NAZ).

When considered at 25% of weight loss, it was found that all pure excipients were sharply decreasing in weight. The forming of the niosome was found to increase thermal stability. Blank niosome tolerated the applied heat to the highest temperature of 344.3 °C more than S60 and CHL alone (326.0 and 332.9 °C, respectively). In the same way, NAZ increased the thermal stability of pure AZM from 281.8 to 315.4 °C.

4.1.6 Powder X-ray diffraction analysis (PXRD)

PXRD analysis was utilized to investigate the crystalline state of AZM after entrapping into the niosome vesicle. The diffraction pattern of all compositions is presented in Figure 4.7.

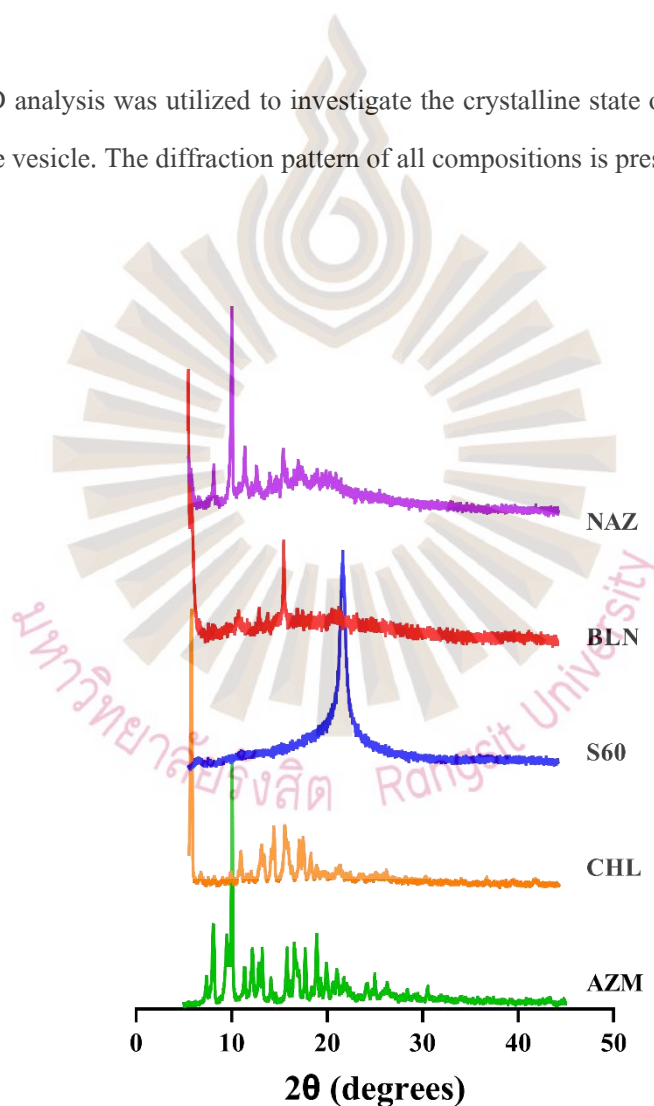


Figure 4.7 PXRD analysis of span 60 (S60), cholesterol (CHL), blank niosome (BLN), azithromycin (AZM), and azithromycin-loaded niosome (NAZ).

Prominent characteristic peaks of drug crystallization were observed at 8 and 10 (2θ). After incorporating AZM into the niosome, the characteristic peaks were also existing in the diffraction pattern of NAZ. This suggested the presence of AZM in crystalline form within the niosomal solution.

4.1.7 Fourier transform infrared spectroscopy (FTIR)

The compatibility of pure AZM and excipients accompanied with AZM-loaded niosomes and blank niosomes formulation was examined by FTIR spectra. Figure 4.8 presents the characteristic spectrum of each composition.

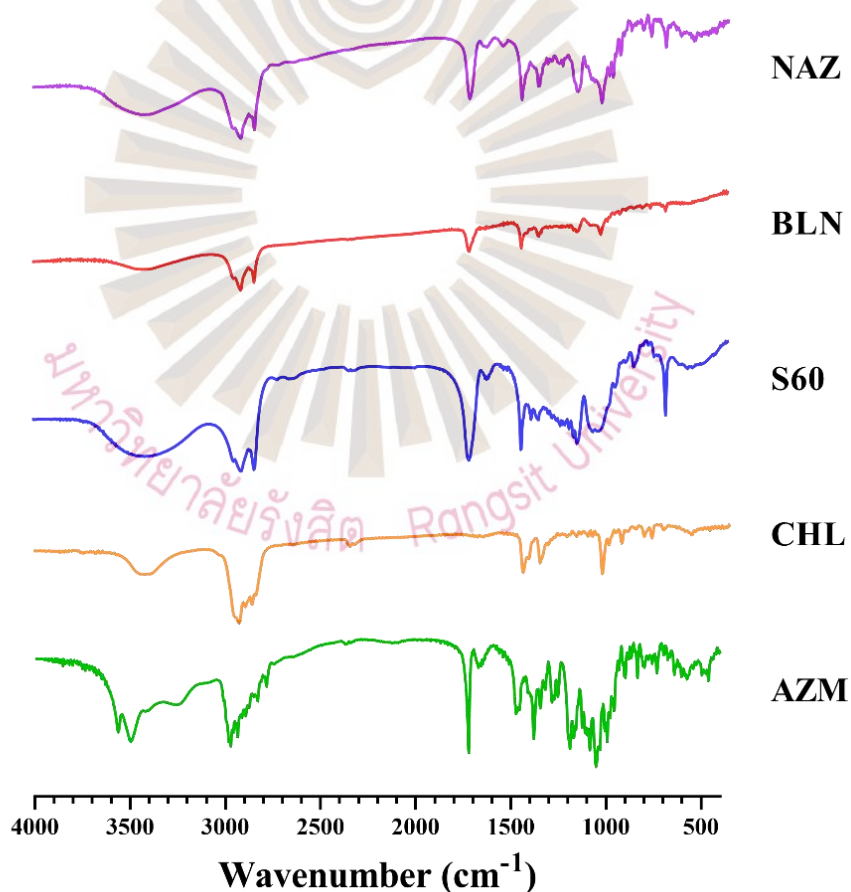


Figure 4.8 FTIR spectra of span 60 (S60), cholesterol (CHL), blank niosome (BLN), azithromycin (AZM), and azithromycin-loaded niosome (NAZ).

The spectrum of AZM revealed that the peak at 3501 cm^{-1} , which is the $-\text{OH}$ functional group. After preparing into niosomes, this peak apparently broadened due to the moisture in the formulation. The presence of water molecules interacting with AZM structure. Apart from that, the peak at 2975 cm^{-1} of AZM was found in NAZ, and the peak between $2800 - 3200\text{ cm}^{-1}$ wavenumber was reported to be the $-\text{CH}_3$ functional group. The peak at 1725 cm^{-1} of AZM was presented in NAZ, the peak ranged from $1705 - 1727\text{ cm}^{-1}$ wavenumber was reported to be the $-\text{C}=\text{O}$ functional group. The peak at 1205 cm^{-1} of AZM existed in NAZ, and the peak in the range of $1000 - 1300\text{ cm}^{-1}$ wavenumber was the $\text{R}-\text{O}-\text{R}$ functional group. Lastly, the peak at 1090 cm^{-1} of AZM was disclosed in NAZ, and the peak within $1000 - 1300\text{ cm}^{-1}$ wavenumber was recognized as $\text{C}-\text{N}$ functional group. Therefore, these characteristic peaks of raw AZM remained intact after being incorporated into niosomes, indicating that there were no major interactions between the compositions, which affected the integrity of the AZM structure.

4.1.8 Confocal microscopy, Scanning electron microscopy (SEM), Transmission electron microscopy (TEM)

Figure 4.9 demonstrates the use of confocal laser scanning microscopy to visualize produced AZM-loaded niosomes dyed with Nile red dye. The lipid droplet emerged as a red-stained vesicle composed of a double layer of S60, which was stabilized by CHL (Moghassemi & Hadjizadeh, 2014).

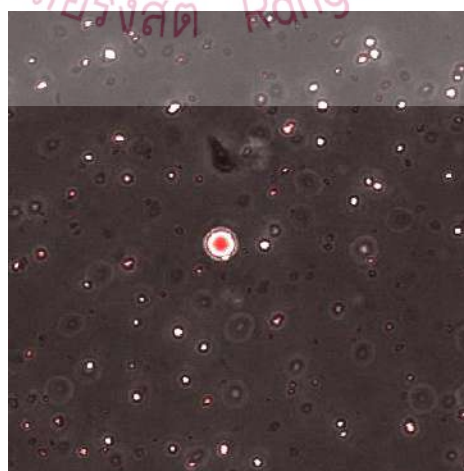


Figure 4.9 Confocal laser scanning microscopy of AZM-loaded niosome.

SEM investigation at different magnifications revealed the niosomal vesicle in the spherical morphology Figure 4.10. TEM image of the NAZ sample showed the well-defined spherical shape of the niosome in the diameter of 300 ± 50 nm (Figure 4.11).

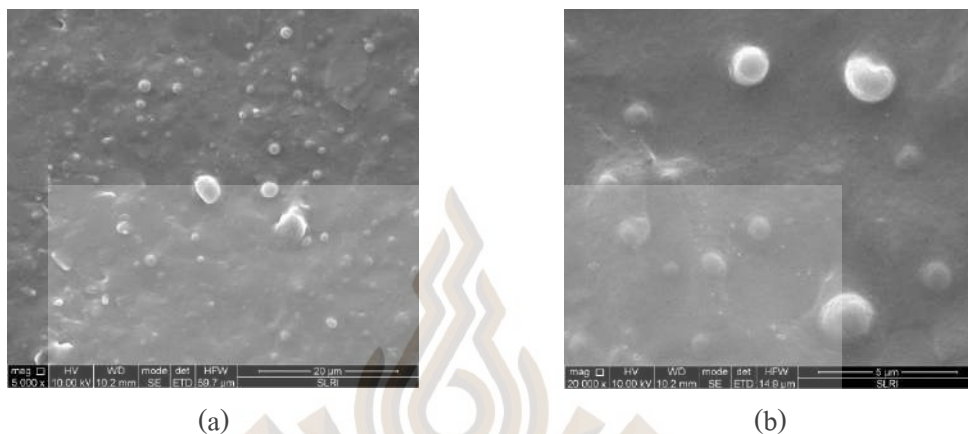


Figure 4.10 SEM image of AZM-loaded niosome at 5000x (a) and 20000x magnification (b).



Figure 4.11 TEM image of AZM-loaded niosome.

According to the findings of morphological studies, it can be hypothesized that the prepared AZM-loaded niosome should consist of double layers of S60, AZM was retained by the hydrophobic tails of S60 despite its low water solubility. (Moghassemi & Hadjizadeh, 2014).

4.1.9 Entrapment efficiency of niosomes

In this analysis, the entrapment efficiency of all niosomal formulations was achieved within the range of 92.24 to 95.51 percent (Table 4.1). However, formulations with low S60 and CHL concentrations relative to the number of drugs (NAZ1, 2) had a lower percent EE value. This was attributed to the reason that there were insufficient quantities of developing niosomes to entrap the amount of AZM in the formulation.

4.1.10 *In vitro* drug release study

In order to imitate the inflammatory state of the periodontal pocket, NAZ formulations were tested for their releasing qualities in PBS with a pH of 6.8. (Watanabe, Soeda, Kobayashi, & Nagao, 1996). The cumulative AZM releases in 8 hours varied from 39.61 to 50.37 percent, as shown by the graph depicting cumulative release (Figure 4.12).

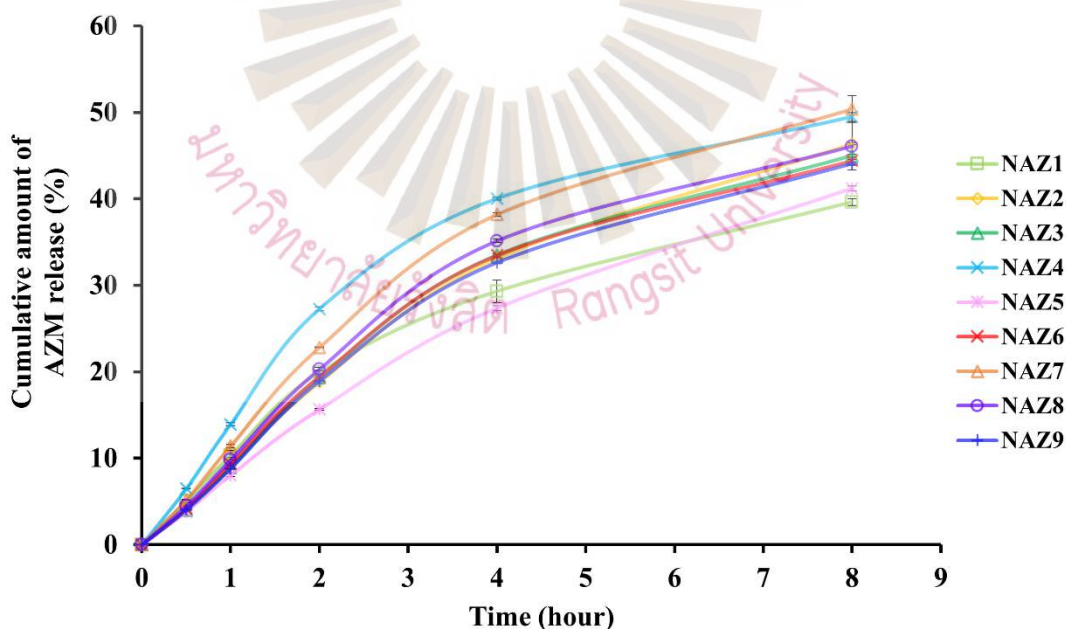


Figure 4.12 *In vitro* percent cumulative release of azithromycin-loaded niosomes (NAZ). The line plots are displayed using the mean, with error bars reflecting S.D.

After thirty minutes, it was discovered that around five percent of the medication included in the formulation had been released. This concentration achieved a level that is more than the minimum inhibitory concentration (MIC) for key periodontal pathogens. (Lai, Ho, Jain, & Walters, 2011). Additionally, the release of AZM was kept going for a total of 8 hrs. This demonstrated that the niosomes that were produced had a controlled-release function (Limsitthichaikoon, Priprem, & Damrongrungruang, 2020). When compared to the bigger particle size, it was discovered that the NAZ 4, 7, 8, and 9 formulations that produced smaller particle sizes (286.7 – 319 nm) tended to display a greater drug release rate. In this particular experiment, a membrane with an MWCO of 12 kDa was adopted, and it was capable of allowing the passage of both free and entrapped AZM. This may suggest that free AZM and NAZ would release to the target location, which is the periodontal pocket, in clinical conditions. When the high entrapment efficiency of this formulation is taken into consideration, the quantity of NAZ that is released from the formulation may facilitate for AZM to penetrate the connective tissue of the periodontium through the advantages of niosomes.

Niosomes that had been prepared were evaluated for their release processes by fitting them with a series of kinetic models. The zero-order release patterns were the most appropriate to correlate with any and all formulations (Table 4.3), which indicated no correlation between AZM release and its concentration. Additionally, the release data was quite similar to the Higuchi model. This revealed that the synthesized niosomes may operate as matrices and regulate the release of AZM that had been entrapped. (Dash, Murthy, Nath, & Chowdhury, 2010).

Table 4.3 Kinetic models fitting of AZG formulations.

Formulation	Kinetic model								
	Zero-order		First-order		Higuchi		Korsmeyer-Peppas		
	K_0	r^2	K_1	r^2	K_H	r^2	K_{KP}	n	r^2
NAZ1	7.3005	0.9635	0.3107	0.7187	15.309	0.9552	10.748	0.741	0.7891
NAZ2	8.3602	0.9946	0.3348	0.7905	16.918	0.9182	9.385	0.917	0.8261
NAZ3	8.4918	0.9930	0.3379	0.7942	17.176	0.9158	9.456	0.922	0.8307
NAZ4	10.0200	0.9633	0.3339	0.6933	20.969	0.9511	14.472	0.753	0.7969
NAZ5	6.8394	0.9938	0.3156	0.7921	13.925	0.9288	8.143	0.880	0.8132
NAZ6	8.4506	0.9923	0.3349	0.7834	17.154	0.9218	9.722	0.901	0.8262
NAZ7	9.5957	0.9889	0.3391	0.7489	19.617	0.9318	11.728	0.861	0.8185
NAZ8	8.8591	0.9931	0.3371	0.7766	17.979	0.9221	10.195	0.901	0.8239
NAZ9	8.2569	0.9927	0.3343	0.7971	16.729	0.9186	9.344	0.911	0.8276

K_0 , K_1 , K_H , K_{KP} are equation parameters of zero-order, first-order, Higuchi, Korsmeyer-Peppas, respectively. The n values are release exponents of Korsmeyer-Peppas equation.

4.1.11 Cell viability evaluation

The cell viability of AZM niosomes and AZM solution was tested using the human gingival fibroblast (HGF) culture. MTT test was utilized to measure cell viability. Niosomes and AZM solution demonstrated dose-dependent cytotoxicity at a given concentration. According to the results of a preliminary investigation, the appropriate concentration of AZM on cultured HGF was 10 µg/ml. Furthermore, the effective dosage against periodontal bacteria did not exceed 10 µg/ml. (Lai et al., 2011). Consequently, this concentration was used to determine the cell viability of AZM-loaded niosomes (NAZ) and blank niosomes (BNAZ) as presented in Figure 4.13a, b. There were substantial discrepancies between the prepared niosomal formulation and the negative control. Niosomes were shown to produce negative impacts on the viability of HGF when compared to the negative control in the experiment. Except for NAZ6 and 9, which were shown to demonstrate higher cell viability comparable to the negative control. Blank niosome formulations also presented cytotoxic effects in the same manner as NAZ.

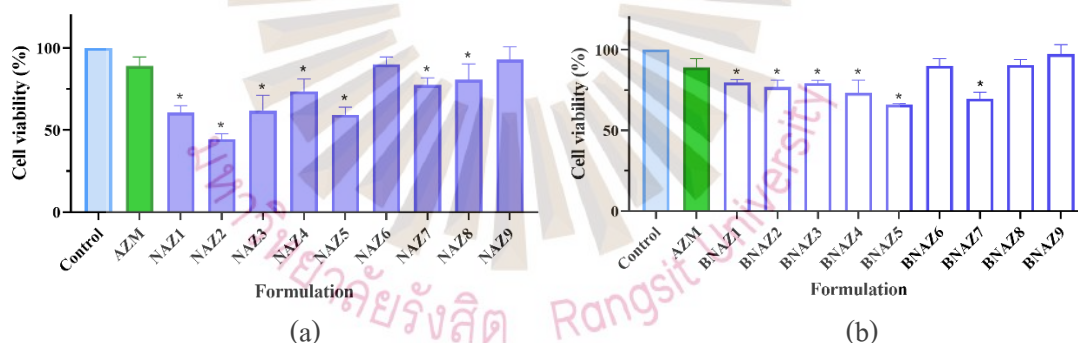


Figure 4.13 Cell viability of HGF cultured with AZM-loaded niosomes (NAZ) formulations (a), blank niosome (b), azithromycin solution (AZM) compared to the culture medium (Control), which served as a negative control. Statistical analysis was performed with ANOVA and Dunnett's multiple comparisons test. Asterisks indicating statistically significant differences compared to Control ($P < 0.01$)

When the cell viability pattern of both NAZ and BNAZ was considered, it was found that BNAZ1, 2, 3, and 8 had higher cell viability than the same formulation of NAZ. The zeta potential

could be the factor because the zeta potential of the particular formulations of the blank niosome was higher in negative charge (Figure 4.2a, b). This finding was in agreement with the other study, which stated that those nanoparticles that exerted positive or stronger similar charges caused more toxicity due to stronger interactions with the cell membrane and were detrimental to the biological activity of the cells (Shao et al., 2015). Therefore, NAZ6, 9, were the most compatible charged with the cultured cell and had high cell viability equivalent to the negative control.

4.2 Formulation of thermoresponsive AZM-loaded niosomes gel (AZG)

4.2.1 Preparation of thermoresponsive niosomes gel

AZM is a promising medication for the treatment of periodontitis (Hirsch et al., 2012). However, AZM is classed as a BCS class II drug due to its limited solubility in water. This may alter the bioavailability of AZM in periodontal tissue for the local delivery formulation. Consequently, the establishment of an appropriate delivery system is essential. During the course of this inquiry, a niosome system was utilized in order to construct a carrier that is effective for AZM delivery. In application, the niosomal vesicle system improves the formulation's stability, as well as the solubility of hydrophobic pharmaceuticals and the enhancement of drug penetration. (Damrongrungruang et al., 2021; Moghassemi & Hadjizadeh, 2014). After the AZM was properly entrapped in the niosome, AZM-loaded niosomes were further synthesized into a thermoresponsive gel for the purpose of intra-periodontal pocket delivery in clinical settings. This was accomplished so that the AZM could be administered directly into the periodontal pocket for clinical intervention in periodontitis treatment.

Thermoresponsive AZM-loaded niosomes gel (AZG) was synthesized into nine distinct formulations so that the physical interactions of P407 and HA with the niosomal formulation could be studied. The concentrations of P407 (17 to 19 percent w/v) and HA (0.2 to 2 percent w/v) were varied to create these formulations (Table 4.4). Due to the appearance of the niosomal suspension made from CHL and S60, the created formulations displayed as a homogeneous, creamy, white,

opaque solution. All formulations maintained homogeneous mixes independent of the P407 and HA concentrations. In dentistry, injectable gel formulations are often utilized for a variety of dental materials. Dentists are knowledgeable about this dosage kind. Thus, the injectable gel should be administered to the patient's periodontal pocket with no effort. Furthermore, in the treatment of chronic conditions like periodontitis, which are caused by bacterial infections, the formulation development process should prioritize prolonged drug retention and sustained drug release in the target region to completely eradicate pathogenic bacteria. The formulation, which is capable of transforming into a semi-solid state, may be useful for this application because it can withstand temporal variations in the oral environment. Consequently, P407, which has phase change characteristics, was selected. The formulation's adherence to biological tissues is an additional significant factor that may contribute to retention time. (Jung, Park, W., Park, H., Lee, & Na, 2017).

HA has beneficial mucoadhesive characteristics, in addition to other positive features, such as anti-inflammatory and enhanced wound healing effects, that are useful in the treatment of periodontal disease. (Dahiya & Kamal, 2013). As a direct result of this, HA was incorporated into the creation of the formulation. In addition, the periodontal formulation needs to be biocompatible with the environment of the periodontal pocket. P407 is used in a broad range of pharmaceutical formulations, including periodontal formulations, due to the fact that it is considered by the FDA to be an inactive component as its safe and biocompatible (Carvalho, Bruschi, Evangelista, & Gremião, 2010; Dumortier et al., 2006). The low cytotoxicity and biodegradability of hydrogels made from poloxamer have been demonstrated and documented (G. C. Carvalho et al., 2021). HA is a naturally produced biopolymer that is synthesized in the plasma membrane by the enzyme hyaluronan synthase. It is commonly found in the extracellular matrix of human epithelial tissues as well as connective tissues. Consequently, because it is a glycosaminoglycan, HA possesses exceptional biocompatibility and does not induce an immune response. In addition, HA may be easily broken down by hyaluronidase and other oxidative species that are present in the human body (Liao et al., 2005).

Table 4.4 Composition of thermoresponsive azithromycin-loaded niosomes gel (AZG) and physicochemical properties of AZG includes pH, drug content, gelation temperature and gelation time (mean \pm SD, n = 3).

Formulation code	Niosomes of AZM		Thermoresponsive gel compositions		Physicochemical properties			
	AZM (%w/v)	S60:CHL (Molar ratio)	P407 (% w/v)	HA (% w/v)	pH	Drug content (%)	Gelation temperature ($^{\circ}$ C)	Gelation time (s)
AZG1	1	3:3	17	0.2	6.91 \pm 0.02	93.86 \pm 0.81	40.33 \pm 0.06	227.00 \pm 3.61
AZG2	1	3:3	17	1.1	6.90 \pm 0.03	94.02 \pm 1.28	36.60 \pm 0.10	171.67 \pm 3.51
AZG3	1	3:3	17	2.0	6.92 \pm 0.04	93.90 \pm 1.18	36.23 \pm 0.15	87.33 \pm 3.06
AZG4	1	3:3	18	0.2	6.89 \pm 0.01	94.38 \pm 0.56	34.20 \pm 0.10	200.67 \pm 3.05
AZG5	1	3:3	18	1.1	6.89 \pm 0.01	93.87 \pm 1.23	32.43 \pm 0.38	125.33 \pm 2.52
AZG6	1	3:3	18	2.0	6.90 \pm 0.01	94.49 \pm 0.81	33.10 \pm 0.10	85.00 \pm 4.58
AZG7	1	3:3	19	0.2	6.90 \pm 0.02	93.09 \pm 0.94	32.67 \pm 0.15	173.33 \pm 3.06
AZG8	1	3:3	19	1.1	6.90 \pm 0.02	93.37 \pm 0.92	29.60 \pm 0.20	107.00 \pm 3.00
AZG9	1	3:3	19	2.0	6.92 \pm 0.01	93.64 \pm 1.37	27.83 \pm 0.55	68.00 \pm 2.00

4.2.2 Physicochemical properties

4.2.2.1 pH determination

All of the completed formulations had a pH that ranged from 6.89 ± 0.01 to 6.92 ± 0.04 according to the measurements (Table 4.4). When compared to the pH of the prepared AZM-loaded niosomes, which was 7.04 ± 0.06 , the pH of the AZG formulation was found to be rather lower. The pH of the periodontal pocket may fall below the mean value of 6.92 ± 0.03 if periodontitis is present, which was the value at which it was normally measured (Eggert, Drewell, Bigelow, Speck, & Goldner, 1991). Because of this, the finished formulations should be compatible with the environment of the periodontal pocket while also being able to avoid disturbing the patient's biological tissues.

4.2.2.2 Drug content

According to the data on drug content, the amount of loaded AZM was found to range from 93.09 ± 0.94 to 94.49 ± 0.81 (Table 4.4), which was in the adequate range. The amount of AZM loaded in AZG was dependent on the entrapment efficiency of the AZM-loaded niosomes that were produced.

4.2.2.3 Gelation temperature and gelation time

The inclusion of P407 enabled AZG to transform from a solution to a gel following injection into a periodontal pocket. The phase transition of the formulations was assessed based on gelation temperature and gelation time (Table 4.4). The temperature at which gelation occurred ranged from 27.83 ± 0.5 to 40.33 ± 0.06 °C on average. The effects of P407 were found in the formulation groups that included an equivalent quantity of HA. The gelation temperature significantly dropped by a substantial amount as a direct result of the gradual increase in P407 concentrations ($P < 0.01$). P407 is a triblock co-polymer made up of double hydrophilic polyethylene oxide (PEO) and a single hydrophobic poly-propylene oxide (PPO) molecule in between. During rising temperatures, PPO groups engage with each other via van der Waals forces to produce the hydrophobic cores of micelles, whereas PEO groups form the hydrophilic shell of

micelles via hydrogen bonds to the water molecule in the system (Dumortier et al., 2006). As the temperature rises higher, micelles assemble at a specific temperature and organize themselves into three-dimensional cubic shapes in order to accomplish the gel-state transition. The elevation in P407 concentration caused an increase in the number of co-polymers, which in turn facilitated the construction of micelles. (Giuliano, Paolino, Fresta, & Cosco, 2018).

The gelation time, which is a measure of how long it takes the formulation to set into gel state, was in the range of 68.00 ± 2.00 to 227.00 ± 3.61 s. Along the same lines as the gelation temperature, an increase in P407 concentrations from 17 to 19 % resulted in a significant reduction in the amount of time required for phase transformation ($P < 0.01$). On the other hand, AZG1 did not succeed in achieving a gel state since the gelation temperature was more than 37°C . An increase in HA content from 0.2 to 1.1 % significantly lowers the gelation temperature in formulation groups when there is an equivalent quantity of P407 ($P < 0.01$). The increase in HA from 1.1 to 2 % did not display any significant changes in the gelation temperature, with the exception of the group that included 19 % of P407, which demonstrated a significant decrease in the gelation temperature ($P < 0.01$). In addition to this, it was discovered that an increase in HA concentration led to a significant reduction in the gelation time ($P < 0.01$). Nonetheless, the increment in P407 concentration from 17 to 18 % only indicated a tendency of decrease in the group that possessed 2 % of HA.

Using experimental design, the relationship between P407 and HA concentration and gelation temperature and time was also examined. Two factors and three levels full factorial design was utilized. Both the concentration of P407 and HA were designated to be independent variables C and D, respectively. The design layout was shown in Table 4.5.

Table 4.5 Experimental design layout for AZG formulation optimization.

Run	Formulation composition		Independent variable	
	P407 (% w/v)	HA (% w/v)	P407 (C)	HA (D)
1	17	0.2	-1	-1
2	17	1.1	-1	0
3	17	2	-1	1
4	18	0.2	0	-1
5	18	1.1	0	0
6	18	2	0	1
7	19	0.2	1	-1
8	19	1.1	1	0
9	19	2	1	1
10	18	1.1	0	0

The results indicated that response data of gelation temperature (Y_3), and gelation time (Y_4) significantly fit with linear models with $P < 0.01$ for both responses. The linear models were presented as the following equations.

$$Y_3 = 33.67 - 3.84C - 1.67D \quad (4-3)$$

$$Y_4 = 138.37 - 22.94C - 60.11D \quad (4-4)$$

The model equation of gelation temperature (Equation 4-3) expressed the correlation coefficient (r^2) at 0.9305. Each independent variable was analyzed for its effects by ANOVA. The results revealed that variable C, which was P407 concentration exerted a significant reverse relationship to response Y_3 ($P < 0.01$), and variable D (concentration of HA) also exhibited a significant reverse relationship to response Y_3 ($P < 0.05$). The 3D response surface for linear equation 4-3 is presented in Figure 4.14a. Response Y_4 was analyzed and the linear equation 4-4 was acquired. Equation 4-4 expressed the relationship of variables C and D, which were the

concentration of P407 and HA, accordingly. The r^2 of this equation was 0.9693. It was found that both variables significantly exerted negative relationship to the response Y_4 ($P < 0.01$). The 3D response surface of this equation is displayed in Figure 4.14b.

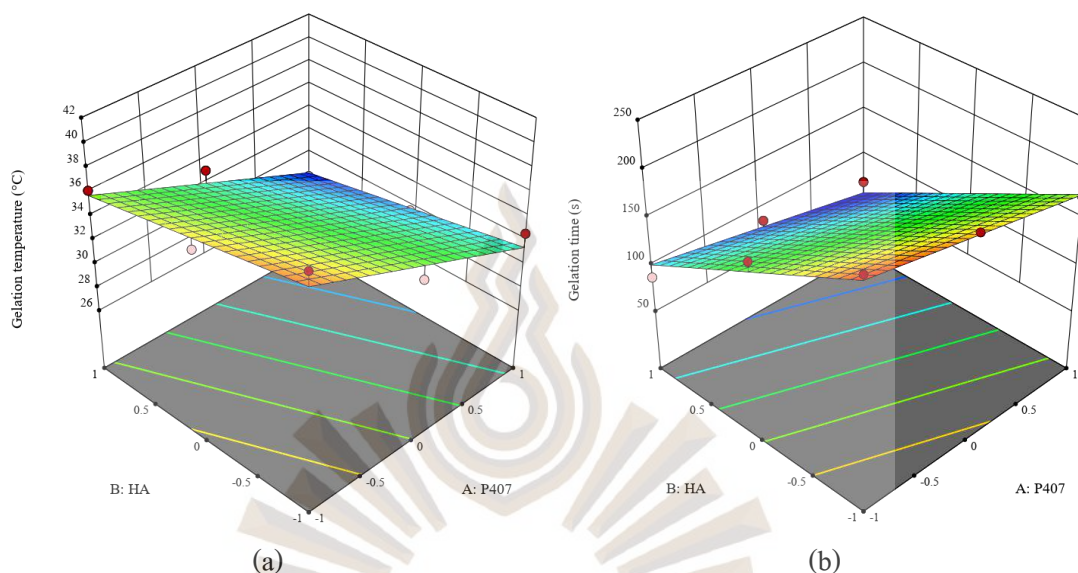


Figure 4.14 Response surface plot indicating the effect of variables C (P407) and D (HA) on the responses: gelation temperature (a) and gelation time (b).

The incorporation of HA into the formulation had the effect of lowering both the gelation temperature and gelation time. This behavior might be explained by the inclusion of high-molecular-weight HA produced the densely packing of HA and P407 molecules together. This could make the micellization process of P407 easier to accomplish. (Pereira et al., 2013). Furthermore, any additives that are used in the formulation of P407, which are capable of forming non-covalent bonds with P407, lower the gelation temperature by minimizing the attraction of P407 with water in the system (Dumortier et al., 2006; Giuliano et al., 2018). In this circumstance, the hydroxyl and carboxyl groups of HA, which are readily available, have the potential to establish hydrogen bonds with P407 (Mayol et al., 2011). This contributed to dehydration, which facilitated the micellization process by reducing the number of water molecules that acted as an obstacle to the combining of PPO in the hydrophobic cores of the micelles. This was possible since there were less water molecules (da Silva, Cook, & Bruschi, 2020). It's also conceivable that the intense

hydrophilicity of HA, which is a great humectant, was pulled the water component from the molecular chain of the poloxamer, which contributed to the decrease in gelation time. This would be another possible explanation (Choi, Lee, Kim, M., & Kim, C., 1999). The development of a formulation has the potential to make use of a wide variety of phase transformation mechanisms, such as pH, temperature, and solvent exchange. Temperature is one of the most prevalent physiological states that can be found in the human body, and it is possible that it is the most basic mechanism that can set off an event. At the active site, the developed formulation would easily be able to undergo phase change. In clinical practice, the amount of time it takes for the dosage form to set shouldn't be excessively long. If it is, the formulation runs the risk of prematurely detaching from the periodontal pocket.

4.2.3 Mechanical properties

4.2.3.1 Viscosity

Table 4.5 provides an overview of the viscosity of each produced formulation. The formulations were in a state of solution when they were maintained at 4 °C. The viscosity that was measured lay in the limit of 2.24 ± 0.25 to 143.53 ± 15.55 cps. Viscosity increased significantly as HA concentration increased from 17 to 18 % ($P < 0.05$) and from 18 to 19 % ($P < 0.01$). In contrast, the increment in the concentration of P407 did not have any influence on the viscosity since the micellization process did not take place.

Table 4.6 Mechanical properties of thermoresponsive azithromycin-loaded niosomes gel (AZG) such as viscosity, injectability and textural properties.

Data are presented in mean \pm SD, n = 3.

Formulation code	Viscosity (cps)		Injectability (N)	Texture profile analysis		
	4 °C	37 °C		Hardness (mN)	Springiness (ratio)	Resilience (ratio)
AZG1	2.24 \pm 0.25	162.77 \pm 5.75	0.78 \pm 0.01	249.80 \pm 6.90	0.25 \pm 0.01	0.002 \pm 0.00
AZG2	29.86 \pm 0.44	194.20 \pm 10.14	0.94 \pm 0.01	418.89 \pm 18.60	0.24 \pm 0.00	0.002 \pm 0.00
AZG3	124.67 \pm 13.51	216.07 \pm 11.47	1.26 \pm 0.06	554.96 \pm 1.04	0.24 \pm 0.00	0.003 \pm 0.00
AZG4	2.60 \pm 0.52	189.03 \pm 4.28	1.24 \pm 0.03	378.39 \pm 4.14	0.25 \pm 0.00	0.002 \pm 0.01
AZG5	36.98 \pm 4.43	195.10 \pm 6.30	1.32 \pm 0.03	472.05 \pm 14.37	0.24 \pm 0.00	0.002 \pm 0.00
AZG6	125.30 \pm 6.85	241.53 \pm 9.56	1.50 \pm 0.04	562.11 \pm 0.03	0.24 \pm 0.01	0.002 \pm 0.01
AZG7	2.55 \pm 0.30	218.97 \pm 12.62	1.13 \pm 0.03	400.60 \pm 5.85	0.25 \pm 0.00	0.002 \pm 0.00
AZG8	34.73 \pm 3.23	247.23 \pm 13.21	1.55 \pm 0.41	508.22 \pm 12.91	0.24 \pm 0.00	0.002 \pm 0.00
AZG9	143.53 \pm 15.55	283.77 \pm 3.75	1.94 \pm 0.04	617.29 \pm 14.31	0.24 \pm 0.00	0.003 \pm 0.01

At 37 °C, every formulation went through a phase transition and became a gel state except AZG1. The viscosity increased to levels that ranged between 162.77 ± 5.75 and 283.77 ± 3.75 cps. It was discovered that increases in HA concentration resulted in a significant rise in the viscosity of the AZG in its gel state. ($P < 0.05$). The variations in HA from 1.1 to 2 % only displayed an upward trend of viscosity, with the exception of the group that comprised 17 % P407. The influence of P407 showed that raising the concentration of P407 from 17 to 18 percent showed an increasing trend, but the difference was not statistically significant. Yet, increasing the concentration of P407 from 18 to 19 percent significantly increased the gel-state viscosity ($P < 0.05$). The greater concentration of P407 and HA in the formulation was one factor that contributed to the higher viscosity seen across all of the different formulations. The gel-state viscosity was directly impacted by the phase change that occurred through P407 as a result of micellization. Due to the high molecular weight of HA (2.05×10^6 Da) contained in AZG, the effect of HA on the viscosity increase was present in the formulation solution state.

4.2.3.2 Rheological study

Flow behavior of the AZG solution state was examined. Figure 4.14 portrays the shear stress and shear rate curves of the developed formulations. According to the nonlinear correlation between shear stress and shear rate, all AZG formulations expressed a non-Newtonian fluid flow. The slope of the curves suggested that the viscosity of the prepared AZG formulations reduced with increasing shear force, clearly showing pseudoplastic characteristic (Srivastava, Kohli, & Ali, 2016). The higher quantities of P407 and HA in the formulation are responsible for the viscosity and shear stress increases that were observed.

Analyzing the plots with rheological equations revealed that the Herschel-Bulkley model, which is reminiscent of non-Newtonian fluids, provided the best fit for the rheological data. The flow index (n value) derived from the Herschel–Bulkley equation for all formulations varied between 0.189 ± 0.003 and 0.585 ± 0.023 , which suggested flow characteristics of shear-thinning (n value < 1).

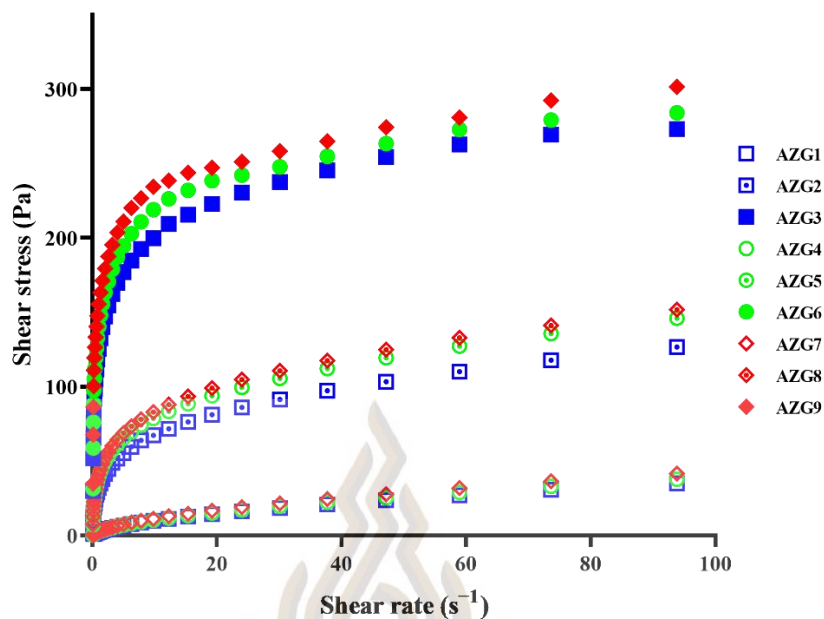


Figure 4.15 Shear stress and shear rate plots indicated rheological behavior of all AZG formulations at 4 °C (mean value).

Considering the injectable dose form, it was believed that pseudoplastic behavior was desirable. Flow of pseudoplastic fluids requires force. When the shear force was exerted to the formulation, the entangled molecule structure changed and became oriented parallel to the shear force's direction (Swain, Patel, Gandhi, & Shah, 2019). After that, the formulation would be able to flow to the target site via the barrel of the syringe and the tip of the needle. After injection, the formulation had a lower viscosity, allowing it to more easily penetrate the intricate anatomical structure of the periodontal pocket. This was made possible by the injection force that was applied during the procedure. After being evenly distributed across the treatment area, the formulation should resume its viscosity and eventually settle within the periodontal pocket without dripping attributable to the pseudoplastic shear-thinning action (Ghica, Hîrjău, Lupuleasa, & Dinu-Pîrvu, 2016).

4.2.3.3 Injectability

All formulations' solution states were assessed for injectability. The outcome is presented in Table 4.5. Similar trends were seen between the injection force and viscosity of the

prepared formulations. It was discovered that the greater the viscosity, the greater the necessary injection force. In general, the greatest force required to expel the formulations via the needle tip of the syringe was below 2 N for every formulation. Consequently, all formulations were regarded as injectable. This should enable administration within the intraperiodontal pocket. Thus, professionals may easily and with minimal force inject the formulation into the confined area of periodontal pocket.

4.2.3.4 Texture profile analysis

Texture profile analysis is commonly employed in the food sciences to characterize textural qualities such as hardness, springiness, and resilience. These characteristics are also applicable in the context of pharmaceutical technology. Consequently, numerous newly published research implement this approach to evaluate novel dose forms (Agossa et al., 2017; Bassi da Silva et al., 2018; da Silva et al., 2020). Gel-state AZG was studied for its textural features (Table 4.5) in order to have a better understanding of the behavior of the gel while it was in residence in the periodontal pocket. The hardness of a gel is measured by the highest force required for the first compression to penetrate the gel composition (Agossa et al., 2017). It was revealed that increasing the amount of HA led to a significant enhancement in the gel-state hardness ($P < 0.01$). During the process of analyzing the effects of P407, it was discovered that an increase in the concentration of P407 resulted in a significant rise in gel hardness. ($P < 0.05$). However, in the group containing 0.2 and 2 % HA, the rise in P407 from 17 to 18 % did not demonstrate a statistically significant increase in hardness; rather, it only demonstrated an upward trend in hardness. According to the findings, the degree of hardness shown by the gel state was found to be directly proportional to the amount of P407 and HA included within the formulation. The gel matrix's strength, as measured by the hardness of the gel, varied between between 249.80 ± 6.90 and 617.29 ± 14.31 mN. The gel strength of each formulation was equivalent to that of earlier periodontal formulation studies (Agossa et al., 2017; da Silva et al., 2020).

In spite of the fact that P407 is capable of performing phase transition, the gel matrix that is formed has a restricted use in the pharmaceutical application due to structural

weaknesses and a high rate of dissolution in water. It may be possible to increase the strength of the P407 matrix gel by either adding the second polymer or modifying its chemical structure (Abou-Shamat, Calvo-Castro, Stair, & Cook, 2019).

The AZG matrix was enhanced in this study by the inclusion of HA. The interaction of P407 with HA was caused by secondary bonding, such as hydrogen bonds, and the development of massive micelles embedded in the coil structures of HA, which enhanced the rheological characteristics of the hydrogel matrix (Mayol et al., 2011). The more robust matrix has the potential to be efficiently preserved in the periodontal pocket. On the other hand, the gel matrix shouldn't be too strong, since this would prevent it from deforming spontaneously inside the periodontal pocket and the gel state would impede the periodontal healing procedure. In addition, springiness refers to how effectively a material "springs back after being deformed". Resilience is the degree to which a product "fights to restore its former height" (Agossa et al., 2017). The springiness was discovered to be in the range of 0.24 to 0.25, while the resilience was found to be low and in the range of 0.002 to 0.003. According to the findings, the gel state of any and all prepared formulations did not display any signs of bounce-back activity. Increased concentrations of P407 and HA had no effect on the springiness and resilience of the gels. These findings were consistent with those obtained in earlier textural investigations (Agossa et al., 2017). Within the periodontal pocket, the AZG gel state need to be capable of undergoing spontaneous deformation. As a result, AZG should not interfere with the tissue growth of the periodontium in the healing phase.

4.2.3.5 Bioadhesive property

The retention duration of the formulation within the periodontal pocket is extended not only by the phase transition property of the formulation, but also by the adherence of the formulation to the biological tissues. According to histopathological anatomy of the periodontal pocket, one side of the periodontal pocket is bordered by pocket epithelium, while the other side is the tooth-root surface. The junctional epithelium is found at the base of the pocket. (Bartold, Walsh, & Narayanan, 2000). The bioadhesive qualities of AZG were investigated in this work for both sides

of the periodontal pocket region. These properties include mucoadhesion to the pocket epithelium and the adherence of AZG to the tooth-root surface.

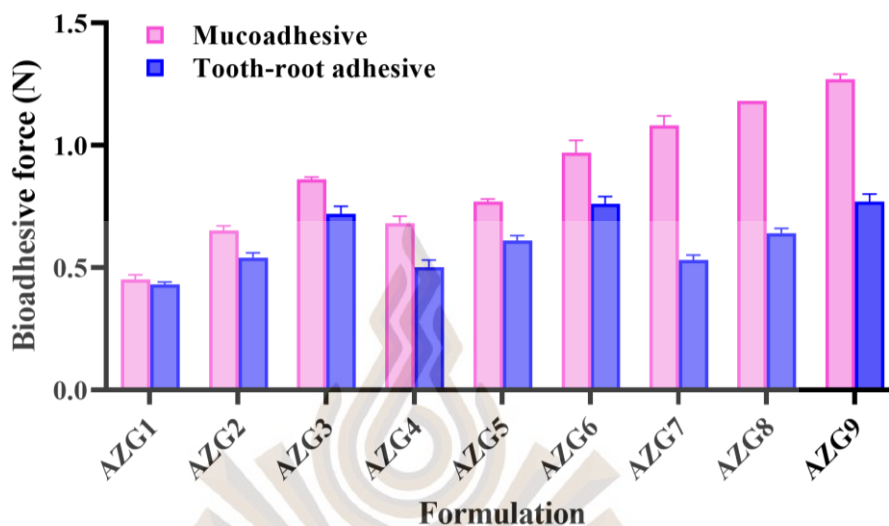


Figure 4.16 Bioadhesive force of AZG formulations represented the adhesion to the mucosa and tooth-root surface (mean \pm SD, n = 3).

(1) Mucoadhesion

Figure 4.15 illustrates the results of an assessment of the mucoadhesive characteristics of every AZG formulation. The mucoadhesive force ranged between 0.45 ± 0.02 and 1.27 ± 0.02 N. A formulation with a higher proportion of HA exhibited a significantly increased mucoadhesive force ($P < 0.01$). In formulations containing the same quantity of HA, a greater concentration of P407 also significantly increased the mucoadhesive force. ($P < 0.01$). This exemplifies the synergistic effect that P407 and HA have on the improvement of mucoadhesive properties. In spite of the fact that P407 is a versatile excipient, the bioadhesion of P407 on its own was rather poor, which may have a negative effect on the topical formulations (Abou-Shamat et al., 2019). In order to improve the mucoadhesive characteristics of formulations based on poloxamer, additives are required. In this setting, HA can be used as a mucoadhesive biopolymer, which has the potential to contribute to improvements in mucoadhesive capabilities in a multitude of dosage forms. (Hsieh et al., 2020; Mayol et al., 2008; Trombino, Servidio, Curcio, & Cassano, 2019). It is possible to explain the mucosal bonding of HA with mucoadhesive theories.

First, the molecular structure of HA causes it to form hydrogen bonds with the surfaces of biological tissues (Pritchard et al., 1996). Second, the structures of the HA comprise coils, and these coils have the potential to become entangled in the mucous membranes (Russo et al., 2016). High-molecular-weight HA is characterized by the presence of numerous coil configurations, which facilitate the entanglement mechanism. Consequently, this investigation utilized high-molecular-weight HA, which demonstrated a greater mucoadhesive force than low-molecular-weight HA (Snetkov, Zakharova, Morozkina, Olekhovich, & Uspenskaya, 2020).

(2) Tooth-root surface adhesion

According to the findings of the adhesion to the tooth-root surfaces, the adhesive force of AZG on the tooth-root surface specimens varied from 0.43 ± 0.01 to 0.77 ± 0.03 N, as shown in Figure 4.15. The significantly improved adhesion was the direct consequence of the increase in HA content ($P < 0.01$). It was shown that an increase in P407 could only significantly improve tooth-root adhesion in the group that included 0.2 and % of HA, an increase in P407 from 17 to 18 % significantly raised the adhesion ($P < 0.05$), but the other groups did not demonstrate any statistically significant variations when the P407 concentrations were changed. In contrast to the mucoadhesive investigation, the results showed that tooth-root surface adhesion was mostly reliant on HA concentration. The mechanism of root surface adhesion is explicable by mechanical interlocking theory, which is a mucoadhesive substance bonded to rough or irregular surfaces with an enhancement of the adhesive interface contact area (Leung & Robinson, 1990).

Cementum, which has a structure that is porous, covers the surface of the root of human teeth. There is a possibility that the adhesiveness of the formulation was enhanced by penetrating and entangling the coil structures of HA within the microporosity of the root surface. In clinical settings, mucin from saliva penetrates the root microporosity, which further assists in the adherence of the formulation. Investigation into the formulation's ability to adhere to the tooth structure is currently under progress by many researchers. According to the histopathologic characteristics of the periodontal pocket, the epithelium lining the periodontal pocket was ulcerated as a result of the inflammatory phase of periodontitis. The rate of turnover of the healing epithelium

was high, and the loss of the fragile epithelium layer was sufficient to remove the adherent formulation from the periodontal pocket (Agossa et al., 2017). Accordingly, adherence to the surface of the tooth root minimizes formulation dislodgement. Increased HA concentrations appear to increase the tooth-root surface adhesion of the AZG formulation.

From the mechanical properties point of view, in this investigation, AZG formulations were able to undergo phase change at physiological temperatures utilizing various gelation periods. These formulations might be administered into the periodontal pocket. However, the long setting time would make its clinical application as a dental material problematic. In aspects of viscosity and rheology, the formulations that had low viscosity and pseudo-plastic characteristics might be difficult to manage during injection due to the free-flowing fluids. The formulations that had a moderate viscosity might make it easier to deliver them through injection, which would provide physicians more control over the amount of the formulations that were given to patients. The formulation with a moderate viscosity requires a larger injection force. From a rheological standpoint, this should assist push the formulation to efficiently penetrate through the small enclosed space in the soft tissue located inside the periodontal pocket. In addition, the formulations that demonstrated significant mucoadhesive and tooth-root adhesion forces had the potential to accomplish both a prolonged retention duration and continuous drug release within the periodontal pocket. As a result, taking into account all of the characteristics that have been discussed so far, the formulations AZG3, 6, 8, and 9 were determined to have a high potential and were selected for future research.

4.2.4 Stability of the formulations

To evaluate the stability of AZG formulations, the prepared formulations were kept at 4 ± 2 , 25 ± 2 , and 45 ± 2 °C with 75% of relative humidity for 30 days (Table 4.6). The results disclosed that the pH of the formulation was steady through the period of 30 days. At 4 ± 2 °C, all formulations remained their AZM content at approximately 100%, while at 25 ± 2 °C, the formulations started losing AZM content by 2 – 5% on day 14th. For the formulations stored at

45 ± 2 °C, the AZM content notably deteriorated from day 7th. Thus, the optimal storage condition for AZG formulation in this preliminary stability test was 4 ± 2 °C. In addition, it was found that AZG9, which contained the highest concentration of P407 and HA, endured inappropriate conditions and remained its AZM content apparently higher than other formulations. This could be explained by the dense packing of the polymeric structure of AZG9 generating high gel strength and protecting the matrix content.

Table 4.7 Percentage of AZM content and pH of each formulation in different storage conditions at 0, 7, 14, and 30 days. Data presented in mean \pm SD, n = 3.

Formulation	Day	pH	Percentage of drug content (%)		
			4 ± 2 °C	25 ± 2 °C	45 ± 2 °C
AZG3	0	6.92 ± 0.04	102.44 ± 0.53	102.36 ± 0.66	101.52 ± 0.39
	7		102.30 ± 0.45	101.68 ± 0.52	75.36 ± 0.52
	14		100.57 ± 0.59	95.69 ± 0.37	67.95 ± 0.59
	30		101.00 ± 0.76	89.90 ± 0.45	53.54 ± 0.76
AZG6	0	6.90 ± 0.01	101.50 ± 0.69	101.58 ± 0.78	101.61 ± 0.44
	7		100.48 ± 0.46	100.35 ± 0.77	76.83 ± 0.44
	14		100.45 ± 0.59	95.16 ± 0.50	61.95 ± 0.69
	30		100.86 ± 0.42	93.17 ± 0.76	55.67 ± 0.84
AZG8	0	6.90 ± 0.02	100.20 ± 0.57	101.45 ± 0.67	102.05 ± 0.40
	7		99.98 ± 0.42	98.32 ± 0.35	74.23 ± 0.56
	14		102.01 ± 0.73	89.15 ± 0.51	71.95 ± 0.68
	30		99.42 ± 0.60	84.77 ± 0.57	51.59 ± 0.54
AZG9	0	6.92 ± 0.01	101.24 ± 0.75	102.10 ± 0.27	101.77 ± 0.85
	7		100.29 ± 0.67	100.05 ± 0.67	77.96 ± 0.75
	14		100.58 ± 0.75	97.63 ± 0.53	69.2 ± 0.54
	30		100.19 ± 0.76	95.15 ± 0.30	59.6 ± 0.31

4.2.5 Model drug analysis

4.2.5.1 *In vitro* drug release and kinetic profiles

Figure 4.16 depicts the cumulative release plots of AZM for 72 hours from AZG3, 6, 8, and 9. The behavior of the four formulations' release patterns was comparable, and all formulations exhibited no lag time. AZG8 was shown to have the greatest rate of drug release, followed by AZG3, 6, and 9. In the fourth hour, AZG8 release significantly increased, surpassing all others, and persisted for the next 72 hours. The cumulative release plots divide the release profile into three phases: (1) rapid release during the first 12 hrs; (2) sustained release over the next 12 to 48 hrs; and (3) steady level of release during the next 48 to 72 hrs (Jain, Rhodes, Railkar, Malick, & Shah, 2000). It was anticipated that the development of an AZG formulation for the treatment of periodontitis would result in a rapid drug release following administration, followed by a sustained release that would achieve antimicrobial activity inside the periodontal pocket for a period of 72 hrs as per the AZM oral administration dosage (Hirsch et al., 2012). The release scheme that was gathered from the cumulative plots showed that every formulation that was evaluated displayed release patterns that were quite comparable to one another, with prompted and sustained AZM release for up to 72 hrs. Nevertheless, AZG8 had the greatest release rate when compared with the other formulations.

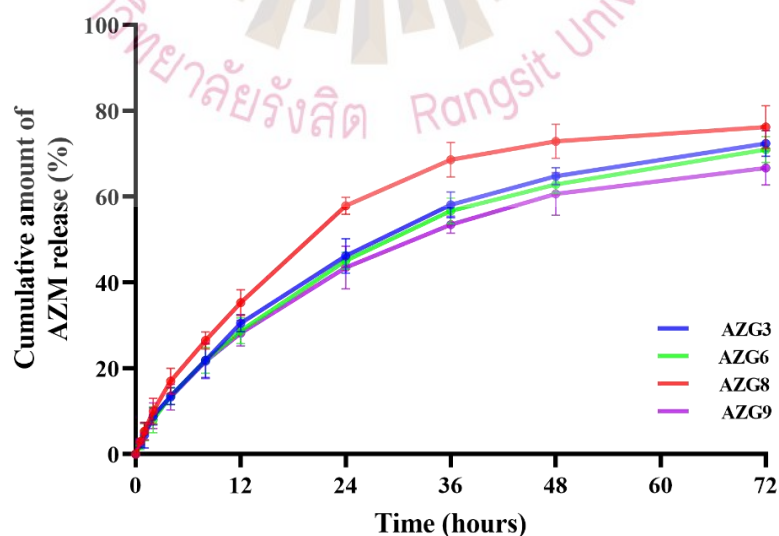


Figure 4.17 Percent cumulative drug release of AZG formulations.

Data are mean \pm SD, n = 3.

The data on the cumulative drug release was evaluated using a variety of kinetic models, including the zero-order model, the first-order model, the Higuchi model, and the Korsmeyer-Peppas model. Table 4.7 presents the findings of a linear regression analysis performed with the equation parameters of each different formulation. It was revealed that the Korsmeyer-Peppas model gave the greatest fit for the AZG formulation release rates, which suggested that the polymeric matrix drug delivery system was responsible for the AZG formulation's distribution of the drug. (Mhlanga & Ray, 2015). The release exponent (n) of the Korsmeyer-Peppas equation had values in the range of $0.45 < n < 0.89$ (Korsmeyer, Gurny, Doelker, Buri, & Peppas, 1983). Accordingly, the drug is released in a non-Fickian diffusion manner. AZM formulation release was caused by both the dispersion of the polymeric matrix and its erosion (Ritger & Peppas, 1987). The release behavior was significantly influenced by the AZG's physical characteristics. The formulation AZG8, which had the greatest rate of release, was made up of 18 %P407 and 1.1 % HA. This group that was examined had a low hardness as a direct consequence of the decreased amounts of P407 and HA. As a consequence of this, the AZG8 gel matrix degraded very easily, which enabled a more rapid release of the drugs. Similar explanations might be given to the AZG3, 6, and 9 releases. These formulations contained 2 % HA, and the gel matrices' hardness was exclusively determined by the quantities of P407. AZG3, with 17% P407, had the lowest gel hardness compared with AZG6 (18% of P407) and 9 (19% of P407). Consequently, AZG3 had the greatest rate of drug release, followed by AZG6 and 9.

As stated in the texture profile study, the interactions between P407 and HA produced a more robust hydrogel matrix (Mayol et al., 2011). Due to its enhanced structural integrity and stability, the P407-HA hydrogel matrix might be employed as a controlled release device to maintain and delay drug release (Jung et al., 2017). Considering the AZM oral regimen, the short course of treatment consists of 500 mg taken orally once a day for three days (Hirsch et al., 2012). As a result, the effective sustained release method would be able to provide AZM with just a single dose. This ought to increase patient compliance and could minimize dental visits for periodontal therapy, which is especially important during the COVID-19 pandemic.

Table 4.8 Kinetic models fitting of AZG formulations.

Formulation	Kinetic models								
	Zero-order		First-order		Higuchi		Korsmeyer-Peppas		
	K_0	r^2	K_1	r^2	K_H	r^2	K_{KP}	n	r^2
AZG3	2.699	0.964	0.032	0.982	7.756	0.944	4.797	0.741	0.998
AZG6	2.600	0.953	0.030	0.975	7.505	0.952	4.905	0.715	0.998
AZG8	3.186	0.954	0.039	0.980	9.191	0.950	5.972	0.718	0.998
AZG9	2.567	0.938	0.030	0.963	7.452	0.963	5.211	0.681	0.999

K_0 , K_1 , K_H , K_{KP} are equation parameters of zero-order, first-order, Higuchi, and Korsmeyer-Peppas, respectively. The n values are release exponents of the Korsmeyer-Peppas equation.



4.2.5.2 *Ex vivo* drug permeation study

Figure 4.17 depicts the quantity of AZM that permeated the mucosal specimen. The permeated AZM in AZG8 was greatest due to its lowest HA composition when compared to other examined formulations, followed by 9, 6, and 3. As a consequence, the resultant molecular structure was loosely packed, had low textural hardness, and was prone to erosion. Furthermore, AZG8's high mucoadhesion contributed to the high penetration rate by producing a strong mucoadhesive interface that bonded closely to the mucosal membrane (Pedreiro, Cury, Chaud, & Gremião, 2016). When comparing AZG3, 6, and 9, which all contained the same amount of HA (2%), AZG9 with 19% of P407 showed the highest permeated rate, followed by 6 (18% of P407) and 3 (17% of P407). The concentration of P407 may account for the increased penetration rate. P407 was discovered to improve transmucosal drug delivery (Bodratti & Alexandridis, 2018). Aside from that, AZG9 had the highest mucoadhesive characteristics.

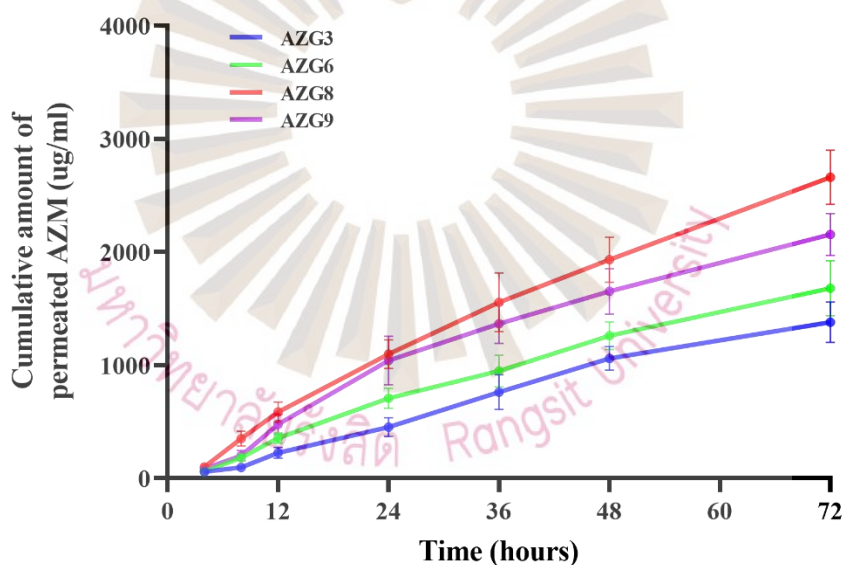


Figure 4.18 Cumulative permeated drug from *ex vivo* mucosal permeation model.

Data are mean \pm SD, n = 3.

In this work, the porcine esophagus was used as a model for mucosal penetration due to its anatomical similarities to the human oral mucosa. The preparations for the standardized esophageal specimens were simple in comparison to the porcine buccal mucosa, which may be damaged during mastication, varies in texture, and have limited availability (Diaz del

Consuelo et al., 2005). When considered the log P value of AZM, which is 3.98, indicated that AZM has low solubility in water and a tendency to disseminate in lipids. (Vanić et al., 2019). This implies that the low number of permeated drugs was due to AZM being mostly dispersed in the lipid bilayer of the mucosal tissue. This circumstance would be advantageous for the treatment of periodontitis. It was anticipated that the topical formulation would play the role of providing slow drug release within the periodontal pocket, delivering the drugs permeating through the periodontal pocket epithelium, and then maintaining the drugs within the epithelium and connective tissue of the gingiva in order to eradicate the infiltrated periodontal pathogens.

4.2.6 Biocompatibility

4.2.6.1 Cytotoxicity of AZG

AZG formulations were evaluated for cytotoxicity effects utilizing the MTT assay (Figure 4.18). AZG formulation extract was varied in concentration from 10 to 1000 µg/ml and co-culture with human gingival fibroblasts. The optical density of insoluble formazan is produced by tetrazolium reduction of mitochondrial activity within the living cells representing cell viability. The result indicated that the concentration of AZG extracts affected cellular viability in a dose-dependent manner. At 10 µg/ml, the percentage of cell viability of AZG3, 6, 8, and 9 was in the range of 84.84 to 95.52% and decreased to the range of 66.44 to 92.43% at 100 µg/ml of AZG extract concentration. At the higher concentration, the percentage of cell viability of all formulations was less than 80% except in AZG9, which possessed the highest cellular viability among other formulations in every concentration. When the results were compared within the same concentration, AZG9 also yielded the highest cell viability. AZG extract at the concentration of 10 µg/ml was the most compatible with the cultured fibroblasts. In this study, AZG3, 6, and 9 were composed of an equal concentration of HA (2%) but different in the concentration of P407, which was 17, 18, and 19%, respectively. In addition, AZG8 consisted of 19% of P407 and also exhibited high cell viability. This indicated that the high concentration of P407 in the formulation may be contributed to the high percentage of cell viability. P407 was considered a bioinert polymer (Giuliano et al., 2018). However, recent studies of P407 in tissue engineering reported an

improvement in cell viability *in vitro* (Cui et al., 2022; Rezazadeh, Parandeh, Akbari, Ebrahimi, & Taheri, 2019).

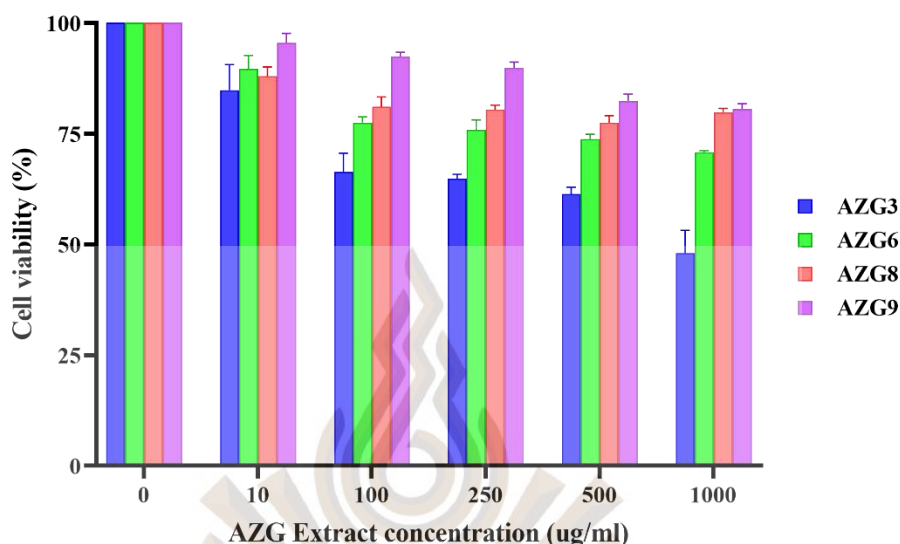


Figure 4.19 Percentage of cell viability of AZG formulations in various concentrations, Data are mean \pm SD, n = 3.

4.2.6.2 Biodegradability

Gel-state of AZG formulations was determined for weight loss, which represents the biodegradability of the gel matrix in a simulated biological environment. The formulations were injected into the customized container mimicking the periodontal pocket and submerged in phosphate buffer pH 6.8 under the moving environment. The percentage of weight loss data (Figure 4.19) revealed that after 12 hrs, the formulations became swelling as the weight was gained by approximately 2.9 – 11.8% due to the micellization process. AZG8 exhibited less weight gain from swelling compared to other formulations because of the lower amount of HA in its composition (1.1% compared to 2% of HA in AZG3, 6, 9). The swelling hydrogel matrix of AZG3, 6, and 9 remained its weight until 48 hrs, while AZG8 lost 25% of its weight. At 72 hrs, hydrogel matrix erosion was observed since 8 – 15% of weight loss presented in AZG3, 6, 9. AZG9 preserved its weight at 92% higher than AZG6 (87.4%) and AZG3 (85.6%), respectively. The weight loss pattern remained in this order until 120 hrs. The results of this experiment clearly explained that HA contributed to gel stability. AZG8 possessed lower HA composition and could

poorly maintain its matrix integrity. In AZG3, 6, and 9, which were composed of 2% HA, P407 seemed to elevate matrix strength to resist matrix erosion. These results may imply that AZG formulation could remain inside the periodontal pocket for 72 hrs as intended for AZM administration. The observation at 120 hrs showed that the gel matrices of AZG3, 6, and 9 remained in the range of 40.9 – 55.0%.

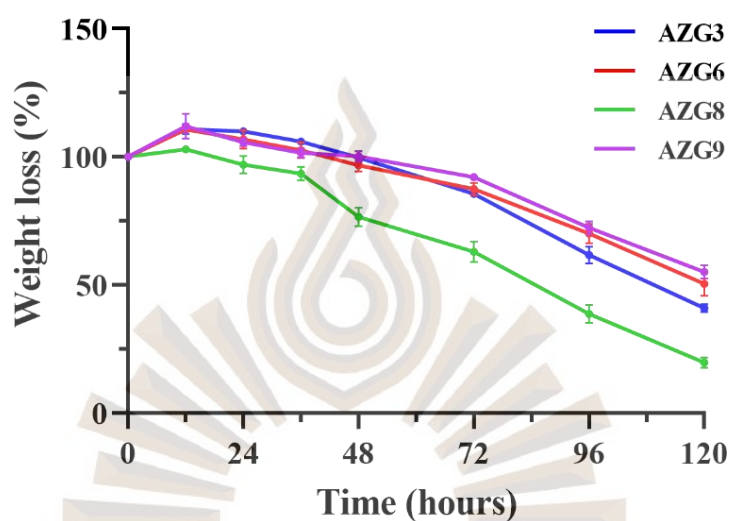


Figure 4.20 Biodegradability of the formulation represented by the percentage of weight loss.

Data are mean \pm SD, n = 3.

In an oral environment, there are more complicated dynamic changes such as muscle movement from mastication, speaking, saliva, and gingival crevicular fluid flow. The formulation could be expelled from the periodontal pocket. However, the remaining formulation of 85.6 – 92.0% was observed at 72 hrs combined with the bioadhesive properties of AZG. The formulation matrix should suffice for drug delivery. The prepared gel formulations were further investigated for 120 hrs (5 days). According to the data of the oral form of AZM, the concentration of drugs was present up to 7 days after the oral intake regimen of once daily for 3 days with the help of fibroblasts, which act as biological drugs reservoir (Lai et al., 2011). From the data of release and biodegradability studies, it may be postulated that AZG formulation, which preserved its matrices at 50% on the 5th day, should provide drug distribution within the periodontal pocket comparable to the oral form of AZM. However, there must be further investigations into this statement.

4.3 Efficacy evaluation of thermoresponsive AZM-loaded niosomes gel

4.3.1 Antibacterial activity

In this study, AZG formulations were tested for their antibacterial efficacy against major periodontal pathogens, namely *Aa.*, *Pg.* (Figure 4.20). According to the findings of the inhibitory zone, every AZG formulation showed significantly higher antibacterial activity ($P < 0.01$) compared to the AZM solution, which was prepared at the same drug concentration. The hydrogel matrix of AZG may have enhanced the dispersion of the drugs. The findings were the same for both pathogens. When comparing the antibacterial activity of each AZG formulation, however, no significant differences were detected. *Aa.* and *Pg.* are considered significant periodontal pathogens involved with severe periodontitis (Torrungruang, Jitpakdeebordin, Charatkulangkun, & Gleebua, 2015). The invasion of these organisms into the sub-epithelium and connective tissue results in a chronic infection that is difficult to treat with conventional methods. Even the "gold standard" therapy for periodontitis, which is scaling and root planing, was not able to eliminate all of the remaining pathogens. Antibiotics administered locally might eradicate any residual bacteria. However, the formulation must have a prolonged retention duration in the periodontal pocket and improve transmucosal drug delivery.

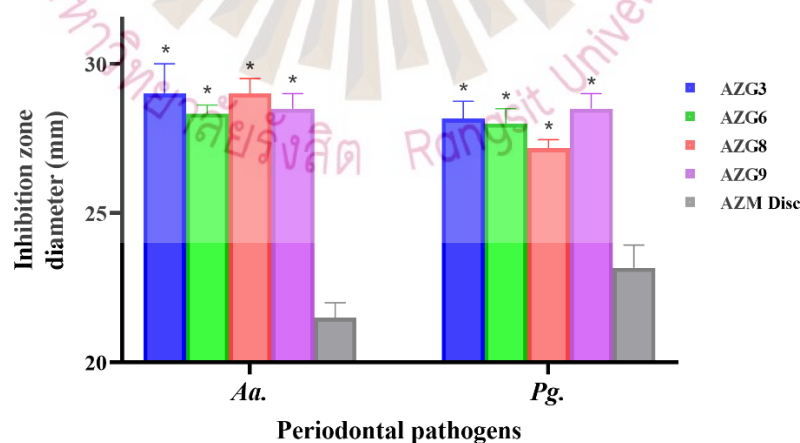


Figure 4.21 Antibacterial activity of AZG against major periodontal pathogens, namely *Aggregatibacter actinomycetemcomitans* (*Aa.*) and *Porphyromonas gingivalis* (*Pg.*), $n = 3$. Asterisks indicate statistically significant differences compared with AZM Disc ($P < 0.01$).

4.3.2 Wound healing effect

4.3.2.1 *In vitro* scratch wound closure

AZG formulations were investigated for wound healing effect by *in vitro* scratch wound closure model. The formulations were extracted and prepared at a concentration of 10 µg/ml and co-cultured with gingival fibroblasts.

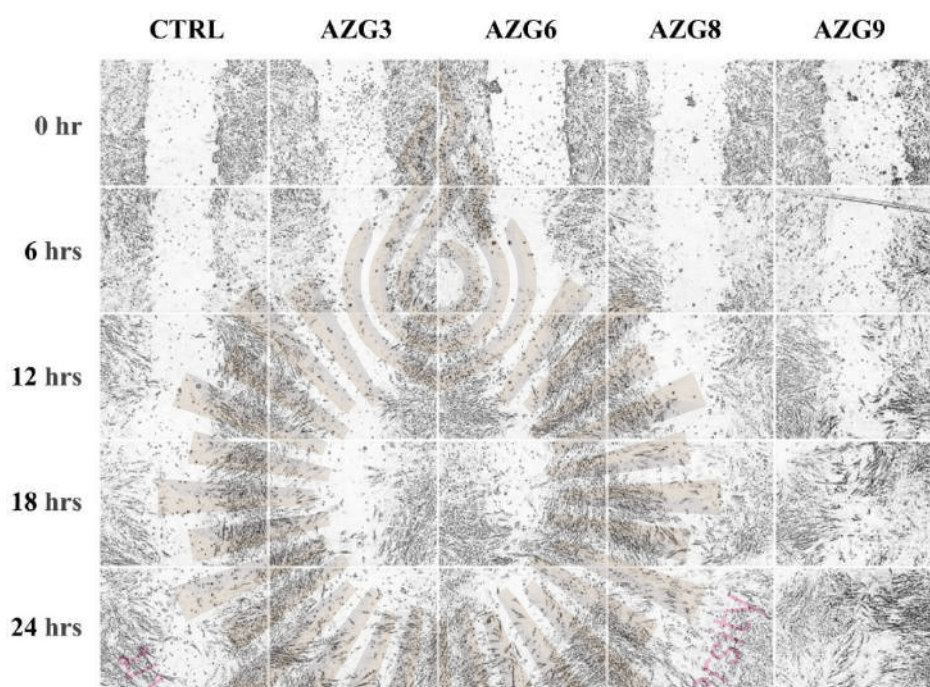


Figure 4.22 Scratch wound assay of gingival fibroblast at 0, 6, 12, 18, 24 hrs.

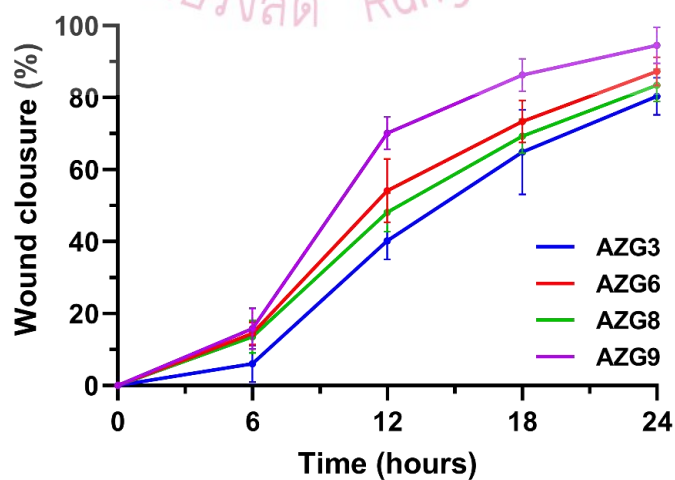


Figure 4.23 Percentage of wound closure, Data are mean \pm SD, n = 3.

The observed wound closure results (Figure 4.21) revealed that the wound area gradually decreased over time. At 12 hrs, the wound area noticeably reduced in the AZG9 group followed by AZG6, 8, and 3, respectively (Figure 4.22). The wound closure pattern was continued in this order for 24 hrs of the observation. Compared to the control group, all AZG-treated groups exhibited a markedly higher number of cells in the scratch area. This indicated the influence of HA in the formulation, which could accelerate cellular migration. This finding was in agreement with the other study on the high-molecular-weight HA contributed to gingival fibroblast wound closure (Chen et al., 2019). Moreover, the concentration of P407 in the formulation was found to affect the wound closure assay. In AZG9 group, which had 19% of P407 concentration, exhibited the highest wound closure area with dense migrated cells into the wound area followed by AZG6 and 3, which had 18, and 17% of P407, respectively. The higher concentration of P407 in the formulation seemed to exert a positive effect on cell migration. These results were consistent with the results of cell viability in section 4.2.6.1.

AZG formulation was intended to be used as the adjunctive to the conventional periodontal treatment. After scaling and root planing, periodontal tissue is healing by granulation forming and re-epithelialization. These events involve cell proliferation and migration. Therefore, the accelerated wound closure feature of AZG would be beneficial to periodontal wound healing. AZG9 performed the highest in wound closure capability. Then, AZG9 was chosen for further experiments.

4.3.2.2 Cell proliferation

The cell proliferation assay was conducted to evaluate the effective concentration of AZG extract, which caused minimum cytotoxicity and stimulated cell proliferation during 48 and 72 hrs. The assay utilized murine macrophage RAW 264.7 which is a common immune cell found in periodontal tissue. AZG9 extract was prepared with the cultured medium in various concentrations and incubated with RAW 264.7 cells. The cell viability result is displayed in Figure 4.23. It was found that cell viability was affected by AZG9 extract in a dose-dependent manner. At the concentration of 500 – 1000 $\mu\text{g/ml}$, the percentage of cell viability was lower than

50% in both 48, 72 hrs incubation periods. At 250 $\mu\text{g/ml}$, cell viability was comparable to the control group (0 $\mu\text{g/ml}$). However, after 72 hrs, cell viability was markedly decreased to lower than 25%. In the group of concentrations 10 – 125 $\mu\text{g/ml}$, the percentage of cell viability was higher than in the control group. This indicated that the extract stimulated cellular proliferation. However, in the 125 $\mu\text{g/ml}$ group, cell viability decreased after 72 hrs. Therefore, the optimal concentration of AZG9 for the cultured macrophage, which could stimulate cell proliferation was 100 $\mu\text{g/ml}$. This concentration was chosen for further mRNA expression and protein secretion study.

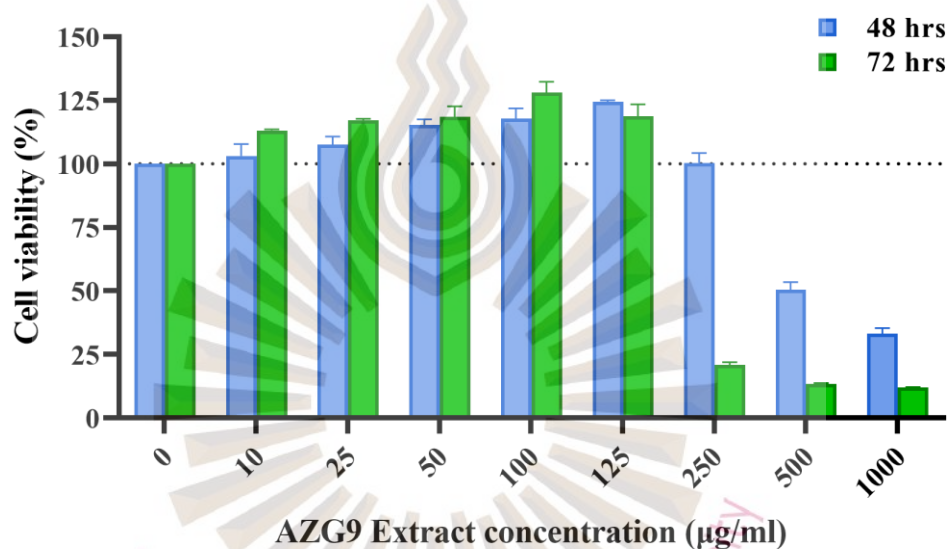


Figure 4.24 Cell proliferation assay indicated the percentage of cell viability of cultured macrophage at 48 and 72 hrs incubation periods.

Data presented in mean \pm SD, n = 3.

4.3.3 Anti-inflammatory effects

4.3.3.1 Real-time reverse transcriptase quantitative polymerase chain reaction (rt-qPCR)

To investigate the anti-inflammatory properties of AZG, mRNA expression of the inflammatory cytokines namely IL-1 β and TNF- α models were employed. As mentioned in the previous section, AZG9 was chosen by overall appropriate properties. However, in this study, AZG7 and 8 were included for comparison to study the influence of HA concentration in the formulation

(all of them were equal in P407 at 19% with variations of HA at 0.2, 1.1, and 2% in AZG7, 8, and 9, respectively). The mRNA expression result of both cytokines (Figure 4.24, 4.25) revealed that the cultured macrophages could be successfully stimulated into the inflammatory condition after being exposed to LPS. The expression of IL-1 β and TNF- α in the LPS-stimulated group was significantly higher than in the control group. Moreover, AZG9 exhibited no IL-1 β and TNF- α stimulation in both genes, which illustrated the biocompatibility of the formulation with the cultured cells. The anti-inflammatory activities were examined in the group with had been treated with AZG extract before being exposed to the LPS. For IL-1 β expression, it showed that all AZG pretreated groups significantly decreased IL-1 β expression compared to the LPS-stimulated group. When compared between each AZG formulation, AZG9 expressed the lowest IL-1 β mRNA followed by AZG8 and 7. Similar to the expression of TNF- α , the AZG pre-treated groups expressed lower TNF- α mRNA. However, the significant decrease was only present in AZG8 and 9 groups. The results of this study indicated that HA in the composition could play an important role in the suppression of inflammatory cytokines. HA is well-documented in its contribution to cell viability and wound healing. However, there was one study that described the inhibition of pro-inflammatory cytokine mRNA expression by HA (Mitsui et al., 2008). Considering the results from both inflammatory cytokines mRNA expression, AZG9 was found to efficiently suppress IL-1 β and TNF- α . Then, AZG9 was chosen for the cytokine secretion study by ELISA.

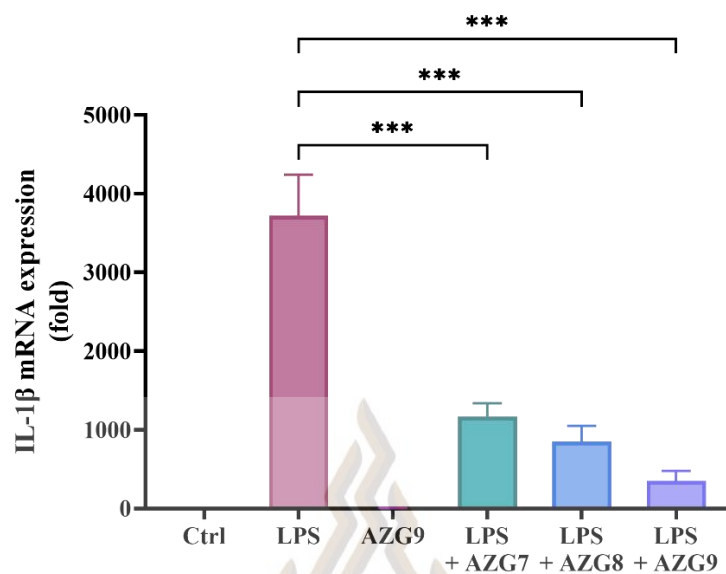


Figure 4.25 IL-1 β mRNA expression of RAW 264.7 in control (Ctrl), LPS-stimulated (LPS), pretreated with AZG followed by LPS stimulation group (LPS + AZG7, 8 and 9).

Data are mean fold to the control group \pm SD, n = 3.

*** indicated statistically significant (P < 0.001).

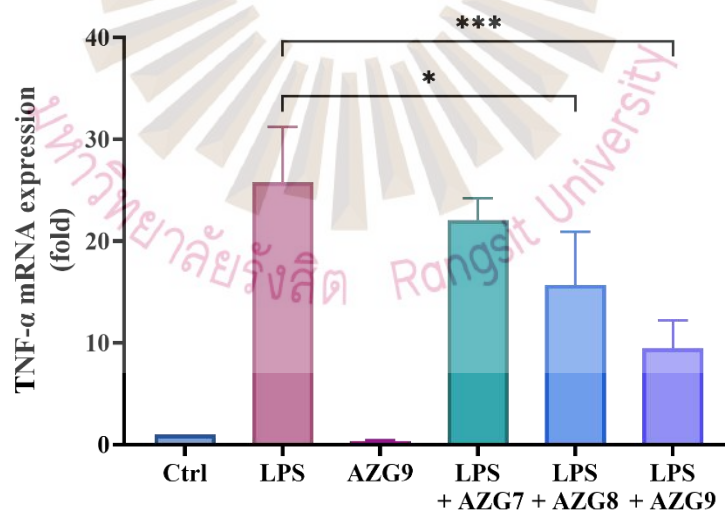


Figure 4.26 TNF- α mRNA expression of RAW 264.7 in control (Ctrl), LPS-stimulated (LPS), pretreated with AZG followed by LPS stimulation group (LPS + AZG7, 8 and 9).

Data are mean fold to the control group \pm SD, n = 3.

*** indicated statistically significant P < 0.001,

* indicated statistically significant P < 0.05.

4.3.3.2 Enzyme-linked immunosorbent assay (ELISA)

AZG9 formulation was further investigated for the anti-inflammatory effects by the inhibition of IL-1 β and TNF- α protein secretion. AZG9 extract was prepared in serial dilutions to confirm its efficacy. After RAW 264.7 was pretreated with AZG9 extract and stimulated into the inflammation stage with LPS. The cultured medium was collected to quantify the amount of secreted cytokines as both IL-1 β and TNF- α were extracellular cytokine secretion. The ELISA result of IL-1 β (Figure 4.26) indicated that the cultured macrophages were induced into an inflammatory condition. LPS stimulated group exhibited higher IL-1 β secretion than the control group. Cultured macrophages which were pretreated with AZG9 extract decreased IL-1 β secretion in a dose-dependent manner. The macrophage groups were pretreated with AZG9 extract at the concentration of 100, 50, and 25 μ g/ml significantly reduced IL-1 β secretion compared to the LPS-stimulated group.

The ELISA result of TNF- α is presented in Figure 4.27. The result showed that the cultured macrophages were successfully induced with LPS to an inflammatory condition. The LPS-treated group secreted a higher amount of TNF- α compared to the control group. Macrophages pretreated with AZG9 extract were found to reduce TNF- α production in a dose-dependent manner. All concentrations of AZG9 extract significantly inhibited TNF- α secretion in this experiment.

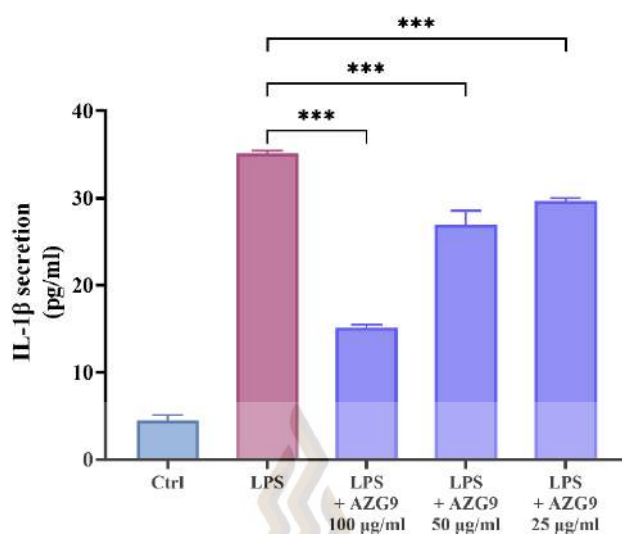


Figure 4.27 IL-1 β secretion of RAW 264.7 in control (Ctrl), LPS-stimulated (LPS), pretreated with AZG9 extract at different concentration followed by LPS stimulation. Data are mean \pm SD, n = 3. *** indicated statistically significant P < 0.001,

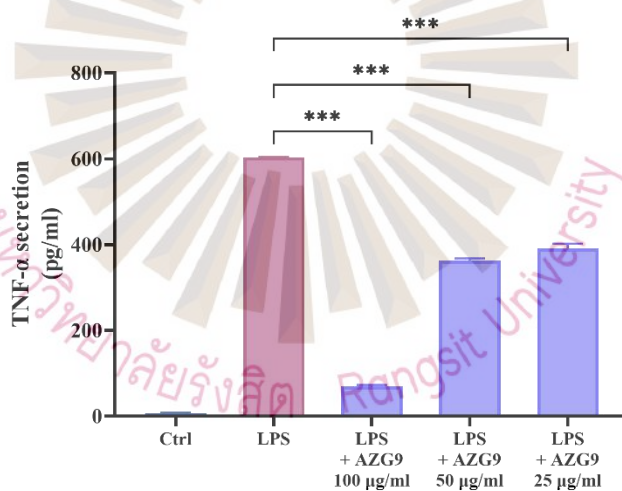


Figure 4.28 TNF- α secretion of RAW 264.7 in control (Ctrl), LPS-stimulated (LPS), pretreated with AZG9 extract at different concentrations followed by LPS stimulation.

Data are mean \pm SD, n = 3. *** indicated statistically significant P < 0.001.

Chapter 5

Conclusion

5.1 Conclusion

The main objective of this study was to formulate the optimal dosage form of AZM for intra-periodontal pocket administration. Although there are many periodontal formulations available in the present-day market, there is no formulation that is particularly aimed at the correction of the main etiologies of periodontal disease comprised of pathogenic bacteria and the host immune response. AZM is a potential drug for periodontitis treatment but because of its poor solubility, categorized as a BCS class II drug, which tampers the bioavailability of AZM in periodontal tissues. The first phase of this research aimed to improve AZM properties by customizing an efficient niosomal system for AZM delivery. The results of phase one could be summarized as that AZM was successfully loaded into the niosome of S60 and CHL. AZM-loaded niosome (NAZ) was successfully prepared with a modified reverse-phase evaporation method. The concentration ratio of S60 and CHL was found to influence particle size and zeta potential of the niosome. The utilization of experimental design provided the polynomial equations and desirability optimization for the favorable niosomal properties. The optimal ratio of niosome composition is obtained. Furthermore, the niosomal formulation achieved controlled release and was associated with the zero-order kinetic model. The prepared NAZ formulation presented proper characteristics as a nano-size particle, and charge stability and was proved to present biocompatibility with periodontal cells, which could potentially correct the disadvantage of AZM in terms of poor solubility and improve bioavailability.

As the adequate form of AZM has been obtained, an efficient carrier for delivering NAZ into the periodontal pocket in actual clinical settings was needed. The second phase of this study intended to develop the practical injectable formulation of NAZ for intra-periodontal administration.

The essential properties of the ideal periodontal formulation are long residence time and sustained-drug release. Therefore, thermoresponsive AZM-loaded niosome gel (AZG) was invented based on these principles. P407 as a thermosensitive polymer and HA as a mucoadhesive polymer were incorporated into the gel formulation. The outcomes of the second phase indicated that AZG exhibited proper thermogelling capacity suitable for the phase transition within the periodontal pocket. The developed gel formulation exerted the proper physical and mechanical properties for the injectable dosage form by the interactions of P407 micelles and the HA network. In addition, AZG provided bioadhesiveness to the mucosa and tooth-root surface as the major component of the periodontal tissues. In the aspect of a delivery system, sustained release behavior was observed along with tissue permeation enhancement. The gel formulations were biocompatible and biodegradable. Finally, the antibacterial properties of AZG were elucidated in this phase.

The critical therapeutic efficacy was further investigated in the third phase. AZG was found to accelerate wound healing in the *in vitro* model. An increase in cell proliferation was also observed. According to the contemporary pathogenesis of periodontitis, the disease is initiated by the invasion of periodontal pathogens followed by the host's defensive mechanism, inflammation, resulting in the collateral damage of periodontal tissues. Therefore, the immune response plays an important role in this context. AZG was investigated for anti-inflammatory effects in this phase. The results illustrated that AZG could suppress inflammatory cytokines expressions such as IL-1 β and TNF- α and proved to decrease IL-1 β and TNF- α secretion of the cultured macrophages.

To the best of our knowledge, this is the first report for an intra-periodontal formulation that emphasizes periodontal tissue penetration, prolonged resident time in the periodontal pocket, and sustained drug release within the periodontal pocket. The physicochemical properties acquired from this development have never been purposed in the other available commercial products. Additionally, the dual effects of this novel formulation in terms of antibacterial and anti-inflammatory would be helpful to the periodontitis treatment.

Finally, with all the results obtained from this study, it is possible to conclude that an efficient delivery system of AZM for intra-periodontal administration has been created in the present study. AZG could be potentially used as an adjunctive for periodontitis treatment to improve the outcome of periodontitis treatment as the main objective of this study aimed for.

5.2 Further Study

To demonstrate the efficacy of the novel AZG formulation, clinical randomized controlled trials need to be carried out.



References

- Abdelkader, H., Ismail, S., Kamal, A., & Alany, R. G. (2010). Preparation of niosomes as an ocular delivery system for naltrexone hydrochloride: physicochemical characterization. *Die Pharmazie*, 65(11), 811–817.
- Abou-Shamat, M. A., Calvo-Castro, J., Stair, J. L., & Cook, M. T. (2019). Modifying the properties of thermogelling poloxamer 407 solutions through covalent modification and the use of polymer additives. *Macromolecular Chemistry and Physics*, 220(16), 1900173. <https://doi.org/10.1002/MACP.201900173>
- Agossa, K., Lizambard, M., Rongthong, T., Delcourt-Debruyne, E., Siepmann, J., & Siepmann, F. (2017). Physical key properties of antibiotic-free, PLGA/HPMC-based in-situ forming implants for local periodontitis treatment. *International Journal of Pharmaceutics*, 521(1–2), 282–293. <https://doi.org/10.1016/J.IJPHARM.2017.02.039>
- Al-Rimawi, F., & Kharaof, M. (2010). Analysis of azithromycin and its related compounds by RP-HPLC with UV detection. *Journal of Chromatographic Science*, 48(2), 86–90. <https://doi.org/10.1093/chromsci/48.2.86>
- Bakheit, A. H. H., Al-Hadiya, B. M. H., & Abd-Elgalil, A. A. (2014). Azithromycin. In *Profiles of Drug Substances, Excipients and Related Methodology* (Vol. 39, pp. 1–40). Cambridge, MA: Academic Press. <https://doi.org/10.1016/B978-0-12-800173-8.00001-5>
- Bansal, M., Mittal, N., Yadav, S. K., Khan, G., Gupta, P., Mishra, B., & Nath, G. (2018). Periodontal thermoresponsive, mucoadhesive dual antimicrobial loaded in-situ gel for the treatment of periodontal disease: Preparation, *in-vitro* characterization and antimicrobial study. *Journal of Oral Biology and Craniofacial Research*, 8(2), 126–133. <https://doi.org/10.1016/j.jobcr.2017.12.005>
- Bartold, P. M., Walsh, L. J., & Narayanan, A. S. (2000). Molecular and cell biology of the gingiva. *Periodontology 2000*, 24, 28–55. <https://doi.org/10.1034/j.1600-0757.2000.224010>

References (Cont.)

- Bassi da Silva, J., Ferreira, S. B. de S., Reis, A. V., Cook, M. T., & Bruschi, M. L. (2018). Assessing mucoadhesion in polymer gels: the effect of method type and instrument variables. *Polymers*, *10*(3), 254. <https://doi.org/10.3390/polym10030254>
- Bodratti, A. M., & Alexandridis, P. (2018). Formulation of poloxamers for drug delivery. *Journal of Functional Biomaterials*, *9*(1), 11. <https://doi.org/10.3390/jfb9010011>
- Braun, S. (2011). 4.431 - Encapsulation of cells (cellular delivery) using sol–gel systems. In P. Ducheyne (Ed.), *Comprehensive Biomaterials* (pp. 529–543). Oxford: Elsevier. <https://doi.org/10.1016/B978-0-08-055294-1.00141-0>
- Bureau of dental health, Ministry of public health. (2018). *The 8th Thailand national oral health survey report*. Bangkok, Thailand: Samchareon phanich.
- Carvalho, F. C., Bruschi, M. L., Evangelista, R. C., & Gremião, M. P. D. (2010). Mucoadhesive drug delivery systems. *Brazilian Journal of Pharmaceutical Sciences*, *46*(1), 1–17. <https://doi.org/10.1590/S1984-82502010000100002>
- Carvalho, G. C., Araujo, V. H. S., Fonseca-Santos, B., de Araújo, J. T. C., de Souza, M. P. C., Duarte, J. L., & Chorilli, M. (2021). Highlights in poloxamer-based drug delivery systems as strategy at local application for vaginal infections. *International Journal of Pharmaceutics*, *602*, 120635. <https://doi.org/10.1016/j.ijpharm.2021.120635>
- Casale, M., Moffa, A., Vella, P., Sabatino, L., Capuano, F., Salvinelli, B., . . . Salvinelli, F. (2016). Hyaluronic acid: Perspectives in dentistry. A systematic review. *International journal of immunopathology and pharmacology*, *29*(4), 572–582. <https://doi.org/10.1177/0394632016652906>
- Chen, M., Li, L., Wang, Z., Li, P., Feng, F., & Zheng, X. (2019). High molecular weight hyaluronic acid regulates *P. gingivalis*-induced inflammation and migration in human gingival fibroblasts via MAPK and NF- κ B signaling pathway. *Archives of Oral Biology*, *98*, 75–80. <https://doi.org/10.1016/j.archoralbio.2018.10.027>

References (Cont.)

- Choi, H., Lee, M., Kim, M., & Kim, C. (1999). Effect of additives on the physicochemical properties of liquid suppository bases. *International Journal of Pharmaceutics*, *190*(1), 13–19. [https://doi.org/10.1016/s0378-5173\(99\)00225-2](https://doi.org/10.1016/s0378-5173(99)00225-2)
- Cui, N., Dai, C.-Y., Mao, X., Lv, X., Gu, Y., Lee, E.-S., . . . Sun, Y. (2022). Poloxamer-based scaffolds for tissue engineering applications: A Review. *Gels (Basel, Switzerland)*, *8*(6). <https://doi.org/10.3390/gels8060360>
- da Silva, J. B., Cook, M. T., & Bruschi, M. L. (2020). Thermoresponsive systems composed of poloxamer 407 and HPMC or NaCMC: mechanical, rheological and sol-gel transition analysis. *Carbohydrate Polymers*, *240*, 116268. <https://doi.org/10.1016/j.carbpol.2020.116268>
- Dahiya, P., & Kamal, R. (2013). Hyaluronic Acid: a boon in periodontal therapy. *North American journal of medical sciences*, *5*(5), 309–315. <https://doi.org/10.4103/1947-2714.112473>
- Damrongrungruang, T., Paphangkorakit, J., Limsitthichaikoon, S., Khampaenjiraroach, B., Davies, M. J., Sungthong, B., & Priprem, A. (2021). Anthocyanin complex niosome gel accelerates oral wound healing: *in vitro* and clinical studies. *Nanomedicine : Nanotechnology, Biology, and Medicine*, *37*, 102423. <https://doi.org/10.1016/j.nano.2021.102423>
- Dash, S., Murthy, P. N., Nath, L., & Chowdhury, P. (2010). Kinetic modeling on drug release from controlled drug delivery systems. *Acta Poloniae Pharmaceutica*, *67*(3), 217–223.
- Diaz del Consuelo, I., Pizzolato, G.-P., Falson, F., Guy, R. H., & Jacques, Y. (2005). Evaluation of pig esophageal mucosa as a permeability barrier model for buccal tissue. *Journal of Pharmaceutical Sciences*, *94*(12), 2777–2788. <https://doi.org/10.1002/jps.20409>
- Dumortier, G., Grossiord, J. L., Agnely, F., & Chaumeil, J. C. (2006). A review of poloxamer 407 pharmaceutical and pharmacological characteristics. *Pharmaceutical Research*, *23*(12), 2709–2728. <https://doi.org/10.1007/s11095-006-9104-4>
- Eggert, F. M., Drewell, L., Bigelow, J. A., Speck, J. E., & Goldner, M. (1991). The pH of gingival crevices and periodontal pockets in children, teenagers and adults. *Archives of Oral Biology*, *36*(3), 233–238. [https://doi.org/10.1016/0003-9969\(91\)90091-8](https://doi.org/10.1016/0003-9969(91)90091-8)

References (Cont.)

- Fakhari, A., Corcoran, M., & Schwarz, A. (2017). Thermogelling properties of purified poloxamer 407. *Heliyon*, 3(8), e00390. <https://doi.org/10.1016/j.heliyon.2017.e00390>
- Garala, K., Joshi, P., Patel, J., Ramkishan, A., & Shah, M. (2013). Formulation and evaluation of periodontal in situ gel. *International Journal of Pharmaceutical Investigation*, 3(1), 29. <https://doi.org/10.4103/2230-973X.108961>
- Ghica, M. V., Hirjău, M., Lupuleasa, D., & Dinu-Pîrvu, C.-E. (2016). Flow and thixotropic parameters for rheological characterization of hydrogels. *Molecules (Basel, Switzerland)*, 21(6). <https://doi.org/10.3390/molecules21060786>
- Giuliano, E., Paolino, D., Fresta, M., & Cosco, D. (2018). Mucosal applications of poloxamer 407-based hydrogels: an overview. *Pharmaceutics*, 10(3). <https://doi.org/10.3390/pharmaceutics10030159>
- Gong, C., Qi, T., Wei, X., Qu, Y., Wu, Q., Luo, F., & Qian, Z. (2013). Thermosensitive polymeric hydrogels as drug delivery systems. *Current Medicinal Chemistry*, 20(1), 79–94. <https://dx.doi.org/10.2174/0929867311302010009>
- Gu, Y., Walker, C., Ryan, M. E., Payne, J. B., & Golub, L. M. (2012). Non-antibacterial tetracycline formulations: clinical applications in dentistry and medicine. *Journal of Oral Microbiology*, 4(2012), 1–14. <https://doi.org/10.3402/jom.v4i0.19227>
- Haffajee, A. D., & Socransky, S. S. (1994). Microbial etiological agents of destructive periodontal diseases. *Periodontology 2000*, 5(1), 78–111. <https://doi.org/10.1111/j.1600-0757.1994.tb00020.x>
- Haffajee, A. D., Socransky, S. S., & Gunsolley, J. C. (2003). Systemic anti-infective periodontal therapy. a systematic review. *Annals of Periodontology*, 8(1), 115–181. <https://doi.org/10.1902/annals.2003.8.1.115>
- Herrera, D., Sanz, M., Jepsen, S., Needleman, I., & Roldán, S. (2002). A systematic review on the effect of systemic antimicrobials as an adjunct to scaling and root planing in periodontitis patients. *Journal of clinical periodontology*, 29 Suppl 3, 136–162. <https://doi.org/10.1034/j.1600-051x.29.s3.8.x>

References (Cont.)

- Hirsch, R., Deng, H., & Laohachai, M. N. (2012). Azithromycin in periodontal treatment: more than an antibiotic. *Journal of Periodontal Research*, *47*(2), 137–148. <https://doi.org/10.1111/j.1600-0765.2011.01418.x>
- Hsieh, H. Y., Lin, W. Y., Lee, A. L., Li, Y. C., Chen, Y. J., Chen, K. C., & Young, T. H. (2020). Hyaluronic acid on the urokinase sustained release with a hydrogel system composed of poloxamer 407: HA/P407 hydrogel system for drug delivery. *PLoS ONE*, *15*(3), e0227784. <https://doi.org/10.1371/journal.pone.0227784>
- Jain, R. A., Rhodes, C. T., Railkar, A. M., Mallick, A. W., & Shah, N. H. (2000). Controlled release of drugs from injectable in situ formed biodegradable PLGA microspheres: effect of various formulation variables. *European Journal of Pharmaceutics and Biopharmaceutics*, *50*(2), 257–262. [https://doi.org/10.1016/S0939-6411\(00\)00062-X](https://doi.org/10.1016/S0939-6411(00)00062-X)
- Jepsen, K., & Jepsen, S. (2016). Antibiotics/antimicrobials: systemic and local administration in the therapy of mild to moderately advanced periodontitis. *Periodontology 2000*, *71*(1), 82–112. <https://doi.org/10.1111/prd.12121>
- Jiang, J., Oberdörster, G., & Biswas, P. (2009). Characterization of size, surface charge, and agglomeration state of nanoparticle dispersions for toxicological studies. *Journal of Nanoparticle Research*, *11*(1), 77–89. <https://doi.org/10.1007/s11051-008-9446-4>
- Jung, Y., Park, W., Park, H., Lee, D.-K., & Na, K. (2017). Thermo-sensitive injectable hydrogel based on the physical mixing of hyaluronic acid and pluronic F-127 for sustained NSAID delivery. *Carbohydrate Polymers*, *156*, 403–408. <https://doi.org/10.1016/j.carbpol.2016.08.068>
- Korsmeyer, R. W., Gurny, R., Doelker, E., Buri, P., & Peppas, N. A. (1983). Mechanisms of solute release from porous hydrophilic polymers. *International Journal of Pharmaceutics*, *15*(1), 25–35. [https://doi.org/10.1016/0378-5173\(83\)90064-9](https://doi.org/10.1016/0378-5173(83)90064-9)
- Lai, P.-C., Ho, W., Jain, N., & Walters, J. D. (2011). Azithromycin concentrations in blood and gingival crevicular fluid after systemic administration. *Journal of Periodontology*, *82*(11), 1582–1586. <https://doi.org/10.1902/jop.2011.110012>

References (Cont.)

- Leung, S.-H. S., & Robinson, J. R. (1990). Polymer structure features contributing to mucoadhesion. II. *Journal of Controlled Release*, *12*(3), 187–194.
[https://doi.org/10.1016/0168-3659\(90\)90099-F](https://doi.org/10.1016/0168-3659(90)90099-F)
- Liao, Y.-H., Jones, S. A., Forbes, B., Martin, G. P., & Brown, M. B. (2005). Hyaluronan: pharmaceutical characterization and drug delivery. *Drug Delivery*, *12*(6), 327–342.
<https://doi.org/10.1080/10717540590952555>
- Limsitthichaikoon, S., Priprem, A., & Damrongrungruang, T. (2020). Niosomes encapsulated anthocyanins complex loaded in a topical oral gel. *Key Engineering Materials*, *859*, 232–238. <https://doi.org/10.4028/www.scientific.net/KEM.859.232>
- Idkaidek, N. M., Najib, N., Salem, I., & Jilani, J. (2014). Physiologically-based IVIVC of azithromycin. *American Journal of Pharmacological Sciences*, *2*(6), 100–102.
<https://doi.org/10.12691/ajps-2-6-1>
- Matesanz-Pérez, P., García-Gargallo, M., Figuero, E., Bascones-Martínez, A., Sanz, M., & Herrera, D. (2013). A systematic review on the effects of local antimicrobials as adjuncts to subgingival debridement, compared with subgingival debridement alone, in the treatment of chronic periodontitis. *Journal of Clinical Periodontology*, *40*(3), 227–241.
<https://doi.org/10.1111/jcpe.12026>
- Mayol, L., Biondi, M., Quaglia, F., Fusco, S., Borzacchiello, A., Ambrosio, L., & La Rotonda, M. I. (2011). Injectable thermally responsive mucoadhesive gel for sustained protein delivery. *Biomacromolecules*, *12*(1), 28–33. <https://doi.org/10.1021/bm1008958>
- Mayol, L., Quaglia, F., Borzacchiello, A., Ambrosio, L., & Rotonda, M. I. La. (2008). A novel poloxamers/hyaluronic acid in situ forming hydrogel for drug delivery: rheological, mucoadhesive and *in vitro* release properties. *European Journal of Pharmaceutics and Biopharmaceutics*, *70*(1), 199–206. <https://doi.org/10.1016/j.ejpb.2008.04.025>
- Meyle, J., & Chapple, I. (2015). Molecular aspects of the pathogenesis of periodontitis. *Periodontology 2000*, *69*(1), 7–17. <https://doi.org/10.1111/prd.12104>

References (Cont.)

- Mhlanga, N., & Ray, S. S. (2015). Kinetic models for the release of the anticancer drug doxorubicin from biodegradable polylactide/metal oxide-based hybrids. *International Journal of Biological Macromolecules*, 72, 1301–1307. <https://doi.org/10.1016/j.ijbiomac.2014.10.038>
- Mitsui, Y., Gotoh, M., Nakama, K., Yamada, T., Higuchi, F., & Nagata, K. (2008). Hyaluronic acid inhibits mRNA expression of proinflammatory cytokines and cyclooxygenase-2/prostaglandin E(2) production via CD44 in interleukin-1-stimulated subacromial synovial fibroblasts from patients with rotator cuff disease. *Journal of Orthopaedic Research*, 26(7), 1032–1037. <https://doi.org/10.1002/jor.20558>
- Moghassemi, S., & Hadjizadeh, A. (2014). Nano-niosomes as nanoscale drug delivery systems: an illustrated review. *Journal of Controlled Release*, 185, 22–36. <https://doi.org/10.1016/j.jconrel.2014.04.015>
- Nair, S. C., & Anoop, K. R. (2012). Intraparodontal pocket: An ideal route for local antimicrobial drug delivery. *Journal of Advanced Pharmaceutical Technology & Research*, 3(1), 9–15. <https://doi.org/10.4103/2231-4040.93558>
- Pedreiro, L. N., Cury, B. S. F., Chaud, M. V., & Gremião, M. P. D. (2016). A novel approach in mucoadhesive drug delivery system to improve zidovudine intestinal permeability. *Brazilian Journal of Pharmaceutical Sciences*, 52(4), 715–725. <https://doi.org/10.1590/s1984-82502016000400016>
- Pereira, G. G., Dimer, F. A., Guterres, S. S., Kechinski, C. P., Granada, J. E., & Cardozo, N. S. M. (2013). Formulation and characterization of poloxamer 407[®]: thermoreversible gel containing polymeric microparticles and hyaluronic acid. *Química Nova*, 36(8), 1121–1125. <https://doi.org/10.1590/S0100-40422013000800008>
- Popova, C., Dosseva-Panova, V., & Panov, V. (2013). Microbiology of periodontal diseases. a review. *Biotechnology & Biotechnological Equipment*, 27(3), 3754–3759. <https://doi.org/10.5504/BBEQ.2013.0027>

References (Cont.)

- Pradeep, A. R., Sagar, S. V., & Daisy, H. (2008). Clinical and microbiologic effects of subgingivally delivered 0.5% azithromycin in the treatment of chronic periodontitis. *Journal of Periodontology*, 79(11), 2125–2135. <https://doi.org/10.1902/jop.2008.070589>
- Pritchard, K., Lansley, A. B., Martin, G. P., Helliwell, M., Marriott, C., & Benedetti, L. M. (1996). Evaluation of the bioadhesive properties of hyaluronan derivatives: detachment weight and mucociliary transport rate studies. *International Journal of Pharmaceutics*, 129(1), 137–145. [https://doi.org/10.1016/0378-5173\(95\)04280-6](https://doi.org/10.1016/0378-5173(95)04280-6)
- Quirynen, M., Teughels, W., De Soete, M., & van Steenberghe, D. (2002). Topical antiseptics and antibiotics in the initial therapy of chronic adult periodontitis: microbiological aspects. *Periodontology 2000*, 28, 72–90. <https://doi.org/10.1034/j.1600-0757.2002.280104.x>
- Rezazadeh, M., Parandeh, M., Akbari, V., Ebrahimi, Z., & Taheri, A. (2019). Incorporation of rosvastatin-loaded chitosan/chondroitin sulfate nanoparticles into a thermosensitive hydrogel for bone tissue engineering: preparation, characterization, and cellular behavior. *Pharmaceutical Development and Technology*, 24(3), 357–367. <https://doi.org/10.1080/10837450.2018.1484765>
- Ritger, P. L., & Peppas, N. A. (1987). A simple equation for description of solute release II. Fickian and anomalous release from swellable devices. *Journal of Controlled Release*, 5(1), 37–42. [https://doi.org/10.1016/0168-3659\(87\)90035-6](https://doi.org/10.1016/0168-3659(87)90035-6)
- Russo, E., Selmin, F., Baldassari, S., Gennari, C. G. M., Caviglioli, G., Cilurzo, F., . . . Parodi, B. (2016). A focus on mucoadhesive polymers and their application in buccal dosage forms. *Journal of Drug Delivery Science and Technology*, 32, 113–125. <https://doi.org/10.1016/j.jddst.2015.06.016>
- Shao, X. R., Wei, X. Q., Song, X., Hao, L. Y., Cai, X. X., Zhang, Z. R., . . . Lin, Y. F. (2015). Independent effect of polymeric nanoparticle zeta potential/surface charge, on their cytotoxicity and affinity to cells. *Cell Proliferation*, 48(4), 465–474. <https://doi.org/10.1111/cpr.12192>

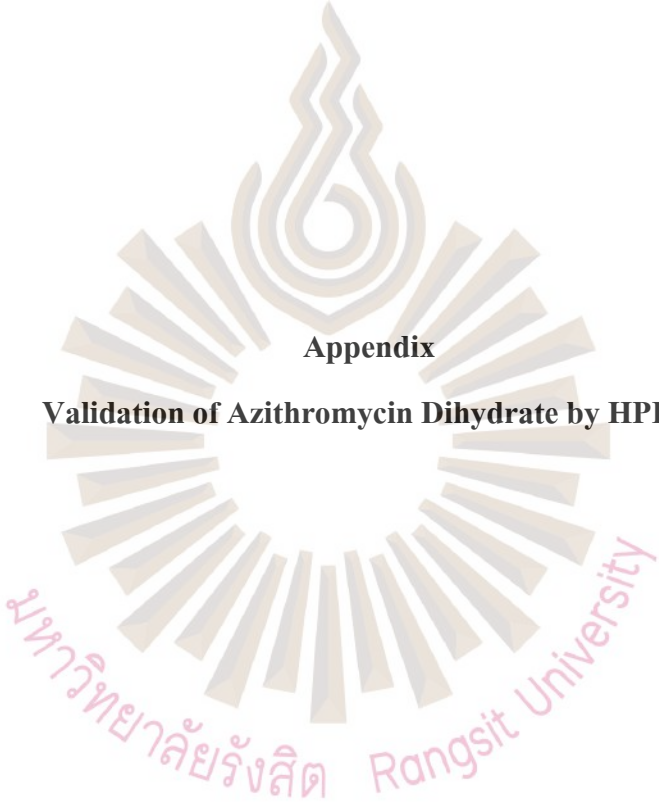
References (Cont.)

- Singh, V. P., Nayak, S. U., Nettemu, S. K., Nettem, S., Lee, Y. H., & Verma, M. B. (2018). Azithromycin in periodontal therapy: beyond the antibiotics. *Journal of Nepalese Society of Periodontology and Oral Implantology*, 2(2), 61–66. <https://doi.org/10.3126/jnspoi.v2i2.23616>
- Snetkov, P., Zakharova, K., Morozkina, S., Olekhnovich, R., & Uspenskaya, M. (2020). Hyaluronic acid: the influence of molecular weight on structural, physical, physico-chemical, and degradable properties of biopolymer. *Polymers*, 12(8). <https://doi.org/10.3390/polym12081800>
- Srivastava, M., Kohli, K., & Ali, M. (2016). Formulation development of novel in situ nanoemulgel (NEG) of ketoprofen for the treatment of periodontitis. *Drug Delivery*, 23(1), 154–166. <https://doi.org/10.3109/10717544.2014.907842>
- Swain, G. P., Patel, S., Gandhi, J., & Shah, P. (2019). Development of moxifloxacin hydrochloride loaded *in-situ* gel for the treatment of periodontitis: *in-vitro* drug release study and antibacterial activity. *Journal of Oral Biology and Craniofacial Research*, 9(3), 190–200. <https://doi.org/10.1016/j.jobcr.2019.04.001>
- Szoka, F., & Papahadjopoulos, D. (1978). Procedure for preparation of liposomes with large internal aqueous space and high capture by reverse-phase evaporation. *Proceedings of the National Academy of Sciences of the United States of America*, 75(9), 4194–4198. <https://doi.org/10.1073/pnas.75.9.4194>
- Talasaz, A. H. H., Ghahremankhani, A. A., Moghadam, S. H., Malekshahi, M. R., Atyabi, F., & Dinarvand, R. (2008). *In situ* gel forming systems of poloxamer 407 and hydroxypropyl cellulose or hydroxypropyl methyl cellulose mixtures for controlled delivery of vancomycin. *Journal of Applied Polymer Science*, 109(4), 2369–2374. <https://doi.org/10.1002/app.28163>
- Torrunguang, K., Jitpakdeebordin, S., Charatkulangkun, O., & Gleebbua, Y. (2015). Porphyromonas gingivalis, Aggregatibacter actinomycetemcomitans, and Treponema denticola / Prevotella intermedia co-infection are associated with severe periodontitis in a Thai population. *PloS One*, 10(8), e0136646–e0136646. <https://doi.org/10.1371/journal.pone.0136646>

References (Cont.)

- Trombino, S., Servidio, C., Curcio, F., & Cassano, R. (2019). Strategies for hyaluronic acid-based hydrogel design in drug delivery. *Pharmaceutics*, *11*(8). <https://doi.org/10.3390/pharmaceutics11080407>
- Vanić, Ž., Rukavina, Z., Manner, S., Fallarero, A., Uzelac, L., Kralj, M., . . . Škalko-Basnet, N. (2019). Azithromycin-liposomes as a novel approach for localized therapy of cervicovaginal bacterial infections. *International Journal of Nanomedicine*, *14*, 5957–5976. <https://doi.org/10.2147/IJN.S211691>
- Watanabe, T., Soeda, W., Kobayashi, K., & Nagao, M. (1996). The pH value changes in the periodontal pockets. *The Bulletin of Tokyo Medical and Dental University*, *43*(4), 67–73. <https://doi.org/10.11480/btmd.430401>



The image features a large, faint watermark of the Rangsit University logo in the center. The logo consists of a stylized flame or sunburst shape at the top, with a circular base containing radiating lines. Below the logo, the text 'มหาวิทยาลัยรังสิต Rangsit University' is written in a semi-circle.

Appendix

Validation of Azithromycin Dihydrate by HPLC

มหาวิทยาลัยรังสิต Rangsit University

HPLC condition and validation of azithromycin dihydrate

Table A1 Validation data of azithromycin dihydrate

Machine	Shimadzu, LC-10, Kyoto, Japan
Column	Zorbax Eclipse XDB-C18 (4.6 × 150 mm, 5 μm) Agilent Technologies, Santa Clara, CA, USA
Oven	50 °C
Detector Wavelength	UV 210 nm
Mobile phase	A = Absolute methanol, B = KH ₂ PO ₄ pH 7.56
Ratio of mobile phase	A:B = 80:20
Injection volume	20 μl
Flow rate	1.0 ml/min
Run time	10 min
Retention time	5.220 min
LOD	7.36 μg/mL
LOQ	22.30 μg/mL
Precision and accuracy	RSD < 2%

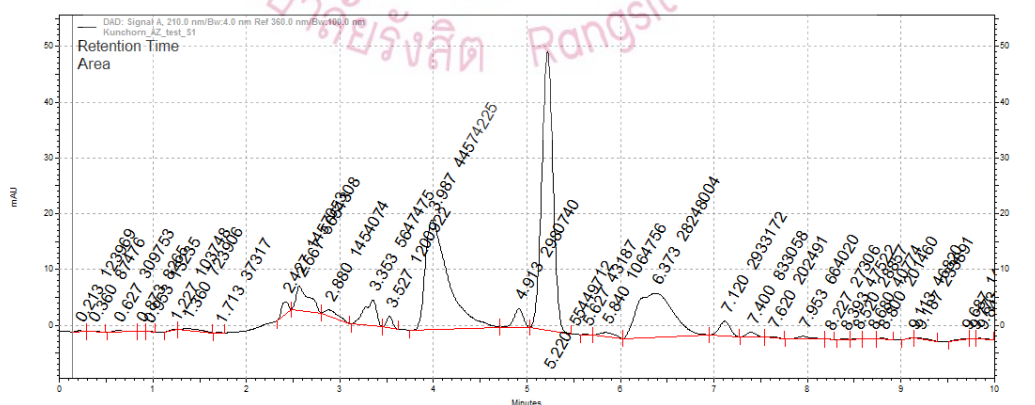


Figure A1 HPLC chromatogram of standard azithromycin dihydrate.

Biography

Name	Kunchorn Kerdmanee
Date of birth	April 9, 1980
Place of birth	Bangkok, Thailand
Education background	Srinakharinwirot University, Thailand Doctor of Dental Surgery, 2004 Srinakharinwirot University, Thailand Master of Science in Clinical Dentistry (Periodontology), 2015 Rangsit University, Thailand Doctor of Philosophy in Pharmacy, 2022
Address	51/063 Muang-ake, Lak-hok, Mueang Pathum Thani, Thailand, 12000
Place of work	College of Dental Medicine, Rangsit University
Work position	Lecturer

